UILU-ENG-96-2004

CIVIL ENGINEERING STUDIES

Structural Research Series No. 609

ISSN: 0069-4274

DYNAMIC STABILITY OF DAMAGE-PRONE INELASTIC STRUCTURAL SYSTEMS

By

Eric B. Williamson

and

Keith D. Hjelmstad

A report to sponsor:
The National Science Foundation

Department of Civil Engineering
University of Illinois at Urbana-Champaign
Urbana, Illinois

May 1996

Dynamic Stability of Damage-Prone Inelastic Structural Systems

Eric B. Williamson
and
Keith D. Hjelmstad

Department of Civil Engineering
University of Illinois at Urbana-Champaign
Urbana, Illinois USA

A report to sponsor:
The National Science Foundation

May 1996

Eric B. Williamson

and

Keith D. Hjelmstad

Department of Civil Engineering
University of Illinois at Urbana-Champaign
205 N. Mathews
Urbana, Illinois 61801
U.S.A.

Dynamic Stability of Damage-Prone Inelastic Structural Systems

Printed in the United States of America.
9 8 7 6 5 4 3 2 1

50272-101

PB96-178587

REPORT DOCUMENTATION PAGE	1 REPORT NO UILU-ENG-96-2004	2	

4. Title and Subtitle
Dynamic Stability of Damage-Prone Inelastic Structural Systems

5 Report Date
May 1996

6.

7 Author(s)
Eric B. Williamson and Keith D. Hjelmstad

8. Performing Organization Rept. No.
SRS 609

9 Performing Organization Name and Address
Department of Civil Engineering
University of Illinois
205 N. Mathews Avenue
Urbana, Illinois 61801

10. Project/Task/Work Unit No.

11 Contract (C) or Grant (G) No
(G) CES 86-58019 (NSF)

12. Sponsoring Organization Name and Address
National Science Foundation, Washington D.C.

13 Type of Report & Period Covered

14

15 Supplementary Notes

16 Abstract (Limit 200 words)

The behavior of a simple mechanical system, experiencing large deformations and inelastic material response with damage, is presented. Because the differential equations that describe the motion are highly nonlinear and coupled for the multi-degree-of-freedom system, a numerical procedure was employed to determine the response. While most engineering approaches to the design of such systems utilize a static approach, results from this research indicate that static analyses cannot effectively predict the behavior of a dynamic, damage-prone system. Most importantly, the rate of damage accumulation will have the greatest impact on the stability properties of the system. In fact, for certain load cases, a system that accrues more damage may be less prone to instability than a system that suffers little damage. For this research, it was assumed that damage caused a reduction in the stiffness such that the structure experienced cyclic softening with increased cycles of loading. Application of the results to seismic-resistant design was considered.

17 Document Analysis a. Descriptors

Stability, Inelastic, Damage, Mathieu equation, Dynamic, Nonlinear, Earthquake, Ramberg-Osgood, Inverted pendulum, Structures.

b Identifiers/Open-Ended Terms

c. COSATI Field/Group

18 Availability Statement	19. Security Class (This Report) Unclassified	21 No. of Pages vii+164
	20. Security Class (This Page) Unclassified	22 Price

Acknowledgements

The research reported herein was supported, in part, by the National Science Foundation (grant number *CES 86-58019*). S.-C. Liu is the cognizant program officer at the National Science Foundation. The support is gratefully acknowledged. The results, opinions, and conclusions expressed in this report are solely those of the authors and do not necessarily represent those of the sponsors.

Contents

1

Introduction

The universe is full of magical things, patiently waiting for our wits to grow sharper.

– Eden Phillpotts

The stability of structures has long been a concern of structural engineers. For many years, researchers have studied why certain structures fail and how to prevent these failures. The first and perhaps the most famous person to study the stability of structures in detail was Leonhard Euler. He is credited with deriving the critical buckling load of an ideal, slender column. This value of the buckling load is well known to most engineers.

The phenomenon of buckling can be illustrated by means of an example. Figure 1 shows a structural system that consists of a rigid bar of length ℓ and an elastic rotational spring of stiffness k. The system is loaded by the vertical load P. Supposing that the bar is disturbed by some external force so that it rotates slightly through a small angle θ, then, if the axial load P is small, the system will return to its original straight configuration after the disturbing force is removed. Under these conditions, the system is termed *stable*. However, if the axial load P is large, the system will continue to rotate around the pin at the base even after the external disturbing force is removed. Under these conditions, the system is *unstable* and is said to *buckle* by undergoing a large rotation of the bar.

A static stability analysis of the displaced system will reveal the smallest axial load that renders the system unstable. As the system rotates, the restoring moment developed in the rotational spring is equal to $k\theta$. Assuming the rotation is small, the overturning moment that is caused by the axial load acting through the displacement at the top of the column is $P\ell\theta$. Equilibrium of the moments about the pin at the base requires that $k\theta - P\ell \sin\theta = 0$. This equation always holds for $\theta = 0$. For equilibrium in the deformed configuration (*i.e.*, $\theta \neq 0$), the axial load P must be equal to $k\theta/\ell \sin\theta$. For values of θ near zero, $P = k/\ell$. This value of P is known as the *critical load* and is given the designation P_{cr}. For axial loads less than the critical load, the system is stable. For axial loads larger than the critical load, the system is unstable and will rotate around the pin at the base.

This example demonstrates that even though a system may be in equilibrium, it is possible for that equilibrium state to be unstable. According to Langhaar (1962),

> an equilibrium configuration of a mechanical system is said to be stable if accidental forces, shocks, vibrations, eccentricities,

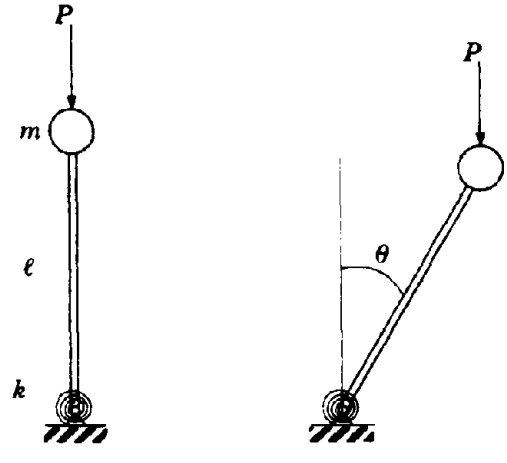

Figure 1 - Simple structural model

> imperfections, inhomogeneities, residual stresses, or other probable irregularities do not cause the system to depart excessively or disastrously from that configuration. In a mathematical sense, stability is usually interpreted to mean that infinitesimal disturbances will cause only infinitesimal departures from the given equilibrium configuration.

The behavior of a long, slender column is similar to the behavior of the spring–bar system in Figure 1. Like the spring–bar system, flexible columns cannot carry arbitrarily large loads and remain stable. As the axial load on the system increases, the critical load will eventually be reached, and the column will buckle. Euler was the first to compute the value of the maximum load the column could carry and remain straight. By studying the equilibrium equations of the column in the deformed configuration, just as we did for the spring–bar system, Euler was able to calculate the critical load. For values of the axial load less than the critical load, the column will remain straight. For axial loads larger than the critical load, the column will buckle.

Failure of structures is a dynamic process. In certain circumstances, it is necessary to approach buckling and stability from a dynamical point of view. For some mechanical systems, the static model is not able to predict the exact path the structure will take in getting to a stable configuration once buckling occurs (Hjelmstad 1994). When the process is fast, the inertia of the system is mobilized, and a method that incorporates the dynamics of the system is required to describe it.

Differential equations of motion can be used to characterize the dynamics of mechanical systems. For example, for an n-degree-of-freedom system, the acceleration of degree-of-freedom i can be described by the differential equation

$$q_i(t) = f_i(q_1, q_2, \ldots, q_n, \dot{q}_1, \dot{q}_2, \ldots, \dot{q}_n, t) \tag{1}$$

where $\ddot{q}_i, \dot{q}_i, q_i$, are the acceleration, velocity, and displacement, respectively, of degree-of-freedom i, t represents time, and f_i, in general, is some nonlinear function of these variables. These nonlinear functions do not require special properties of the restoring force or system damping. For example, the restoring force need not be elastic for Eq. (1) to be valid. The solution to the equations of motion will depend upon the initial conditions and the system parameters. Geometrically, the solution path can be traced as a function of time. For example, one could imagine the trajectory of an object being shot from a canon. The flight of the object will depend upon the initial velocity and the angle at which it was shot. The motion of the object could be described by a curve in a plane. Different paths would result for different initial conditions. Under certain circumstances, some of these curves may intersect one another, and intersecting curves would imply that the same position may correspond to different velocities. Because the trajectory for a given set of initial conditions may intersect other trajectories, many times a different space is chosen to graphically illustrate the motion.

A dynamic process can also be represented graphically in the *phase space* on a plot of velocity versus displacement (Meirovitch 1986, Baker and Golub 1990). The group of all solutions to the governing differential equations that arise because of differing initial conditions is termed the *phase portrait*. The phase portrait has the property that no trajectories intersect one another with the exception of equilibrium points (Meirovitch 1986).

As with static stability, we are most interested in the stability of the motion in the neighborhood of each of the equilibrium points. Most of the early contributions made to the understanding of the stability of dynamical systems are attributed to Lyapunov (*loc. cit.*, Leipholz 1976). Simply put, Lyapunov proposed that a system is stable whenever the motion following a sufficiently small initial dis-

turbance, relative to the perturbed motion, remains as small as desired in the displacements and velocities for all positive time following the disturbance. Mathematically stated, a solution is stable in the sense of Lyapunov if, for any arbitrary positive constant ϵ, there exists a positive quantity δ such that

$$\| \boldsymbol{x}_0 \| < \delta \quad \Rightarrow \quad \| \boldsymbol{x}(t) - \bar{\boldsymbol{x}}(t) \| < \epsilon \qquad 0 \leq t < \infty \tag{2}$$

where $\boldsymbol{x}_0$ defines the initial position and velocity of the system, $\bar{\boldsymbol{x}}(t)$ and $\boldsymbol{x}(t)$ refer to the unperturbed and perturbed motions respectively, and t refers to time. The Euclidian norm is used because it provides a measure of the deviation of the amplitude of the motion from the initial state to any time t. Applying this method requires that the behavior of the dynamic system be addressed for all time subsequent to the perturbation. One difficulty encountered when using the Lyapunov definition is that it is not always clear how to set appropriate limits on ϵ. Clearly, this approach to determining the stability properties of the dynamic system is more complicated than determining the static stability properties of a system.

Poincaré is credited with interpreting Lyapunov's criteria in a geometrical context using phase portraits (see Baker and Gollub 1990 for a more detailed discussion). Poincaré noted certain differences in the trajectories of stable motions versus unstable motions. For example, stable periodic solutions, when plotted in the phase space, produce closed trajectories around an equilibrium point. On the other hand, an unstable equilibrium point has trajectories that form a saddle shape through the equilibrium point or spiral away from the point (for a detailed discussion of phase portraits and the determination of the stability properties in a geometric sense, see Baker and Gollub 1990 or Saaty and Bram 1964). Thus, the stability of the motion for a given system can be ascertained from a phase portrait. To illustrate, consider the free vibration response of the structure shown in

Figure 1. The total energy of the system, which is the sum of the potential energy and the kinetic energy, is given as

$$E(\theta) = \frac{1}{2}m\ell^2\dot{\theta}^2 + \frac{1}{2}k\theta^2 + P\ell\cos\theta = const. \tag{3}$$

For this example, the effect of gravity is included in the axial load P, and it is assumed that the energy is gradually input into the system so that there is no dynamic response associated with the transfer of energy into the system. Conservation of energy requires that $\dot{E}(\theta) = 0$. Computing the derivative of the energy functional allows us to determine the governing differential equation of motion to be

$$\ddot{\theta} + \omega^2[\theta - \eta\sin\theta] = 0 \tag{4}$$

where $\omega^2 = k/m\ell^2$, $\eta = P/P_{cr}$, and $P_{cr} = k/\ell$. Because curves in the phase plane represent trajectories of constant energy when the system is undamped (Meirovitch 1986), Eq. (3) can be used to construct the phase portrait for a particular magnitude of the axial load. Figure 2 shows the phase portraits for three different axial loads – one less than the static buckling load, one equal to the static buckling load, and one larger than the static buckling load. For the different phase portraits shown in Figure 2, $E_1 < E_2 < E_3$. This figure clearly shows that the dynamic stability properties of the system depend upon the amount of energy input to the system via the initial conditions and the amplitude of the axial load.

It is interesting to compare the dynamic stability properties of this model with the static stability properties (for a general discussion on stability criteria for both static and dynamic systems, see the paper by Komarakul-na-nakorn and Arora 990). Initially, the static stability properties of the structure depicted in Figure 1 were determined under the assumption that the rotation would remain small.

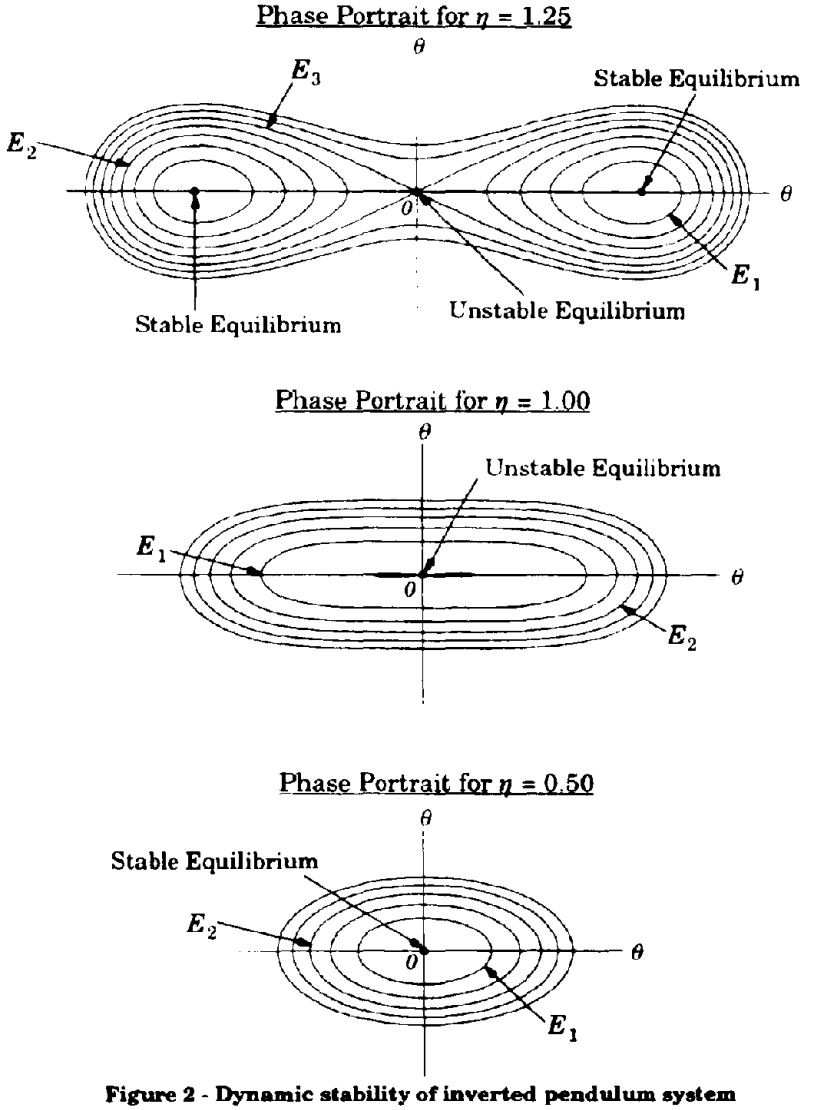

Figure 2 - Dynamic stability of inverted pendulum system

Generally speaking, the critical load is obtained as the solution to a linear eigenvalue problem. As such, the magnitude of the buckled shape is unknown – only the buckled shape itself can be determined. In order to determine the configura-

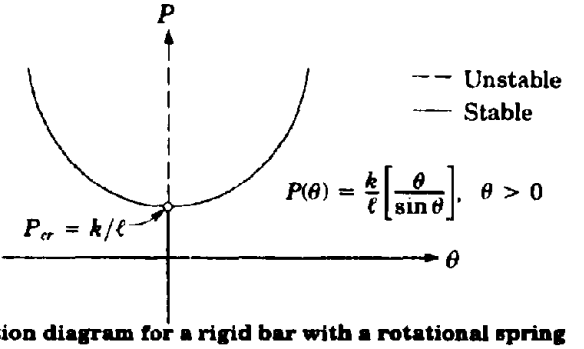

Figure 3 - Bifurcation diagram for a rigid bar with a rotational spring

tion of the structure after buckling takes place, it is necessary to account for large deformations. For the system of Figure 1, considering a large rotation causes the governing equilibrium equation to change. Under these conditions, the overturning moment is calculated from the relationship $P\ell \sin\theta$, and the equation governing the equilibrium of the column is

$$k\theta - P\ell \sin\theta = 0. \tag{5}$$

Equation (5) allows a determination of the equilibrium configuration of the system in the vertical as well as the deformed configuration. The *bifurcation diagram* for the inverted pendulum of Figure 1 is shown in Figure 3. A bifurcation diagram is a plot of the load versus deformation of the system that reveals all static equilibrium states. In Figure 2 we note that, when the axial load is less than P_{cr}, the motion is stable about the origin because the trajectories in the phase plane are closed about this point. In the case of the static loading, this equilibrium configuration corresponds to the stable portion of the bifurcation diagram (Figure 3) when the structure is in the unrotated position (*i.e.*, $\theta = 0$). When the axial load magnitude increases to the value of the critical load, the phase portrait shows that the motion has become larger about the origin and the trajectories have become elongated. The trajectories that intersect this equilibrium point

form a saddle shape which indicates unstable equilibrium. This mode of behavior is consistent with the static bifurcation diagram. For values of axial load that are larger than the static buckling load, the static bifurcation diagram shows that the $\theta = 0$ configuration is not a stable equilibrium position, and a stable equilibrium configuration exists only for larger values of θ. Again, the dynamic response depicted in the phase portrait is consistent with this condition. The origin of the phase portrait for $P/P_{cr} = 1.25$ is an unstable equilibrium point, and stable equilibrium points exist only for larger values of θ. The equilibrium points in the phase portrait correspond exactly to the equilibrium positions indicated by the static bifurcation diagram. Therefore, in light of these comparisons, one can observe that there is a strong relationship between static and dynamic stability analyses.

Although phase portraits allow one to assess the stability of the motion in a direct fashion, it is still necessary to monitor the response as $t \rightarrow \infty$ in order to classify a motion as stable or unstable. It must be pointed out, however, that for a determination of the critical states of the system and the behavior at these points, a complete solution to the dynamic equations of motion may not be necessary. Much research has been devoted to ascertaining the stability limits without actually calculating the response of the system as a function of time. A straightforward approach to this problem, which makes use of an energy criterion, was introduced by Lagrange in 1788. In the early 1800's, the technique was proven by Dirichlet. The basic theorem, which applies only to systems containing conservative forces and dissipative forces derivable from a potential, is as follows: assuming the total energy of the system in question is continuous, the equilibrium of the system is stable provided the Hessian of the energy functional of the system is positive definite.

The law of conservation of energy states that the work of all the forces, both internal and external, acting on a mechanical system is equal to the change of kinetic energy of the system. This law can be used to establish equilibrium equations. When a mechanical system begins to move, the kinetic energy of the system must increase. By the law of kinetic energy, the forces acting on the system must be doing net positive work. From this reasoning, the French mathematician J. Fourier (*loc. cit.*, Langhaar 1962) conversely deduced that a motionless mechanical system remains at rest if the net work done by all the forces in the system is less than or equal to zero for any small displacement that does not violate the constraints. A system is in static equilibrium if the conditions allow the system to remain at rest. Expressing work in variational form leads to the conclusion that in order for the system to be in equilibrium, the first derivative of the energy functional must be equal to zero (Hjelmstad 1994, Langhaar 1962).

A stability criterion can be established by invoking the definition of stability for a mechanical system in the context of the energy functional. If the system can move an infinitesimal amount away from its equilibrium configuration and have positive work done by the forces, then the kinetic energy of the system will increase. Under these conditions, the system is said to be unstable. If only negative work can be done, then the equilibrium state is stable. If either negative or positive work can be done, then the system is said to be in a state of neutral equilibrium. Thus, for a conservative system, stable equilibrium requires that the energy functional be a relative minimum. The second derivative test is used to establish extremum properties of a functional. If the second derivative is greater than zero, the energy is a relative minimum, and the equilibrium state is stable. Conversely, if the second derivative is less than zero, the state is unstable. If the second deriva-

tive is equal to zero, no conclusion can be drawn, and L'Hôpital's Rule must be used to establish the stability characteristics.

The Lagrange-Dirichlet theorem provides a general definition of stability for conservative dynamic systems. For the static case, this theorem yields the same results computed using static stability theory because the static case is a special form of the general dynamic case. Unfortunately, the Lagrange-Dirichlet theorem applies only to dissipative forces derivable from a potential. Whereas dissipative forces that are derivable from a potential (*e.g.*, velocity proportional damping) or are conservative (*e.g.*, gyroscopic forces) cannot destabilize a structure, those which do not meet these criteria can have a destabilizing effect (Bazant and Cedolin 1991, Bernal 1987). Plasticity, as well as viscoelasticity, viscoplasticity, fracture, and other types of damage are dissipative phenomena that are not derivable from a potential. The presence of these types of dissipative forces greatly complicates the problem. The reason dissipative forces that are derivable from a potential cannot destabilize a system is due to the fact that these dissipative forces reduce the energy of the system without altering any of the system parameters. Figure 4 shows the phase portrait of the inverted pendulum when velocity proportional damping is included. For clarity, only part of the phase portrait has been shown for $P/P_{cr} = 1.25$. Note how the motion of the system converges upon the equilibrium point as the energy of the system is dissipated under free vibration. Since the energy of the system is decreasing, (*i.e.*, approaching a minimum), this system must be stable. The same conclusion cannot be drawn for nonconservative forces due to the nature of the path dependency of these forces. For example, the response of a structure following yielding depends not only on its current configuration, but it also depends upon the load path it took in getting to the current state. Black, Wenger, and Popov (1980) have shown that the buckling capacity of

a strut loaded cyclically past its yield state diminishes greatly with increased plastic working of the material. Thus, the strut becomes unstable at a lower applied load. Therefore, while the yielding itself may dissipate energy, its occurrence causes a change in system parameters. The way in which these parameters vary greatly affects the stability properties of the system.

In a very simplistic way, yielding may be thought of as a process that can be associated with the following three phenomena: (1) nonlinear material response; (2) dissipation of energy; and (3) permanent set in the material. Although it is the combination of these three effects acting together that will control the response of the system, a better understanding of the problem might be gained by studying

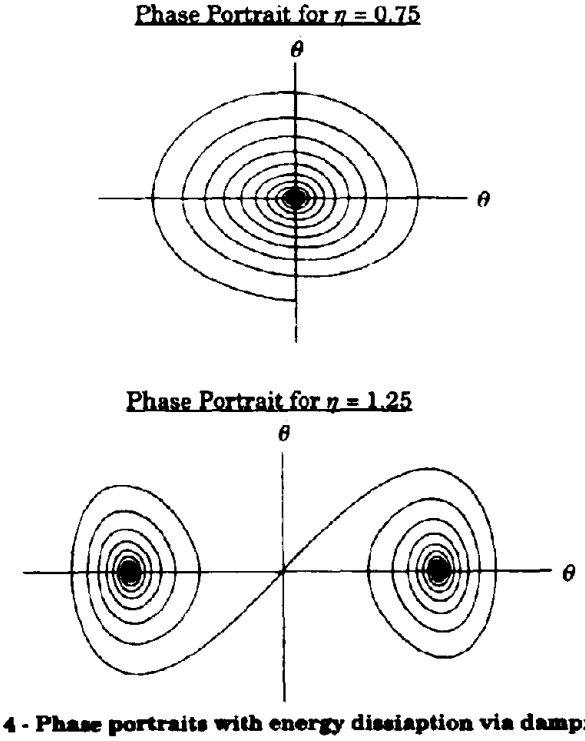

Figure 4 - Phase portraits with energy dissiaption via damping

the individual effects of these three phenomena on the stability properties of the system. Figure 4 shows that energy dissipation, without changes in the other properties of the system, forces the free vibration response toward a stable configuration. Thus, the stability of the system of Figure 1 is improved with energy dissipation.

Next, consider nonlinear material response. Nonlinear material response, even for a static problem, causes difficulty in determining the stability properties of a system (Chen and Lui 1987). To illustrate, Figure 5 shows the response of the inverted pendulum from Figure 1 based upon a nonlinear material model. The assumed relationship between the moment and rotation is given as

$$M(\theta) = \frac{k\theta}{1 + \mu\theta^2} \tag{6}$$

where $\mu = k/M_o$. In Figure 5, it was assumed that $k = 100$ and $M_o = 6$. Comparison between the bifurcation diagrams of Figure 3 and Figure 5 shows that there is a dramatic difference in the static stability properties of the system between the linear model and the nonlinear one. While for the linear system the equilibrium path emanating from the bifurcation point is stable, this path is unstable in the presence of nonlinear material response. Furthermore, the dynamic stability properties, also depicted in Figure 5, change dramatically when nonlinear material properties are considered. For the dynamic response, it was assumed that $\omega^2 = k/m\ell^2 = 1$. The phase portraits for the two levels of axial load considered in Figure 5 show dramatically different stability characteristics from those depicted in Figure 2 even though both models are undamped and assumed to behave elastically. Clearly, the material properties of the system have a large impact on the response of the system as well as its stability properties.

Finally, consider a permanent offset in the material. For the static case, a permanent offset in the material amounts to performing a stability analysis with an initial imperfection. The bifurcation diagram, including an initial imperfection of θ_o, is shown in Figure 6. As one can see, the unrotated configuration $\theta = 0$ is no longer an equilibrium configuration. Two equilibrium paths exist, and the stabil-

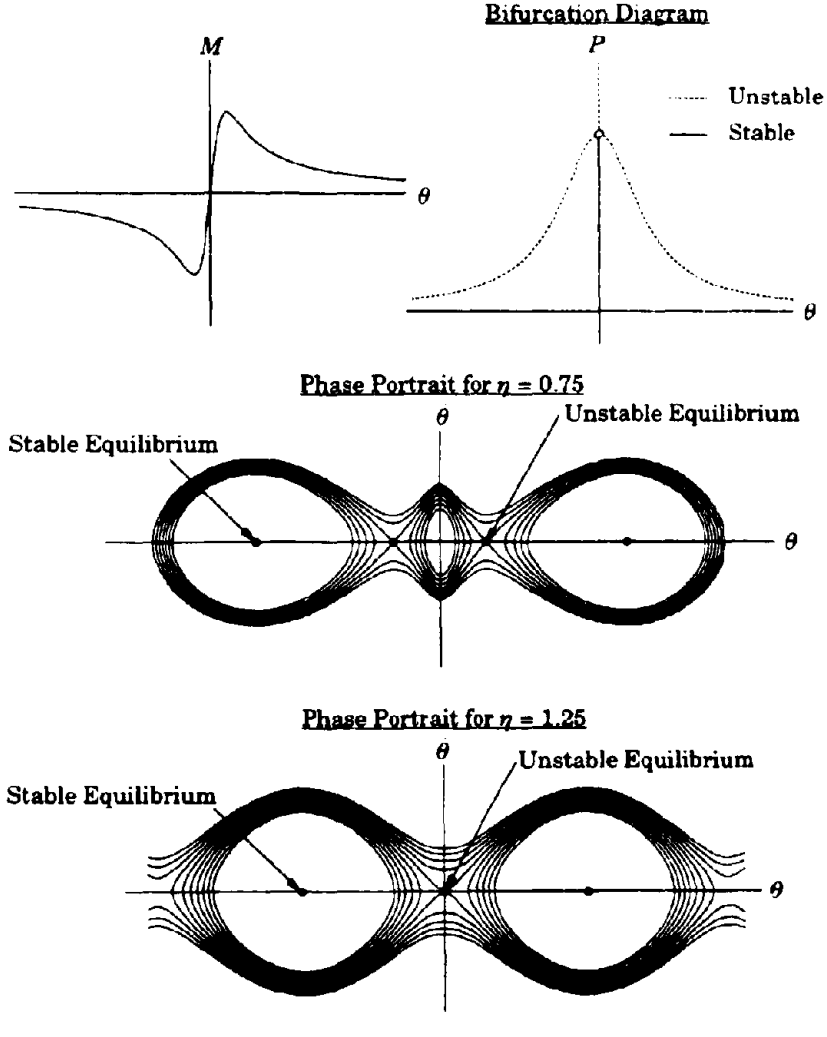

Figure 5 - Response for inverted pendulum with nonlinear material properties

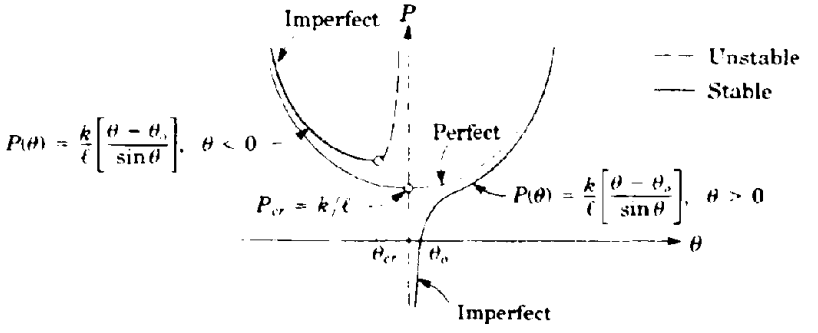

Figure 6 - The effect of an imperfection for inverted pendulum

ity of these paths is shown in Figure 6. For this structure, a limit load is obtained rather than a critical load for the configuration $\theta = \theta_{cr}$. Unlike the perfect system, a stable equilibrium state does not exist for all values of the rotation. As the magnitude of the rotation increases, though, the solution approaches that of the perfect system just as it does when the initial imperfection is small. Clearly, for the static case, the presence of imperfections impacts dramatically upon the stability properties. For the dynamic case, however, the effects of initial imperfections are negligible. The size and direction of the imperfection will simply control the equilibrium point about which the system oscillates. The presence of the imperfection though, unlike the static case, does not affect the stability characteristics. The phase portrait for the inverted pendulum including initial imperfections is also given by Figure 2.

While we are primarily interested in the dynamic stability characteristics of inelastic systems, it is important to first have a thorough understanding of the dynamic stability properties of elastic systems since, at least initially, most structures respond elastically. A significant amount of research literature is available that pertains to the dynamic stability of elastic systems (*e.g.*, Kounadis 1993, Simitses 1990, Leipolz 1976, McIvor and Bernard 1973, Holzer 1970, Bolotin 1964,

etc.). A wide variety of system types with various boundary and loading conditions, including impact loadings (Kounadis 1993, Kounadis 1991) can be found. Most approaches to defining stability limits for elastic dynamical systems are grounded in an energy criterion (Berdichevsky and Kim 1995, Joshi 1995, Lee 1995). Because the forces for an elastic system are conservative, this approach works quite well. Often, nonlinear elastic systems are linearized around an equilibrium point to determine stability characteristics. Doing so allows one to make use of the Routh-Hurwitz criterion which holds that if all of the eigenvalues of the linearized equations are less than zero, then the solution is stable (Afolabi 1995). Chaos theory and graphical methods are also used to help assess stability characteristics via maps. Various researchers have studied chaotic vibrations in simple oscillators and in columns (Addison 1995, Cusumano and Moon 1995, Ravindra and Mallik 1995, Kalathas and Kounadis 1991).

Other types of dynamic stability problems exist for elastic systems other than those mentioned above. One such example is an elastic system under follower forces. Follower forces are nonconservative because their direction changes in accord with the motion of the system. Nonconservative problems of this type have been well covered in the literature (Zuo and Schreyer 1996, Prasad and Herrmann 1972, Bolotin 1963). Another problem is that of parametric resonance. Parametric resonance many times is a result of time dependent coefficients in the governing equations of motion. A classic example of such an equation is the Mathieu-Hill equation (Bolotin 1964, Saaty and Bram 1964). Because the behavior of the Mathieu-Hill equation has been well studied, many researchers try to cast the governing equations of a parametrically excited system of interest in terms of the Mathieu-Hill equation (Chen and Yeh 1995, Lee 1995, Thylwe and Grava-

dor 1995, Yuan and Dickinson 1995, Cederbaum and Mond 1994). A more in-depth discussion of the Mathieu-Hill equation appears later in this manuscript.

For nonconservative systems with inelastic material properties, a different approach is needed for determining the stability properties of the system. It is still desirable, however, to formulate a procedure that does not require integrating the nonlinear differential equations of motion. One approach that has been tried makes use of the second law of thermodynamics (Bazant and Cedolin 1991). Although this approach is general and does not require solution to the differential equations, it does assume that the system loses stability from a static state. Consequently, this approach is not applicable to systems that lose stability in a dynamic way.

Another method that has been introduced makes use of Hamilton's variational principle of dynamics (Komarakul-na-nakorn and Arora 1990). With this approach, the concept of adjacent states is employed. Hence, using the known results for the motion of the system in an unperturbed state, one can study the behavior of the system in an adjacent or perturbed state. It is possible to simplify the expressions for the perturbed motion since this state must satisfy the appropriate boundary conditions. According to Hamilton's Principle, the kinematically admissible deviation from an equilibrium state can be expressed as follows:

$$\delta H(t) = \int_{t_0}^{t_1} (\delta T - \delta \Pi + \delta W_{nc}) dt = 0 \tag{7}$$

where T is the kinetic energy, Π is the potential energy of the conservative forces, and W_{nc} is the work done by the nonconservative forces in going from the state at t_0 to the state at t_1. The equation of motion for the nonconservative system is obtained using Eq. (7). Likewise, using this same procedure, the equation of mo-

tion for the perturbed state can be expressed. To characterize the stability, the perturbed motion must be compared with the unperturbed motion. If it is assumed that the motion in the perturbed state is characterized by

$$\bar{u}_i = \tilde{u}_i e^{\omega t},\ \dot{\bar{u}}_i = \omega \tilde{u}_i e^{\omega t},\ \ddot{\bar{u}}_i = \omega^2 \tilde{u}_i e^{\omega t},\ \text{and}\ \delta\bar{u}_i = \delta\tilde{u}_i e^{\omega t} \tag{8}$$

for some amplitude $\tilde{u}$ and frequency ω, and if the nonlinear material constitutive model can be expressed in an incremental *linearized* form, then the stability of the system may be determined (Komarakul-na-nakorn and Arora 1990). This procedure is an adaptation of the Routh-Hurwitz criterion (Meirovitch 1986). Since the perturbed displacement behaves exponentially, it can be easily shown that the system remains stable for values of ω less than zero. Substituting back into Eq. (8), one is left with a load-frequency dependent, quadratic eigenvalue problem in ω. Due to the nature of the problem, the resulting matrix is typically not symmetric. Accordingly, the resulting eigenvalues are usually complex. The stability criterion is that the real portion of all the eigenvalues be negative for the system to be stable. Because of the load dependency of the eigenvalue problem, an iterative procedure is required to determine the critical load, or the load at which the system changes from being stable to being unstable. At the critical load, the real portion of at least one of the eigenvalues will become zero while the rest remain negative. Thus, the solution procedure commences with determining the eigenvalues for the load currently applied to the structure. If the above criterion is not met, the loads are adjusted. This procedure continues until the critical load is determined. An iterative procedure such as this is typically required for the solution to a nonlinear problem.

Most of the previous research dealing with the dynamic stability of inelastic systems utilizes an elastic-perfectly-plastic material model (Capecchi 1993, Kara-

giozova and Jones 1992, Maier and Pergeo 1992, Yue and Zheng 1992, Jones and Reis 1980) or a bilinear material model (MacRae 1994, Lee 1981). Generally speaking, the study of hysteretic oscillators has not received a great deal of attention in the research literature. The reason this lack of attention exists is that many of the fields for which nonlinear dynamic systems have received extensive study do not typically encounter hysteretic material response (Capecchi 1993, Butenin 1965). Previous study of the response of hysteretic oscillators has proceeded typically in one of two ways. The first approach involves an incremental analysis of the linearized equations to obtain the stability properties of the system. Many times, nonlinear geometrical effects are ignored (Yue and Zheng 1992, Jones and Reis 1980). The second method involves a graphical approach, studying the response of the system in the context of phase portraits for a suitable choice of variables. Using both approaches, significant advancements toward the understanding of hysteretic oscillators have been made.

An example of a study that attempts to characterize the dynamic stability properties of an inelastic system using phase portraits is the one by Sun, Berg, and Hanson (1973). In this study, Sun, Berg, and Hanson monitored the behavior of a structure in free vibration under various initial conditions. The stability of the system was based upon an energy approach similar to the one illustrated for the elastic pendulum discussed earlier. The initial energy input into the system was compared with the amount of energy the system could dissipate through inelastic material response. Sun, Berg, and Hanson assumed an elastic-perfectly-plastic constitutive model for this research. The stability of the system was determined using phase portrait diagrams. As before, if the trajectory in the phase plane remained a closed orbit, the motion was classified as stable. Otherwise, the system was identified as unstable.

Of special interest in the context of civil engineering is the understanding of the inelastic dynamic stability properties of structures subjected to earthquake loadings. Various approaches to this problem have been presented in the literature. For example, Bernal (1987) has suggested a conceptually simple, yet computationally intensive approach. Using the ground motion from various earthquakes as input, the structure can be analyzed repeatedly with different system parameters. The effects of these changes on the response of the system can then be studied. Statistical correlation of the data to the variation of the model parameters can then be used to determine what Bernal has termed an "inelastic P-Δ amplification factor." For Bernal's study, a SDOF system was used, and the material response was assumed to be elastic-perfectly-plastic. The amplification factors were arrived at by comparing the response of the system for the case where no axial load was present to the case where axial load was present. Almost 200 sets of results were computed in this investigation. In order to consolidate all of this information, Bernal tried to statistically correlate the data. By comparing the maximum response to the minimum response and the overall deviation of the data, Bernal was able to prescribe amplification factors for inelastic systems. Using this procedure, it is possible to determine how a certain structure will respond to a given ground motion. Thus, in effect, the inelastic P-Δ amplification factor establishes a serviceability criterion to be employed during design.

In a more recent article, MacRae (1994) extends the results of Bernal's study to include other constitutive models. MacRae's study incorporates a bilinear material response and other hysteresis loops of general shape. MacRae discusses changes in the elastic and inelastic stiffness due to the P-Δ effect. The effects that these changes in stiffness have on the response of structures is discussed in the context of earthquake excitations. MacRae bases the stability of the system with

general-shaped hysteresis loops upon the *hysteresis center curve* concept. The hysteresis center curve is defined as

$$H_c(\Delta) = \frac{1}{2}(H_{yt} + H_{yb}) \tag{9}$$

where H_{yt} and H_{yb} are the upper and lower yield limits on any elastic response line. Conclusions and recommendations for design are based upon the observation that, for earthquake loadings, single degree-of-freedom oscillators tend to oscillate with approximately the same magnitude of acceleration in both the positive and negative directions independent of the shape of the hysteresis curve that describes the material response.

Rationale for the Study

Given the current level of knowledge regarding the dynamic stability of nonlinear, hysteretic systems, there is a great need to develop a better understanding of how such systems behave. Currently, there are not any general observations or classifications of behavior for such systems. Although an extensive amount of information exists regarding the dynamic response of elastic systems and the static response of inelastic systems, very little attention has been directed toward understanding the behavior of inelastic systems under dynamic loadings. As a result, the conditions under which a dynamic, inelastic system becomes unstable remain largely unknown.

Previously, it was claimed that inelastic material behavior may be thought of as the combination of nonlinear material response, energy dissipation, and permanent offset. Of course, in reality, these three effects cannot be separated from one another. In order to determine the dynamic stability properties, it is important to understand the effects of these three phenomena acting in concert. Additionally, the actual response of an inelastic system involves further complication.

With hysteretic behavior, sudden changes in stiffness will take place due to loading and unloading in response to the load. Furthermore, concern must be directed toward understanding the relationship between the energy input to the system by the external loads and the energy dissipated by the inelastic material response. For inelastic material response, unlike the case of velocity proportional damping, energy dissipation is not constantly occurring. At the onset of unloading and reloading, the material will behave elastically, and the energy dissipation will be negligible. Lastly, it is necessary to understand how the external forces acting on the system affect the stability properties since some structures are more efficient at mobilizing this input energy while other structures are more efficient at dissipating it.

Most previous studies in this area have concentrated on using an elastic-perfectly-plastic or bilinear material model. The stability properties for other types of hysteretic behavior have not been explored. In addition, inelastic material behavior implies that the system experiences damage in response to load. Damage to the system, modeled through changes in the constitutive relationship, is an aspect of the dynamic stability of inelastic systems that has yet to be addressed.

Determining the dynamic stability properties of a damage-prone system undergoing large motions, however, has proven to be quite difficult. The differential equation that characterizes such a system is nonlinear and nonconservative, and a closed-form solution has not been obtained under these circumstances. Instability may result during the dynamic excitation or after the external forces cease to act. Thus, study is needed to determine how damage-prone systems respond to dynamic excitations.

Objective and Overview

The objective of this investigation is to provide a definition of what it means for a nonlinear, dynamic system to be stable. Nonlinearity in both the material response and in the geometry of deformation will be considered. Furthermore, the effects of including a damage mechanism in the constitutive relationship will also be addressed. The results presented will discuss the role each parameter of the model has in affecting the behavior of the system. From a practical, civil engineering point of view, of special concern is understanding how structures respond to earthquakes. For this reason, a discussion is included concerning how the results of this study may relate to seismic-resistant design.

The following chapter covers preliminary material on dynamic modeling, numerical integration, and constitutive modeling. Following these preliminary topics, the dynamic stability properties of a hysteretic system are explored. Application of the results are then applied to the earthquake engineering problem. Finally, a summary and conclusions are presented along with recommendations for future research.

2

A Model Problem for the Study of Dynamic Stability

All the mathematical sciences are founded on relations between physical laws and laws of numbers, so that the aim of exact science is to reduce the problem of nature to the determination of quantities by operations with numbers.

– James Maxwell

Introduction

In the analysis and design of structures, engineers often use simple models to help understand and predict the behavior of more complex systems. The main advantage to employing simple models is that they are easier to study and to solve than more complicated ones, yet, they can give an accurate representation of the true structural response despite their simplicity. In addition, for very complicated systems, it is often convenient to analyze simple structures first in order to develop an understanding of the important aspects of the problem. For these reasons, a simple structural model is considered in this research.

Equations of Equilibrium for the *N*-DOF System

Shown in Figure 7 is the structural system used in this investigation. It is comprised of concentrated masses at the end of each rigid link. Rotational restraint of each link is provided by nonlinear springs. These assumptions are often

employed in structural dynamics problems and are known as the *shear building approximation* with *lumped masses* (Berg 1989, Clough and Penzien 1993). The system has N degrees-of-freedom, namely, the rotation of each link measured from the vertical. In this study, both the effects of large rotations and yielding in the springs are considered. Thus, nonlinear effects in geometry and material properties are both taken into account. Constitutive modeling will be discussed in detail in the next section. The structure may be excited dynamically by means of time-dependent axial loads $P(t)$ that can be applied at any or all masses, and/or a horizontal base acceleration of x_g. The system can be set in motion by means of initial velocities and/or displacements at the onset of the analysis. Although it

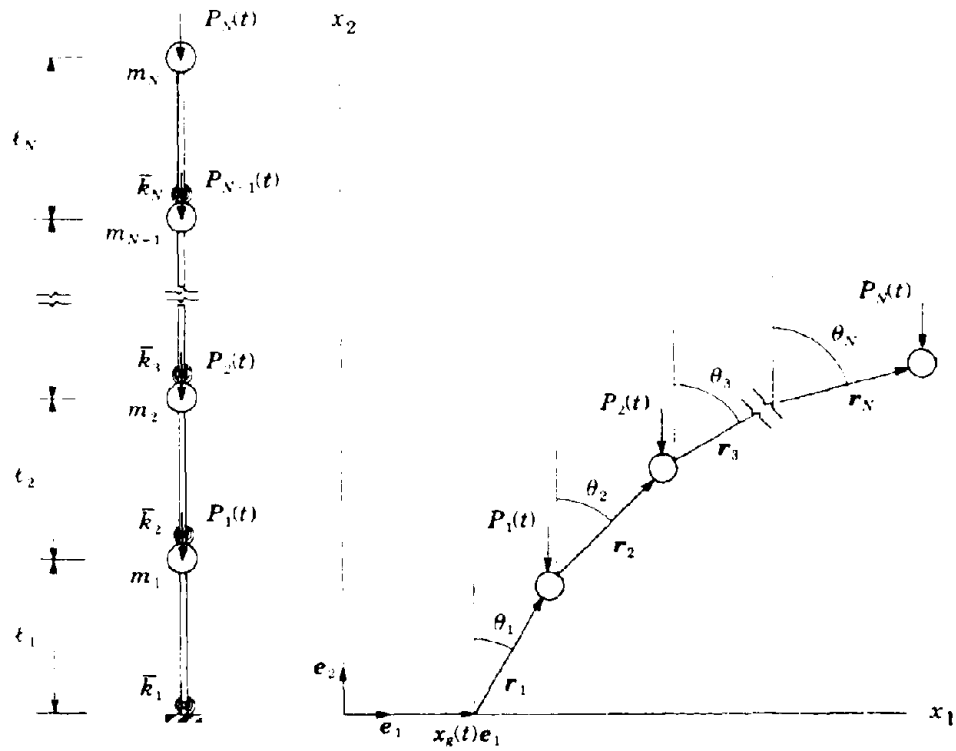

Figure 7 - *N*-DOF model

may appear that such a simple pendulum-type system is incapable of exhibiting complex behavior, the results of this study show otherwise.

In order to proceed with the analysis, the governing equations of motion for the system must be derived. These equations can be constructed using a Newtonian approach (Greenwod 1988, Meirovitch 1986). Referring to Figure 7, it is first necessary to define the position, velocity, and acceleration for each mass. The position of the i^{th} mass is defined as follows:

$$\boldsymbol{R}_i = x_g \boldsymbol{e}_1 + \sum_{j=1}^{i} \boldsymbol{r}_j \tag{10}$$

where $\boldsymbol{r}_j = \ell_j\left(\sin\theta_j \boldsymbol{e}_1 + \cos\theta_j \boldsymbol{e}_2\right)$, and $\boldsymbol{e}_1$ and $\boldsymbol{e}_2$ are unit vectors that point in the direction of the coordinate axes in the x_1–x_2 frame. The velocity is obtained by differentiating the position vector with respect to time. Thus,

$$\dot{\boldsymbol{R}}_i = \dot{x}_g \boldsymbol{e}_1 + \sum_{j=1}^{i} \dot{\boldsymbol{r}}_j \tag{11}$$

and $\dot{\boldsymbol{r}}_j = \ell_j\left(\cos\theta_j \boldsymbol{e}_1 - \sin\theta_j \boldsymbol{e}_2\right)\dot{\theta}_j$. Finaliy, the acceleration is given by

$$\ddot{\boldsymbol{R}}_i = \ddot{x}_g \boldsymbol{e}_1 + \sum_{j=1}^{i} \ddot{\boldsymbol{r}}_j \tag{12}$$

with $\ddot{\boldsymbol{r}}_j = \ell_j\left[\left(\cos\theta_j\ddot{\theta}_j - \sin\theta_j\dot{\theta}_j^2\right)\boldsymbol{e}_1 - \left(\sin\theta_j\ddot{\theta}_j + \cos\theta_j\dot{\theta}_j^2\right)\boldsymbol{e}_2\right]$. For simplicity, define

$$A_j \equiv \cos\theta_j\ddot{\theta}_j - \sin\theta_j\dot{\theta}_j^2 \text{ and } B_j \equiv \sin\theta_j\ddot{\theta}_j + \cos\theta_j\dot{\theta}_j^2 \tag{13}$$

so that $\ddot{\boldsymbol{r}}_j = \ell_j\left[A_j\boldsymbol{e}_1 - B_j\boldsymbol{e}_2\right]$.

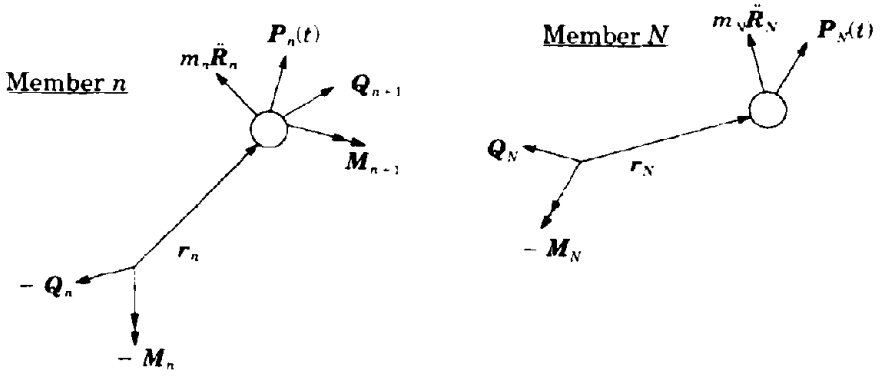

Figure 8 - Free-body diagram

Figure 8 shows a free-body diagram of the system using d'Alembert's principle of dynamic equilibrium (*loc. cit.*, Berg 1989) for the inertial forces. Equilibrium requires

$$-\boldsymbol{M}_n + \boldsymbol{M}_{n+1} + \boldsymbol{r}_n \times \left(\boldsymbol{P}_n + \boldsymbol{Q}_{n+1} + m_n\ddot{\boldsymbol{R}}_n\right) = \boldsymbol{0}, \quad n = 1,\ldots,N-1, \quad (14)$$

$$-\boldsymbol{M}_N + \boldsymbol{r}_N \times \left(\boldsymbol{P}_N + m_N\ddot{\boldsymbol{R}}_N\right) = \boldsymbol{0}. \quad (15)$$

Equilibrium of the free-body diagram shown in Figure 9 requires that

$$\boldsymbol{Q}_n = \sum_{i=n}^{N}\left(\boldsymbol{P}_i + m_i\ddot{\boldsymbol{R}}_i\right). \quad (16)$$

Substituting the relationship for $\boldsymbol{Q}_n$ obtained from Eq. (16) along with the relationships for $\ddot{\boldsymbol{R}}$, A_i, and B_i from Eqs. (12) and (13) respectively, the differential equation of motion for each mass of the system can be determined. To proceed, these values are substituted into Eq. (14). Let us assume planar motion. Noting that all moments cause a couple about the $\boldsymbol{e}_3$ axis, the dot product of both sides of Eq. (14) with the unit vector $\boldsymbol{e}_3$ leads to the scalar equation

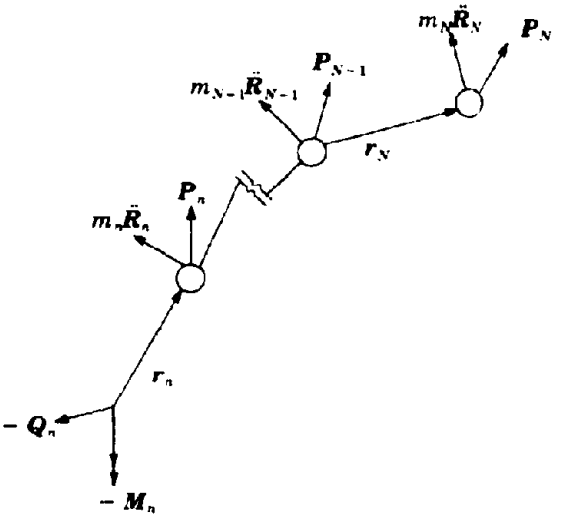

Figure 9 - Free-body diagram of top portion of structure

$$M_n - M_{n+1} + e_3 \cdot r_n \times \sum_{i=n}^{N}\left(P_i + m_i\ddot{R}_i\right) = 0 \tag{17}$$

where $M_n = e_3 \cdot M_n$. Eq. (17) can be simplified by evaluating the cross products and making use of appropriate simplifications. The first cross product reduces to

$$e_3 \cdot r_n \times \sum_{i=n}^{N} P_i = \ell_n \sum_{i=n}^{N}\left(\sin\theta_n P_i - \cos\theta_n F_i\right) \tag{18}$$

where it has been noted that $P_i = F_i e_1 + P_i e_2$. The second cross product is calculated as

$$e_3 \cdot r_n \times \sum_{i=n}^{N} m_i\ddot{R}_i = \tag{19}$$

$$-\ell_n \cos\theta_n \ddot{x}_g \sum_{i=n}^{N} m_i + \sum_{i=n}^{N} m_i \ell_n \sum_{j=1}^{i} \ell_j\left[-\sin\theta_n B_j - \cos\theta_n A_j\right]$$

Substituting Eqs. (18) and (19) into Eq. (17) and making use of trigonometric identities, the governing equations of motion for the system can be calculated. In general, we have the system of equations

$$\boldsymbol{M}(\boldsymbol{\theta})\ddot{\boldsymbol{\theta}} + \boldsymbol{C}(\boldsymbol{\theta})\dot{\boldsymbol{\theta}}^2 + \boldsymbol{R}(\boldsymbol{\theta}) = \boldsymbol{L}(\boldsymbol{\theta}) \tag{20}$$

where $\boldsymbol{\theta} = \{\theta_1, \theta_2, ..., \theta_N\}^T$, $\ddot{\boldsymbol{\theta}} = \{\ddot{\theta}_1, \ddot{\theta}_2, ..., \ddot{\theta}_N\}^T$, and $\dot{\boldsymbol{\theta}}^2 = \left\{\dot{\theta}_1^2, \dot{\theta}_2^2, ..., \dot{\theta}_N^2\right\}^T$. It is possible to express the components of each of the coefficient matrices. First let,

$$\overline{m}_{nj} \equiv \sum_{i=\min(j,n)}^{N} m_i \tag{21}$$

which is the total mass above level $\min(j, n)$. Assuming that the external loads all act in the negative vertical direction so that $\boldsymbol{P}_i = -P_i\boldsymbol{e}_2$, then

$$\overline{P}_n = \sum_{i=1}^{N} P_i \tag{22}$$

is the total vertical load above level n. Then,

$$\boldsymbol{M}_{nj} = \overline{m}_{nj}\ell_n\ell_j\cos(\theta_n - \theta_j), \tag{23}$$

$$\boldsymbol{C}_{nj} = \overline{m}_{nj}\ell_n\ell_j\sin(\theta_n - \theta_j), \tag{24}$$

$$\boldsymbol{R}_n = \boldsymbol{M}_{n+1}(\theta_{n+1} - \theta_n) - \boldsymbol{M}_n(\theta_n - \theta_{n-1}), \tag{25}$$

with $M_{n+1} \equiv 0$ and $\theta_0 \equiv 0$, and

$$\boldsymbol{L}_n = \ell_n\sin\theta_n\overline{P}_n + x_g\ell_n\cos\theta_n\overline{m}_{nn}. \tag{26}$$

Observe that $\boldsymbol{M}_{nj} = \boldsymbol{M}_{jn}$ so that $\boldsymbol{M}(\boldsymbol{\theta})$ is symmetric while $\boldsymbol{C}_{nj} = -\boldsymbol{C}_{jn}$ so that $\boldsymbol{C}(\boldsymbol{\theta})$ is anti-symmetric.

Special Cases: Consider the specific case $N = 1$. The governing differential equation for this case is

$$m\ell^2\ddot{\theta} - P\ell\sin\theta + m\ddot{x}_g\ell\cos\theta + M(\theta) = 0 \tag{27}$$

where $M(\theta)$ is the moment in the nonlinear spring.

For the case $N = 2$, the equations are slightly more involved. To simplify the expressions, let us assume that $m_1 = m_2 = m$, $\ell_1 = \ell_2 = \ell$, $P_1 = 0$, and $P_2 = P$. Then, the coefficient matrices are given as

$$\boldsymbol{M} = \begin{bmatrix} 2m\ell^2 & m\ell^2\cos(\theta_2 - \theta_1) \\ m\ell^2\cos(\theta_2 - \theta_1) & m\ell^2 \end{bmatrix} \qquad \boldsymbol{C} = \begin{bmatrix} 0 & m\ell^2\sin(\theta_2 - \theta_1) \\ -m\ell^2\sin(\theta_2 - \theta_1) & 0 \end{bmatrix}$$

$$\boldsymbol{R} = \begin{Bmatrix} M_2(\theta_2 - \theta_1) - M_1(\theta_1) \\ -M_2(\theta_2 - \theta_1) \end{Bmatrix} \qquad \boldsymbol{L} = \begin{Bmatrix} 2m\ell\ddot{x}_g\cos\theta_1 - P\ell\sin\theta_1 \\ m\ell\ddot{x}_g\cos\theta_2 - P\ell\sin\theta_2 \end{Bmatrix}$$

Constitutive Models

Constitutive theory defines the governing relationships between stress and strain. It represents our ability to accurately determine how a certain material will respond to a given loading. Unlike kinematics and equilibrium, constitutive laws are almost always empirically based. Experimental data are used to help establish the validity of such models. When developing a constitutive model, one tries to formulate mathematical expressions that accurately represent the observed behavior for the material of interest. Certain assumptions, however, may be employed that reasonably approximate the actual system response.

The variety and number of constitutive models that have been studied and proposed in the research literature are tremendous. Many of these models are capable of accounting for complex load histories (Ohno 1982, Chaboche 1989, Ishikawa, Sasaki, and Nakagawa 1994, Sugiura, Chang, and Lee 1991). In order to

evaluate the effects that the constitutive relationship has on the computed response, two different material models are considered in this investigation – an elastic-perfectly-plastic model and a modified, cyclic Ramberg-Osgood model. Both models account for varied, cyclic loads. It should be pointed out that these models are not being used to represent any one particular material. In using the two constitutive relationships, we are focusing on how the response changes with the *type* of model. Accordingly, the greatest concern is understanding the conceptual difference between the two models.

Elastic-Perfectly-Plastic Material Model

Figure 10 shows the stress-strain relationship for an elastic-perfectly-plastic material in a uniaxial stress state. In the subsequent text, "elastoplastic" and "elastic-plastic" share the same meaning as elastic-perfectly-plastic. Prior to yielding, the material responds elastically with stiffness E. After yielding the material offers no further resistance, and upon unloading, the material behaves elastically again. One interesting feature of this model is the abrupt change in stiffness that occurs in the transition from the elastic state to the plastic state or from the plastic state to the elastic state.

This elastoplastic model is often used to model mild structural steels. Although mild structural steels will, after continued loading, exhibit some strain

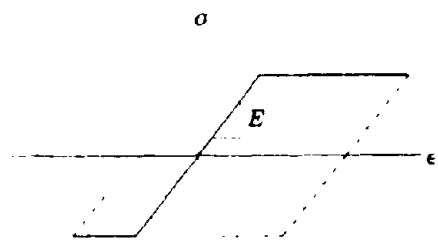

Figure 10 - Elastic-plastic material model

hardening, this feature is not included in the model. Because strain hardening is not included, it is generally assumed that this model conservatively estimates the actual displacements of the real system. While valid for monotonic loadings, this condition may not always hold under cyclic loads. The role of the the material model on the computed results is discussed in detail in Chapter 3.

Local Governing Equations. Although Figure 10 gives a schematic representation of the material model, one must develop a mathematical framework that accurately describes this relationship in order to carry out the desired computations. Once the defining equations have been established, suitable algorithms can be developed to numerically determine the solution in an efficient manner. Already, much research has been devoted to this area (Hill 1950, Simo and Hughes 1988, *etc.*). In fact, the mathematical description of this model was clearly presented in Simo and Hughes (1988) and has been used without modification in this research.

It is assumed that the total strain ϵ is composed of an elastic portion, ϵ^e, and a plastic portion, ϵ^p. Mathematically stated,

$$\epsilon = \epsilon^e + \epsilon^p. \tag{28}$$

The stress is assumed to be linearly related to the elastic strain such that

$$\sigma = E\epsilon^e = E(\epsilon - \epsilon^p). \tag{29}$$

Based on the model we are trying to incorporate, we must recognize certain other physical limitations and describe them mathematically. One such limitation is that the stress σ cannot exceed (either positively or negatively) σ_y. This implies that the *admissible stresses* must lie in the closed interval $[-\sigma_y, \sigma_y]$. Addition-

ally, if the applied stress is less than the yield stress, then there can be no change in the plastic strain. Mathematically, this implies the following:

$$\epsilon^p = 0 \text{ if } f(\sigma) \equiv |\sigma| - \sigma_y < 0. \tag{30}$$

Thus, Eq. (29) along with Eq. (30) imply that

$$f(\sigma) < 0 \Rightarrow \sigma = E\epsilon. \tag{31}$$

Since there is no change in the plastic strain if the stress is less than σ_y, and since the stress cannot exceed σ_y, this leads to the conclusion that the only way in which the the value of ϵ^p can change is if $f(\sigma) = |\sigma| - \sigma_y = 0$. Therefore, if the stress reaches the value of σ_y, then the spring will yield in the direction of the applied force. If we call $\gamma \geq 0$ the absolute value of the plastic strain rate, then we are led to the following:

$$\begin{aligned} \epsilon^p &= \gamma \geq 0 \text{ if } \sigma = \sigma_y, \\ \epsilon^p &= -\gamma \leq 0 \text{ if } \sigma = -\sigma_y. \end{aligned} \tag{32}$$

The sign of the plastic strain rate will depend upon whether or not the structure is under tension or compression.

Reiterating from above, it is first required that the stress at the current configuration be admissible and that the slip rate be positive. Accordingly, if $f(\sigma) < 0$, then the material has not yielded, and the plastic strain rate must be zero. Otherwise, the material has yielded. If the material has yielded, then this implies that $f(\sigma) = 0$ and that the plastic strain rate must be greater than zero. Mathematically,

$$\gamma f(\sigma(t)) = 0. \tag{33}$$

Eq. (33), along with the requirements that $\gamma \geq 0$ and $f(\sigma) \leq 0$, are often referred to as the Kuhn-Tucker conditions (Luenberger 1984). Further, we specify that $\gamma > 0$ only if the material continues yielding or if

$$\gamma f(\sigma) = 0. \tag{34}$$

Eq. (34) is known as the *consistency condition*. With this consistency requirement established mathematically, we can readily determine the state of the system once yielding occurs. From above, we have the following relationship:

$$\dot{f} = \frac{\partial f}{\partial t} = \frac{\partial f}{\partial \sigma}\frac{\partial \sigma}{\partial t} = \frac{\partial f}{\partial \sigma}E(\dot{\epsilon} - \dot{\epsilon}^p) = \frac{\partial f}{\partial \sigma}E\dot{\epsilon} - \gamma\frac{\partial f}{\partial \sigma}\, E\, sign(\sigma) \tag{35}$$

since

$$\frac{\partial}{\partial \sigma}|\sigma| = sign(\sigma) \Rightarrow \frac{\partial f}{\partial \sigma} = sign(\sigma) \text{ and } sign(\sigma) \equiv \begin{cases} +1 \text{ if } \sigma \geq 0 \\ -1 \text{ if } \sigma < 0 \end{cases} \tag{36}$$

Because $[\text{sign } (\sigma)]^2 = 1$, Eqs. (35) and (36) imply that

$$\dot{f} = 0 \rightarrow \dot{\gamma} = \dot{\epsilon}\, sign(\sigma). \tag{37}$$

Using the result of Eq. (37) along with Eq. (32) leads to the result that

$$\dot{\epsilon}^p = \dot{\epsilon} \text{ for } f(\sigma) = 0,\ \dot{f}(\sigma) = 0. \tag{38}$$

Determination of Points on the Stress-Strain Curve. Points on the stress-strain curve are computed using a step-by-step approach. Accordingly, assuming that the current point on the curve is known and the increment in total strain from the previous converged step is given, we desire to determine the corresponding point on the stress-strain curve for the new value of strain. The method for making these calculations is based upon an elastic predictor–corrector meth-

od. The first step in this process is based upon the assumption that over the given time step, the material behaves elastically. Then, based on these trial values, we can determine whether or not yielding actually took place. If yielding did not occur, our elastic prediction was correct, and we can proceed to the next step. Otherwise, we must correct our initial prediction to account for the yielding. The steps needed to determine the stress-strain state of the system are summarized in ***Algorithm 1***.

Algorithm 1

1. Starting conditions: $n = 0$, $\sigma_0 = 0$, $\epsilon_0 = 0$, $\epsilon_0^p = 0$
2. Given the increment in the total strain, update the strain field for the body (*i.e.*, $\epsilon_{n+1} = \epsilon_n + \Delta\epsilon_n$).
3. Compute $f_{n+1}^{trial} = |\sigma_n + E\Delta\epsilon_n| - \sigma_y$
   If $f_{n+1}^{trial} \leq 0$, then
   $\sigma_n \leftarrow \sigma_n + E\Delta\epsilon_n$
   $\epsilon_n^p \leftarrow \epsilon_n^p$
   $n \leftarrow n + 1$
   Otherwise, yielding has occurred
   $\sigma_n \leftarrow \sigma_y \cdot sign(\sigma_n + E\Delta\epsilon_n)$
   $\epsilon_n^p \leftarrow \epsilon_n^p + (f_{n+1}^{trial}/E) \cdot sign(\sigma_{n+1})$
   $n \leftarrow n + 1$
4. Go to step 2.

Cyclic Ramberg-Osgood Material Model

In order to model the behavior of a material such as mild structural steel, our constitutive relationship should include the features of strain hardening and the Baushinger effect. In addition, the transition from the elastic state to the plastic state should be smooth. None of these features are included in the elastic-perfectly-plastic material model covered in the last section. In this section, the modified

Ramberg-Osgood model used in this investigation is presented. For this model, unlike its original form, it is assumed that the response of the material is elastic prior to yielding and that the material response is governed by the monotonic stress-strain curve prior to unloading.

Based upon a large pool of experimental data, one can observe various trends in the behavior of steel subjected to varied, cyclic loads. The first general observation is that, prior to any load reversals, the response of the material is governed by the *monotonic load curve*. This curve is characterized by three separate regions. The first region is the linear-elastic response. With continued loading, the stress eventually exceeds the proportional limit, and yielding occurs. After yielding, the material remains on the yield plateau, the second region of the curve, until strain hardening ensues. The strain hardening portion of the curve is a nonlinear relationship between the stress and strain and represents the third and final region of the monotonic load curve.

A second general observation is that, at a load reversal point, the initial response for unloading in the opposite direction is elastic. With continued loading, the material eventually responds plastically. As the material makes the transition from the elastic state to the plastic one, the tangent modulus changes from E, the initial elastic stiffness, to some constant value E_t. Dafalias and Popov (1975) called this final, constant slope a *bounding line*, for it represents a bound in the stress-strain space. Aktan, Karlson, and Sozen (1973) made similar observations for steel reinforcing bars. They termed the curve that best described this behavior an *envelope curve*. Once a load reversal occurs, the subsequent behavior of the material, as suggested by various investigations, is entirely nonlinear. This nonlinearity is attributed to the *Baushinger* effect. According to Black, Wenger, and Popov (1980), inclusion of the Baushinger effect is essential for cap-

turing the deterioration of buckling strength of a steel member due to previous plastic working of the material. Furthermore, experimental data for structural steel under cyclic loads have shown that the response to subsequent loadings depends not only on the current configuration, but it also depends to a large extent upon the load path taken in getting to the current configuration (see, for example, Dafalias and Popov 1975). Thus, in addition to the Baushinger effect, the load history plays a crucial role in determining the response of the material.

Another key observation, which makes sense from a theoretical point of view, is that loading in one direction has a significant influence on the response of the material for loading in the opposite direction. Accordingly, the position of the bounding line or envelope curve will depend upon the current stress state and the previous loading history. If a load reversal occurs from a point that represents a maximum stress excursion for loading in that direction (*i.e.*, a point on the yield surface), the bounding line for loading in the other direction will shift. If, on the other hand, a load reversal occurs at a point that is less than the maximum stress in that direction (*i.e.*, a point not on the yield surface), the bounding line for loading in the opposite direction will remain unchanged. Instead, the curve will merge with the bounding line defined from the previous maximum stress (see Figure 11).

As with the elastic-plastic model, it is necessary to first establish the mathematical equations that describe the general observations mentioned above before any analyses can be performed. In what follows, the local governing equations that describe these general observations are presented.

The cyclic stress-strain relationship for a typical structural steel under a complex loading is shown in Figure 11. The well-known Ramberg-Osgood equation has been implemented in this study to characterize this complicated relationship between stress and strain. One drawback, however, in using the Ramberg-Osgood

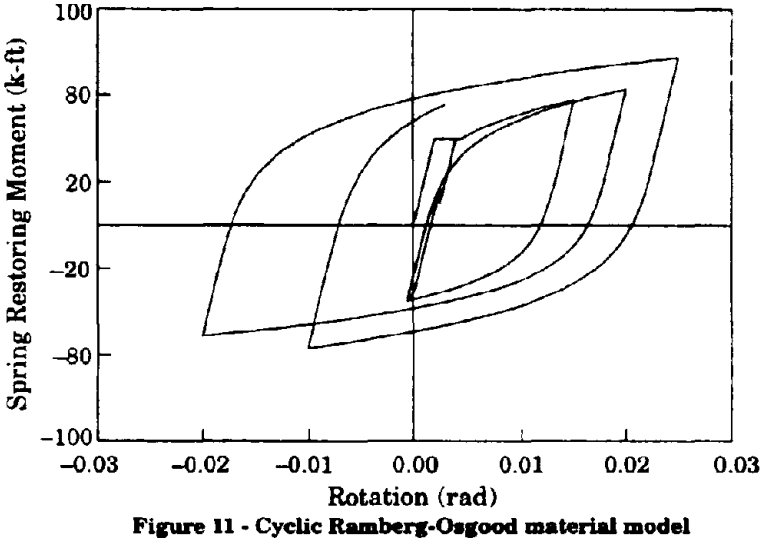

Figure 11 - Cyclic Ramberg-Osgood material model

equation is that, in its original form, it does not include provisions for cyclic loading conditions. Accordingly, modifications must be made before it can be incorporated into our model.

The basic form of the Ramberg-Osgood equation is given as

$$\epsilon - \epsilon_i = \frac{\sigma - \sigma_i}{E}\left[1 + \left|\frac{\sigma - \sigma_i}{\sigma_o - \sigma_i}\right|^{\psi - 1}\right] \tag{39}$$

where ϵ_i, σ_i are the strain and stress, respectively, at the beginning of the curve, E is the initial modulus of elasticity, and σ_o and ψ are constitutive parameters. The value ψ can take on a wide range of values to account for different amounts of hardening. Because the stress-strain relationship is history dependent, the parameters σ_o and ψ will vary as the analysis proceeds. The method for determining their value is given below.

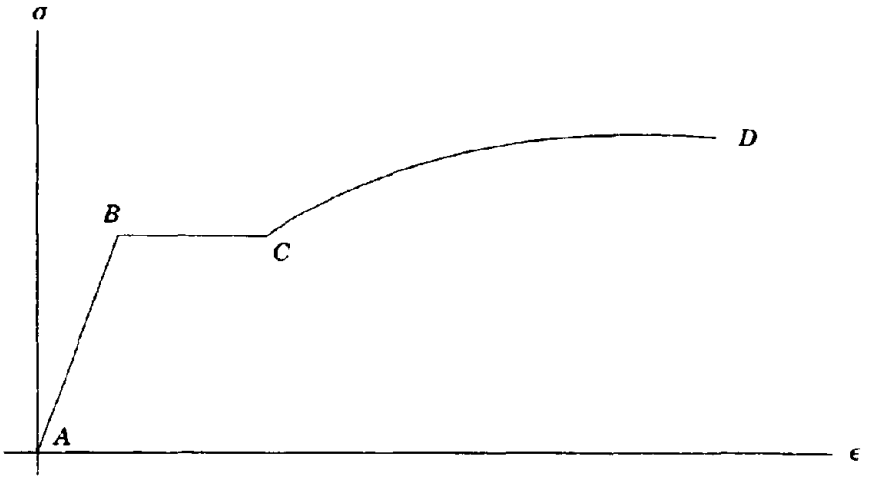

Figure 12 - Monotonic stress-strain curve

Although use of the Ramberg-Osgood equation with the scaling parameters may seem to be somewhat *ad hoc*, it does provide a convenient means of consistently reproducing experimental data. Basically, two different forms of the equation are used. At the start of the analyses, before any load reversals take place, the monotonic curve is used to determine the relationship between stress and strain. Once a load reversal occurs, the parameters used in the modified form of the Ramberg-Osgood equation will depend upon the current stress state and loading history. Details of the procedure are given subsequently.

The Monotonic Load Curve. The monotonic load curve for a typical structural steel is shown in Figure 12. The curve consists of three regions – the linear or elastic region (*A*-*B*), the yield plateau (*B*-*C*), and the strain-hardening region (*C*-*D*). A modified form of Eq. (39) is used to determine the stress-strain relationship for the monotonic load curve:

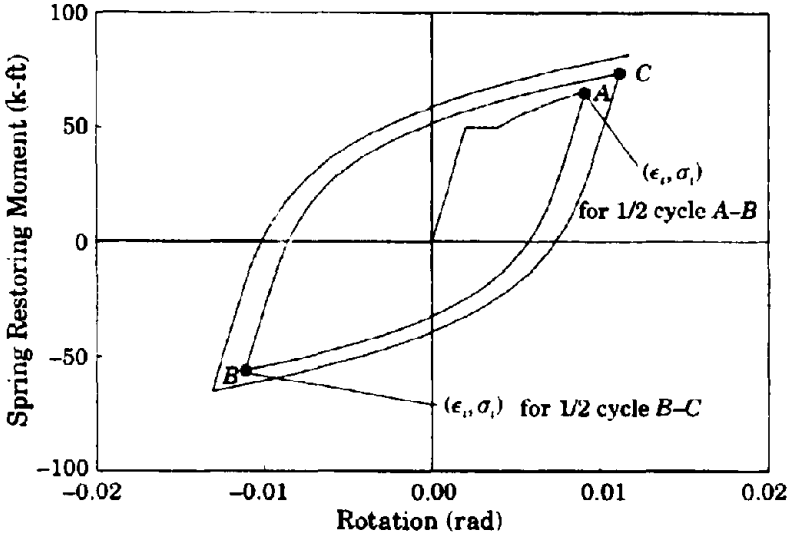

Figure 13 - Envelope curve

$$\frac{\epsilon}{\epsilon_o} = \frac{\sigma}{\sigma_o} + \left[\frac{\sigma}{\sigma_o}\right]^m \tag{40}$$

where $\epsilon_o = \sigma_o/E$, and σ_o and m are parameters that are determined from experimental test data.

Envelope Curves. Figure 13 shows the envelope curves for the cyclic stress-strain relationship defined herein. One complete stress-strain cycle (*A*-*B*-*C*) is assumed to be comprised of two half-cycles. One half-cycle loads in compression (*A*-*B*), and the other half-cycle loads in tension (*B*-*C*). The point at which the half-cycle starts is given the designation (σ_i, ϵ_i), and the slope of the stress-strain curve at the reversal point is equal to the elastic stiffness. The following formula, which is a modified form of the Ramberg-Osgood equation, is used to define the stress-strain relationship for each half-cycle:

$$\frac{\epsilon - \epsilon_t}{\epsilon_o} = \frac{\sigma - \sigma_t}{\sigma_o} + \left|\frac{\sigma - \sigma_t}{\sigma_o}\right|^{\psi} sign(\sigma - \sigma_t). \tag{41}$$

The quantity ϵ_o is defined as σ_o/E, and the function $sign(x)$ is defined as follows:

$$sign(x) \equiv \begin{cases} +1 \text{ if } x \geq 0 \\ -1 \text{ if } x < 0 \end{cases} \tag{42}$$

As mentioned above, we will need to adjust the parameters σ_o and ψ during the analyses. These two parameters will reflect the history dependency of the nonlinear stress-strain relationship. The way in which these parameters are determined will depend upon the point from which unloading commences and upon the stress history up through the latest half-cycle. The two separate ways of determining the values of σ_o and ψ will depend on whether or not the absolute value of the stress at the load reversal point (σ_t in Figure 13) is larger in magnitude than the previous maximum stress. The details are included in the following section.

Determination of Ramberg-Osgood Envelope Parameters. If the unloading curve originates at an initial stress that is greater in magnitude than the previous maximum stress, then the parameters σ_o and ψ can be calculated from the following equation (Aktan, Karlson, and Sozen, 1973):

$$\sigma_o = \lambda + \tau(\sigma_{max} - \sigma_{min}). \tag{43}$$

In Eq. (43), the constants λ and τ, as well as the exponent ψ, are chosen so as to match up well with the experimental curve. For example, for Grade 60 reinforcing steel, Aktan, Karlson, and Sozen (1973) reported the following data:

$\psi = 6$, $\lambda = 0.7938$, $\tau = 0.55723$ for 1/2 cycle from compression, and

$\psi = 7$, $\lambda = 0.7735$, $\tau = 0.47989$ for 1/2 cycle from tension.

Although these values matched the test data, in reality it would be difficult to determine the values of λ and r with such high precision. Also in Eq. (43), σ_{max} refers to the maximum tensile stress prior to the current half-cycle, and σ_{min} refers to the maximum compressive stress prior to the current half-cycle. These parameters can be adjusted to account for other types of steels different than Grade 60 reinforcing steel (see Sittipunt and Wood 1993).

The main drawback of Eq. (43) is that it is only accurate for stress histories that are *symmetric*. The values of the parameters have been determined from load cycles in which the amount of strain in both the compression half-cycle and tension half-cycle are the same. Because not all loading situations encountered are symmetric, it is necessary to develop an alternate method for calculating σ_o and ψ that addresses this issue. Based on observations of various unsymmetric load tests, the following two guidelines are used to help determine the values of the parameters σ_o and ψ when unsymmetric load cycles occur (Dafalias and Popov 1975):

> **G1**. When the initial stress σ_i is less than the previous maximum stress for loading in that direction, the stress-strain curve will join up with and follow the previous half-cycle of loading in that direction (*i.e.*, there is no further expansion of the yield surface).
>
> **G2**. The ultimate strength of the material will control the maximum attainable stress in both tension and compression. When the stress approaches this limiting value, the stress-strain curve tends to flatten out so that this maximum value is not exceeded.

Based on these two guidelines, Sittipunt and Wood (1993) introduce the notion of a *common point* and an *ultimate point* (see Figure 14). A *common point* is defined as the point on the stress-strain curve where the curve from the current half-cycle of loading joins up with the stress-strain curve from the previous half-cycle of

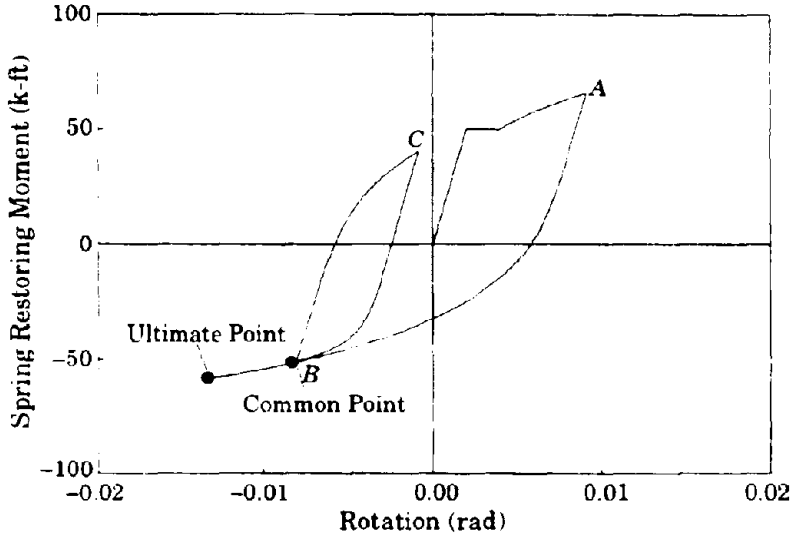

Figure 14 - Definition of common point and ultimate point

loading. An *ultimate point* is defined to be the point on the stress-strain curve that is the limiting value of stress for loading in that direction. Its value is determined from both the properties of the material and the maximum stress excursion in the current loading direction. The way in which these two points are incorporated into the analysis procedure can best be illustrated by means of an example.

Consider the loading history shown in Figure 14. Starting from the origin, the material is loaded in tension until it reaches point A. Because point A represents the maximum stress for loading in this direction, loading in the compression half-cycle from A to B is controlled by Eq. (41) with σ_o calculated from Eq. (43) and ψ obtained from experimental results. Again, since the stress at B represents the maximum in that direction, loading of the curve in tension from B to C is controlled by the same equations. We now must determine the parameters for loading in compression from C. Based on the guideline **G1**, since the stress at C is less than the stress at A (the maximum from the previous half-cycle in that direction), the

stress-strain curve should merge with the previous curve at the common point. Therefore, we need to determine the values of σ_o and ψ that will force the stress-strain curve to merge with the previous envelope curve from A to B at the common point. At the common point, both curves will have equal values for the stress, strain, and tangent stiffness E_t. Since we know the value of the stress, strain, and stiffness at the initial point, we can determine the parameters σ_o and ψ (Sittipunt and Wood 1993). Defining,

$$\breve{\sigma} \equiv \frac{\sigma_2 - \sigma_i}{E(\epsilon_2 - \epsilon_i) - (\sigma_2 - \sigma_i)} \tag{44}$$

then

$$\psi = \left(\frac{E}{E_t} - 1\right)\breve{\sigma}, \text{ and} \tag{45}$$

$$\sigma_o = \breve{\sigma}^{\left(\frac{\psi}{\psi - 1}\right)} \tag{46}$$

where ϵ_i and σ_i are the strain and stress, respectively, at the beginning of the current half-cycle of loading, ϵ_2 and $\sigma_2$are the strain and stress, respectively, at the common point or ultimate point, E is the elastic modulus of the material, and E_t is the tangent modulus of the curve at point (ϵ_2, σ_2).

The correctness of these calculations must now be verified. The procedure for doing so consists of first evaluating Eqs. (45) and (46) at the common point. After calculating σ_o and ψ, the stress at the ultimate point should be calculated based on these values of the parameters. If the calculated stress at the ultimate point is less than the maximum allowable stress, the curve needs no adjustment. If, however, the calculated stress at the ultimate point is greater than the bounding line value or maximum allowable stress for loading in that direction, then the curve needs to be adjusted. At the ultimate point, the stress should equal the max-

imum allowable stress and the tangent stiffness should equal zero. Under these conditions, it is necessary to recompute σ_o and ψ by evaluating Eqs. (45) and (46) at the ultimate point.

The Ramberg-Osgood equation, with the modifications presented above, can adequately describe the cyclic response of mild structural steel. ***Algorithm 2*** summarizes the procedure used to determine a point on the stress-strain curve. As with the elastoplastic model, a step-by-step approach is used.

Algorithm 2

1. The data base and increment in total strain are assumed known. The data base includes the values of all variables needed for subsequent calculations including the maximum tensile stress and strain, the maximum compressive stress and strain, the value of the stress and strain at the last load reversal, curve parameter constants, the total strain increment from the previous step, and the values of stress and strain from the last step.

2. With the given increment in strain, determine if loading is changing directions. Thus, if

$$\Delta\epsilon_{old} \cdot \Delta\epsilon_{new} < 0 \Rightarrow \text{change in loading directions.} \qquad (47)$$

   If the load is changing directions, this indicates loading from a new initial point. If the value from the previous step is greater than the previous maximum for loading in that direction, update the value of the maximum stress and strain. Also update the values of stress and strain from the last load reversal. If the loading is in the same direction as the previous strain increment, the data base does not need to be updated.

3. Now, with the strain and loading direction known, we need to determine the stress. The appropriate equation must be used based upon the following tests:

   3.a. Has the material yielded yet? If not, then $\sigma = E\epsilon$. Otherwise, go to 3.b.

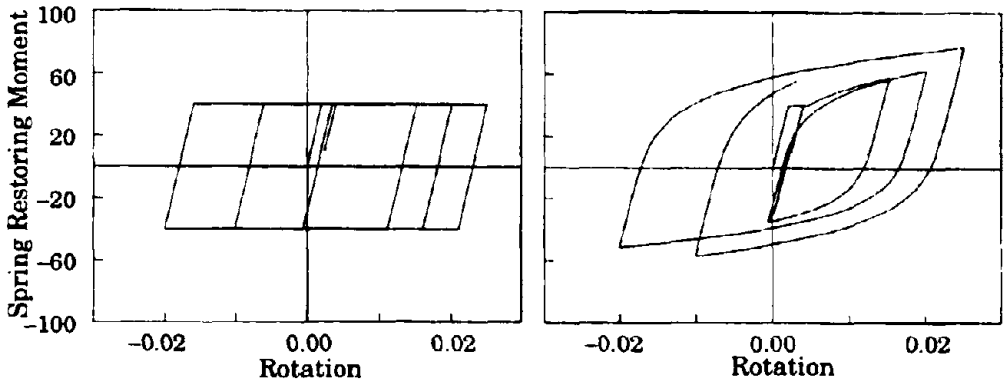

Figure 15 - Elastic-plastic vs. Ramberg-Osgood material models

3.b. Has the material undergone a load reversal yet? If not, then use Eq. (40). Otherwise, go to 3.c.

3.c. Is the value of the initial stress larger than the previous maximum? If so, use Eq. (41) in conjunction with Eq. (43). Otherwise, calculate the stress at the common point using Eq. (41) in conjunction with Eqs. (45) and (46). Also, calculate the stress at the ultimate point. If the calculated stress at the ultimate point exceeds the maximum allowable stress, recalculate the parameters in Eqs. (45) and (46) using the ultimate point instead. Otherwise, use the values obtained previously.

Summary and Comparison of Models. Figure 15 shows a comparison of the two material models presented in this chapter that are used in subsequent analyses. Both models represent loading along the same strain path. That is, starting from the origin, both models are given the same strain increment, and the corresponding stress is determined based upon the guidelines presented earlier. Clearly, there are differences in the response calculated for the two different models. While the stress never exceeds the yield stress for the elastic-plastic mod-

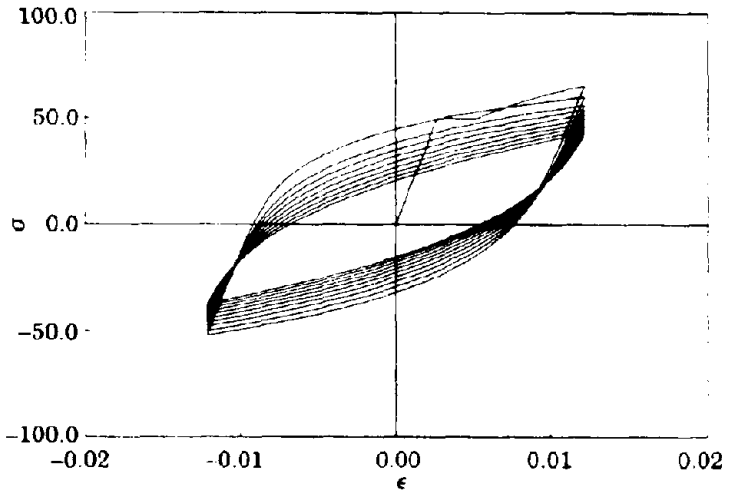

Figure 16 - Cyclic strain softening

el, the Ramberg-Osgood model produces a stress that is much larger than this value in both tension and compression. Furthermore, the energy dissipated, as measured by the area under the stress-strain curve, is much larger for the Ramberg-Osgood model for a given maximum strain. Chapter 3 includes further discussion on how the choice of material model affects the computed results.

Incorporation of Damage in the Constitutive Models

Figure 16 shows the cyclic response of a material that displays *cyclic strain softening*. A consequence of strain softening is that the stiffness of the material degrades under constant amplitude strain cycling. Empirical data suggest that one possible way to model this damage is to modify the modulus of elasticity of the system (Lemaitre and Chaboche 1994, Kachanov 1986). Thus, if E_o is Young's Modulus of the virgin material, free from damage, then

$$E(D) = E_o(1 - D) \tag{48}$$

represents the the damaged modulus. According to Kachanov (1986), the choice of variable(s) to affect the damage model is not simple. For this study, it would have also been possible to include the strain hardening exponent ψ and/or the constitutive parameter σ_o in the damage model. The choice of variables to include is generally based upon a direct generalization of observed behavior. In addition, from a practical point of view, it is desirable to choose as simple a model that will yield acceptable results. In our model, simply reducing the elastic modulus according to Eq. (48) without modifying σ_o or ψ gives good agreement between the calculated results and observed behavior.

Various researchers have introduced different measures of damage D that a system experiences in response to load (Kachanov 1986, Lemaitre and Chaboche 1994, McCabe and Hall 1989, Lubarda 1994, Fajfar 1992, Kutt and Bieniek 1988, Sugiura, Chang, and Lee 1991). Damage models for inelasticity generally depend on the maximum deformation and the accumulated energy dissipated by the system. Other factors, such as temperature, radiation, and corrosion, could also cause damage but are less important in applications involving large strain cycling of the material. A good first approximation for the damage model is to consider a linear dependence upon the maximum deformation and energy dissipated. To wit,

$$D = \alpha \mathfrak{D} + \beta \mathfrak{E} \tag{49}$$

where α and β are constants that depend upon material properties, $\mathfrak{D} = d/d_y$ is the deformation normalized by the yield deformation, $\mathfrak{E} = E_H/\sigma_y d_u$ is the hysteretic energy dissipated normalized by $\sigma_y d_u$ where d_u is the ultimate displacement of the material under monotonic loading conditions, and σ_y is the yield strength of the material. The coefficients α and β can be interpreted as the parameters that determine the rate of damage of the material under cyclic loading.

At the end of each converged step, the total amount of damage is calculated, and the modulus $E(D)$ is modified. Thus, for both the elastoplastic model and the cyclic Ramberg-Osgood model, one simply replaces the value of E with $E(D)$ in each formula it occurs. The damage form of the Ramberg-Osgood equation is now given as

$$\epsilon - \epsilon_i = \frac{\sigma - \sigma_i}{E(D)}\left[1 + \left|\frac{\sigma - \sigma_i}{\sigma_a - \sigma_i}\right|^{r-1}\right] \tag{50}$$

The effects of including a damage mechanism in the constitutive relationships are discussed in detail in Chapter 3.

Numerical Integration of Governing Nonlinear Equations

Since the differential equations that describe the motion of the system being considered cannot be solved analytically, one must resort to a numerical procedure in order to make any headway toward a solution. Accordingly, one must ensure that the numerical procedure used gives accurate results. Otherwise, the results obtained from the analysis can be at best misleading, and at worst, completely unrepresentative of the motion the system actually experiences. In addition to accuracy, the numerical solution procedure used must be stable. In the context of numerical integration, *stability* implies that any errors in the displacements, velocities, and accelerations at some time t, which may be due to computer round-off error, do not grow with the integration (Bathe 1982). The *accuracy* of the numerical integration scheme refers to the ability of the method to replicate the exact solution. The accuracy and stability properties of the numerical integration scheme control the maximum allowable time step size that yields results with the desired level of precision.

Direct Integration Methods: A Brief Introduction. Using *direct integration* to solve the equations of motion implies that the solution will be found at discrete times only. Therefore, a step-by-step numerical procedure is used to advance the solution from the last converged state to the next converged state. Many different direct integration techniques exist (Bathe 1982). The assumed variation of the displacements, velocities, and accelerations over the time step Δt are what determine the accuracy and stability properties of the numerical procedure. It is generally agreed that among the different direct integration procedures available that the Newmark Method provides the best overall performance with regard to stability and accuracy (Bathe 1982).

Even though the Newmark Method is unconditionally stable for linear problems, the time step size must still be chosen appropriately. According to Bathe (1982), using a step size of $\Delta t = 0.01\ T_n$ will ensure sufficient accuracy. Some additional issues arise when applying direct integration techniques to nonlinear problems. For nonlinear problems, the system can experience sudden changes in stiffness or resistance due to yielding and unloading. If the time step chosen is too large, these effects may not be accurately captured. Because nonlinear problems are path-dependent in their solution by nature, any errors introduced during the incremental analysis can have a large impact on the behavior calculated at a later time. Consequently, when using direct integration techniques to solve nonlinear problems, the user should employ a procedure that is unconditionally stable for the linear case and include equilibrium iterations with a tight enough tolerance to ensure that the true behavior of the system is accurately determined (Hughes 1977). For this research, the tolerance was set so that the magnitude of the residual forces or load imbalance (as determined from the equilibrium equations), normalized by the magnitude of the load vector, was less than 10^{-6} (see Bathe

(1982) for general guidelines on setting tolerances for numerical integration of nonlinear problems).

Newmark's Method. Newmark's Method for numerical integration of the equations of motion is based upon the following assumptions:

$$\boldsymbol{v}_{i+1} = \boldsymbol{v}_i + \Delta t\left[(1-\gamma)\boldsymbol{a}_i + \gamma \boldsymbol{a}_{i+1}\right] \tag{51}$$

$$\boldsymbol{d}_{i+1} = \boldsymbol{d}_i + \Delta t \boldsymbol{v}_i + \Delta t^2\left[\left(\frac{1}{2}-\beta\right)\boldsymbol{a}_i + \beta \boldsymbol{a}_{i+1}\right] \tag{52}$$

where $\boldsymbol{d}_i \approx \boldsymbol{u}(t_i)$, $\boldsymbol{v}_i \approx \dot{\boldsymbol{u}}(t_i)$, and $\boldsymbol{a}_i \approx \ddot{\boldsymbol{u}}(t_i)$. The parameters β and γ can be selected to obtain different stability and accuracy characteristics. Typically, the choices of $\beta = 1/4$ and $\gamma = 1/2$ are made. The reason for this choice of parameters is that, for linear systems, Newmark's Method is unconditionally stable and second order accurate. The Newmark estimations for $\boldsymbol{d}_{i+1}$ and $\boldsymbol{v}_{i+1}$ must be augmented by an equilibrium equation to complete the estimate of the state at time t_{i+1}.

In general, we are interested in the following system of equations:

$$\boldsymbol{G}(\ddot{\boldsymbol{U}}, \dot{\boldsymbol{U}}, \boldsymbol{U}) = \boldsymbol{0}. \tag{53}$$

For nonlinear problems, the solution proceeds iteratively. The iteration procedure can be efficiently implemented as a Newton-Raphson scheme. Because we will be considering increments in the displacement, it is convenient to rearrange Eqs. (51) and (52) in terms of the unknown displacements. Thus, for $\beta = 1/4$ and $\gamma = 1/2$, the acceleration and velocity in terms of the unknown displacement are given as

$$\boldsymbol{a}_{i+1} = \tilde{\boldsymbol{a}}_i + \frac{4}{\Delta t^2}\boldsymbol{d}_{i+1} \tag{54}$$

$$\boldsymbol{v}_{i+1} = \tilde{\boldsymbol{v}}_i + \frac{2}{\Delta t}\boldsymbol{d}_{i+1} \tag{55}$$

where

$$\tilde{\boldsymbol{a}}_i = -\boldsymbol{a}_i - 4(\boldsymbol{d}_i + \boldsymbol{d}_{i+1})/\Delta t^2 - 4\boldsymbol{v}_i/\Delta t \tag{56}$$

$$\tilde{\boldsymbol{v}}_i = -\boldsymbol{v}_i - 2(\boldsymbol{d}_i + \boldsymbol{d}_{i+1})/\Delta t \tag{57}$$

Eq. (53) requires that

$$\boldsymbol{G}(\boldsymbol{a}_{i+1}, \boldsymbol{v}_{i+1}, \boldsymbol{d}_{i+1})\boldsymbol{0}. \tag{58}$$

Substituting the Newmark relationships from above leads to the expression

$$\boldsymbol{G}\left(\tilde{\boldsymbol{a}}_i + \frac{4}{\Delta t^2}\boldsymbol{d}_{i+1}, \tilde{\boldsymbol{v}}_i + \frac{2}{\Delta t}\boldsymbol{d}_{i+1}, \boldsymbol{d}_{i+1}\right) = \boldsymbol{0} = \tilde{\boldsymbol{G}}(\boldsymbol{d}_{i+1}). \tag{59}$$

Linearizing $\tilde{\boldsymbol{G}}(\boldsymbol{d}_{i+1})$ about the configuration $\boldsymbol{d}^{\nu}_{i+1}$ gives

$$\tilde{\boldsymbol{G}}(\boldsymbol{d}^{\nu}_{i+1}) + \left[\frac{4}{\Delta t^2}\frac{\partial \boldsymbol{G}}{\partial \boldsymbol{a}} + \frac{2}{\Delta t}\frac{\partial \boldsymbol{G}}{\partial \boldsymbol{v}} + \frac{\partial \boldsymbol{G}}{\partial \boldsymbol{d}}\right]\Delta \boldsymbol{d}^{\nu}_{i+1} = \boldsymbol{0} \tag{60}$$

where the general model $\boldsymbol{G} = \boldsymbol{M}(\boldsymbol{\theta})\ddot{\boldsymbol{\theta}} + \boldsymbol{C}(\boldsymbol{\theta})\dot{\boldsymbol{\theta}}^2 + \boldsymbol{R}(\boldsymbol{\theta}) - \boldsymbol{L}(\boldsymbol{\theta}) = \boldsymbol{0}$ is used in Eq. (60) (see Eq. (20)). Finally, the displacements are updated with the expression

$$\boldsymbol{d}^{\nu+1}_{i+1} = \boldsymbol{d}^{\nu}_{i+1} + \Delta \boldsymbol{d}^{\nu}_{i+1}. \tag{61}$$

Eventually, the difference in the new estimate and the old estimate will be within the set tolerance. At this point, the state of the system is known for the current time step, and now the state of the system should be determined for the next time step. This procedure continues until the response of the nonlinear system has been determined for all time.

Variable Time Stepping for Newmark's Algorithm. An interesting phenomenon occurs when using Newmark's Method to solve single degree-of-freedom problems with an elastic-plastic material model. In order to avoid problems with the numerical integration, it may be necessary to use a time step smaller than the recommended 0.01 T_n for linear systems. Figure 17 shows the effects of using too large a time step in calculating the maximum displacement of the system shown in Figure 1. The system response has been determined for a sinusoidal ground excitation with the system starting from rest. The large spikes in the graph appear due to error accumulation during the course of the analysis. For certain time steps, the error in defining the transition from the elastic state to the plastic state or from the plastic state to the elastic state is such that errors systematically accumulate. A closer examination shows that only very specific time step increments will lead to this type of error. If the time step size is changed slightly, the error disappears. Figure 18 demonstrates this phenomenon.

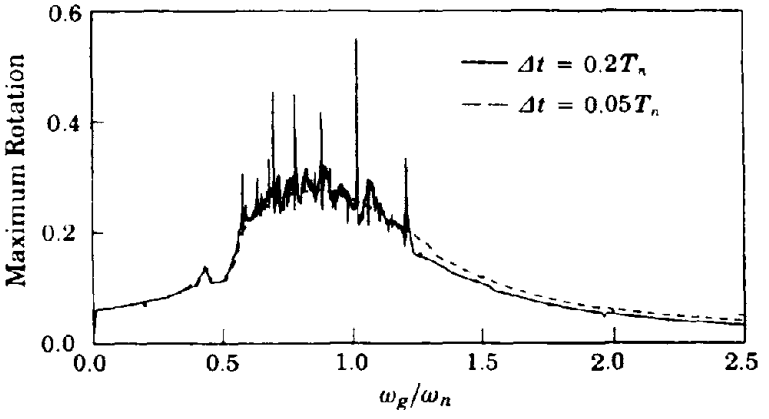

Figure 17 - Effect of time step size on maximum computed displacement

The systematic errors accrue because of one-sided dipping at the elastic-plastic interface. Figure 19 shows this rounding of the corner effect for a particular time step increment. In order to make the Newmark algorithm accurate, one must subdivide the time step in the transition regions. Using a uniformly small time step in the regions away from the corners is not efficient. Hence, one should allow the time step to adapt. When the material is near the transition region, make the time step size small enough to accurately determine the corner of the curve. Away from this region, allow the time step to increase in size in order to

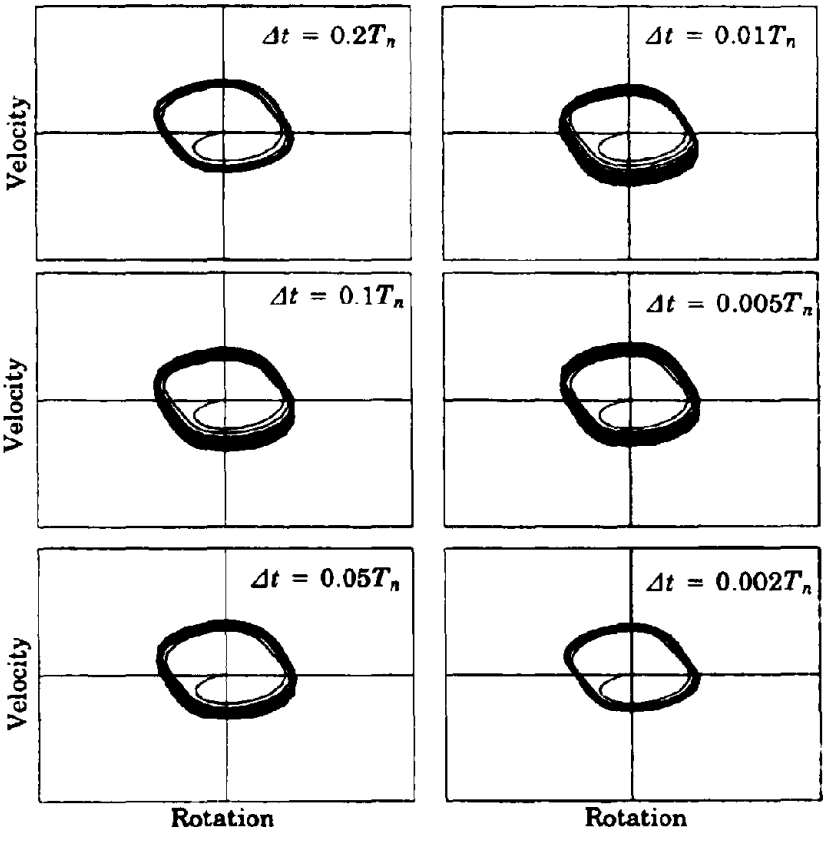

Figure 18 - Effect of time step size on stability of Newmark's Method

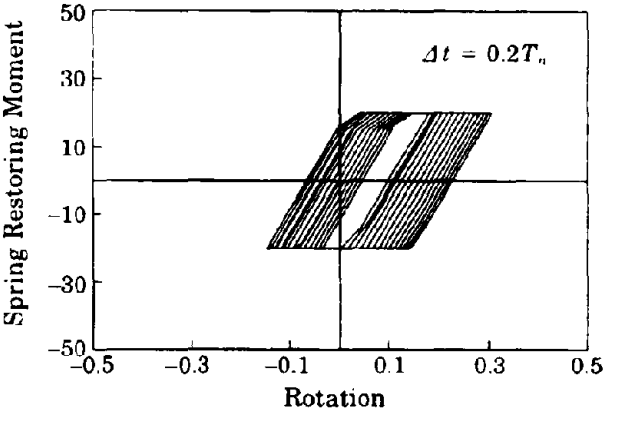

Figure 19 · Error accumulation for Newmark's Method

speed up the analysis. Of course, since the integration constants used in the Newmark procedure are dependent on the time step duration, these values must be updated every time the time step changes. Using this strategy works very well. In fact, for maximum time steps even greater than those that led to the large error accumulations above give results that are quite acceptable.

Successive Symmetric Quadratures. Another approach to dealing with the problems of the Newmark Method for nonlinear problems is to use an altogether different integration scheme. Chen and Robinson (1993) have developed an integration method that includes the following two essential features: (1) use of time integration for its smoothing effect; (2) use of an improved quadrature rule over the trapezoidal rule. This method works quite well and was employed for determining the response for the SDOF system in this research. The details of implementing this method are presented in Appendix A1.

Summary

A mechanical model was presented that will be used to study the dynamic stability characteristics of a damage-prone system. The corresponding differential equations of motion were derived for the general case. These equations account for inelastic material behavior and large rotations. Two nonlinear constitutive relationships were introduced that will be used to determine the restoring moments developed in the rotational springs located at the base of each rigid link. The role of the constitutive model on the observed behavior is studied in detail in Chapter 3. Following the material on the constitutive models, a damage model was introduced. The damage model, which depends upon the maximum deformation and hysteretic energy dissipated, has the effect of reducing the elastic modulus with increasing damage. Finally, the numerical integration procedure used to determine the response of the system was presented. For nonlinear problems, provisions must be made to account for sudden changes in stiffness that arise due to yielding and unloading of the material.

3

Dynamic Stability of Hysteretic Systems

There is nothing stable in the world – uproar's your only music.
- John Keats

Dynamic Response without Base Excitation

Even though the primary focus of this study is to investigate the dynamic stability characteristics of hysteretic, damage-prone systems, it is important to first consider the linear-elastic response of the system. As discussed previously, studying the linear-elastic response allows one to locate possible regions of instability, and it provides a benchmark for comparing the dynamic stability properties of the damage prone system. In this chapter, the structural model presented in Chapter 2 is analyzed. First, the SDOF system is considered, and the response is computed assuming a linear-elastic response. Initially, the lateral base acceleration is set equal to zero. The effects of accounting for large rotations and inelastic material properties are then investigated. After, the response of the system to lateral base excitation and constant axial load is presented. Following this material, the response of a 2-DOF model is considered. Finally, the role of including a damage mechanism in the constitutive relationship is explored.

Linearized Geometry and Elastic Material Properties. If we make the assumptions that the rotation is small, the material is elastic, and the base acceleration is equal to zero, then the governing differential equation of motion for a SDOF system is given as

$$m\ell^2\ddot{\theta} + (k - P(t)\ell)\theta = 0. \tag{62}$$

If we further assume that the system is undamped, the force due to gravity is negligible compared to the magnitude of the applied axial load, and the axial load varies with time according to $P(t) = P_o \cos(\Omega t)$, then Eq. (62) reduces to

$$m\ell^2\ddot{\theta} + (k - P_o\ell\cos\Omega t)\theta = 0. \tag{63}$$

Eq. (63) is the Mathieu Equation (Bolotin 1964, Saaty and Bram 1964). Many properties of this equation have been well established in the literature (Bolotin 1964, Saaty and Bram 1964, Grimshaw 1990, Shirts 1993). One of its most important characteristics is that for certain combinations of axial load magnitude and frequency, the system becomes dynamically unstable (in the sense of Lyapunov). In order to determine the regions of stability for the Mathieu Equation, it is first assumed that the solution is periodic and can be described by an infinite Fourier series. Substituting the Fourier series back into Eq. (63) leads to a linear set of algebraic equations that involve the unknown coefficients of the Fourier series. It is known from linear algebra that the system of homogeneous equations has a solution different from zero only when the determinant of the matrix of the system coefficients is zero. Since we are considering an infinite series, we must calculate an infinite determinant. In order to compute an actual value for the determinant, it is necessary to consider a finite subset. The accuracy of the computed determinant is improved as the number of terms considered increases.

In Figure 20, the shaded regions indicate the combination of model parameters that lead to the first three regions of dynamic instability for the Mathieu Equation. The axes have been normalized such that the ordinate is the ratio of the frequency of the axial load to the natural frequency, and the abscissa is the axial load magnitude divided by the static buckling load. In Figure 20, the system is unstable, both in a dynamic sense and a static sense, when $P_o/P_E \geq 1$. As Figure 20 indicates, the primary region of instability corresponds to the case where the frequency of the pulsing vertical load is twice the natural frequency of the system. Under these conditions, the system becomes dynamically unstable for any magnitude axial load greater than zero. For very small values of the axial load, the effects of gravity become more significant. In this research, however, only axial loads greater than approximately 40% of the static buckling are consid-

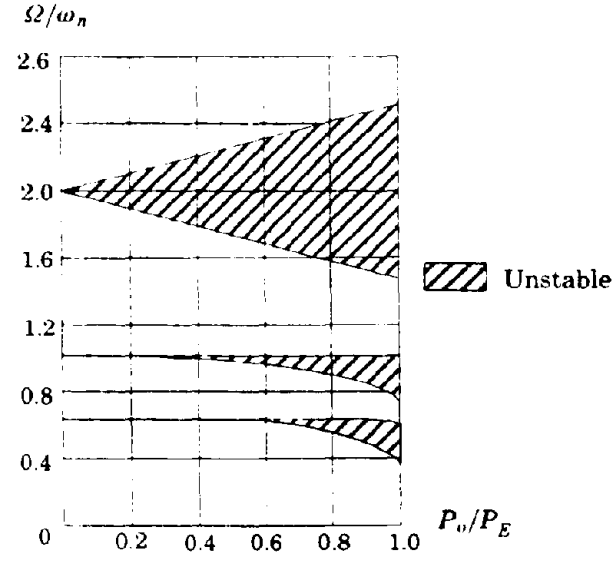

Figure 20 - Regions of dynamic instability for the Mathieu Equation

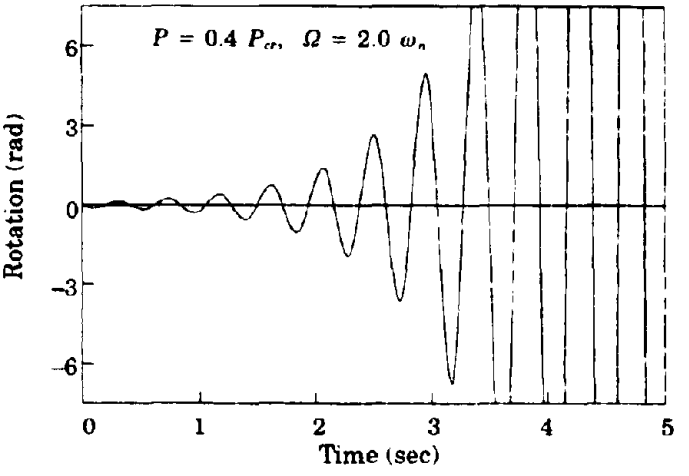

Figure 21 - Displacement vs. time for unstable region of Mathieu's Equation

ered so that the effect of gravity is small in comparison to the amplitude of the axial load.

Figure 21 shows a plot of the rotation versus time for a set of model parameters that falls into one of the regions of instability for the Mathieu Equation. With increasing time, the rotations approach infinity, and, by any definition, we can conclude that the system has become unstable. This response confirms the expected behavior for the given model parameters and the Mathieu Equation. Using Eq. (63) to calculate the response, one would be led to believe that, in the time duration shown, the pendulum rotates completely about the hinge at the bottom more than twice. Clearly, the calculated response is not consistent with the assumption of small rotations.

In order to gain a better understanding of the response of the system for a set of model parameters that falls into one of the regions of instability, we must refine our original hypothesis to include the possibility of large rotations. Although us-

ing the geometrically exact model complicates the analysis, it is necessary to obtain more information about the system after the rotations become large. It should come as no surprise that one must consider large deformations for this problem. This step is also essential for static stability problems (Hjelmstad 1994). For such problems, the linearized analysis may indicate the critical load, but it cannot provide information about the system once buckling has occurred. Consequently, the next step in our analyses will be to investigate the response of the geometrically exact model.

Exact Geometry and Elastic Material Properties. If we modify our previous assumptions to account for large rotations, then the governing equation of motion takes the form

$$m\ell^2\ddot{\theta} + k\theta - (P_o\ell\cos(\Omega t))\sin\theta = 0. \tag{64}$$

While the geometrically exact model gives more accurate results, it is much more difficult to solve analytically. In fact, a closed form solution of Eq. (64) has not been found for the case where the nonlinear differential equation has time-varying coefficients (Bolotin 1964, Grimshaw 1990). Consequently, the analysis is accomplished by numerically solving Eq. (64) for a wide array of model parameters. By considering a variety of different system properties, we can gain a better understanding of the general nature of this structure. Figure 22 compares the results of the geometrically exact analysis with those of the linearized analysis. The properties of the system for both analyses are the same, the only difference is the approximation that $\sin\theta \approx \theta$ for the linearized system. Thus, Figure 22 illustrates the difference between using Eq. (63) and Eq. (64) to compute the response.

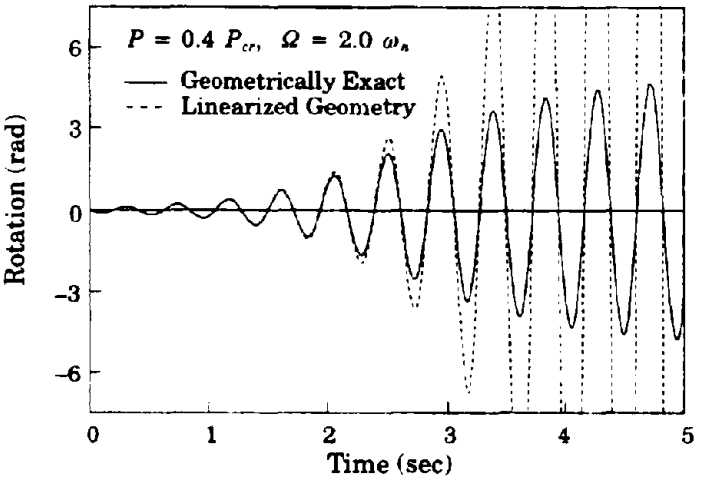

Figure 22 - Comparison of geometrically exact vs. linearized analysis

While the linearized model helps us locate potential regions of instability, it fails to capture some significant aspects of the behavior.

If the response of the system computed from Eq. (64) is monitored for a longer period of time, a peculiar phenomenon is observed. Figure 23 shows the variation of the displacements with time for the same system considered above but for a greater duration. Figure 23 shows that the system experiences some sort of "beating" phenomenon. Classical beating motion occurs in the presence of two vibrations of different frequencies that are very close to one another (den Hartog 1985, Timoshenko 1948, Meirovitch 1986, Lu and Hall 1990). Beating occurs frequently with acoustic vibrations and in other areas of the physical sciences. Figure 24 shows a plot of the displacement versus time for a classical beating system. What is interesting about the fact that beating occurs in our model is that it will take place even when the driving frequency is much different than the natural frequency of the system.

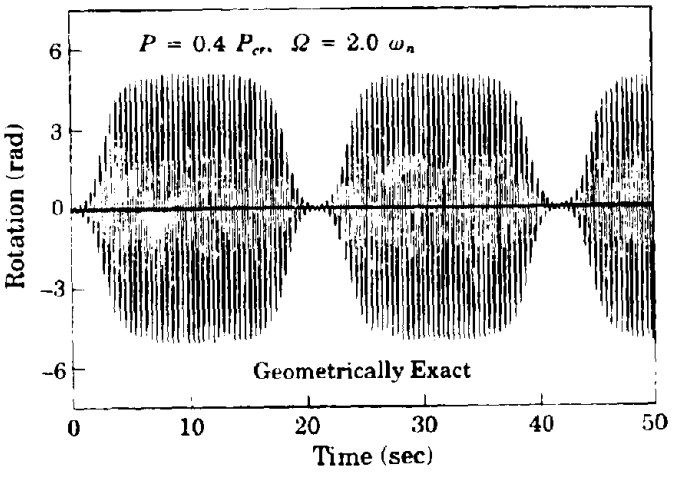

Figure 23 - Beating phenomenon

Two key factors contribute to the pattern of behavior shown in Figure 23. First, unlike the linearized system, the frequency of the motion is not constant

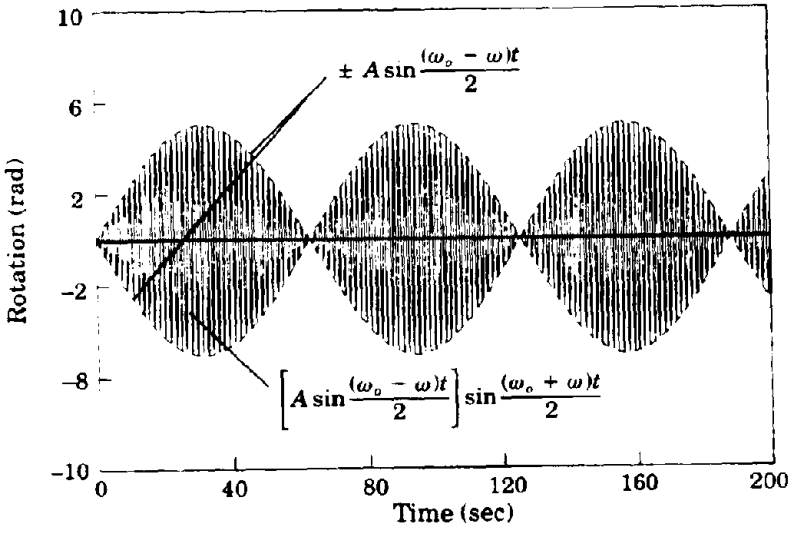

Figure 24 - Classical beating system

(Meirovitch 1986) but is affected by the amplitude. The free vibration of a geometrically exact oscillator is not exactly sinusoidal (the analytical solution is in terms of elliptic integrals (Kamke 1959, Saaty and Bram 1964)). Consequently, at certain times, the frequency of vibration due to the initial conditions is in phase with the driving frequency, and at other times, it is not. When the two frequencies are in phase, the motion becomes large. When they are out of phase, the amplitude diminishes. Whether or not the two parts of the response are in phase will depend upon the displacement amplitude, which in turn depends upon the axial load magnitude and the initial conditions. Based on these observations, one could speculate that the system would respond similarly for other types of periodic axial loads.

The impact the initial conditions have on the observed behavior can be demonstrated by considering the response of the system when a very small amount of damping is included (0.005 of critical damping). The response for the damped system is shown in Figure 25. Initially, before the steady-state is reached, one can see the start of the beating behavior due to the interaction between the steady-state and transient responses. However, with time, as the transient portion of the motion gets damped out, a steady-state oscillation of the same frequency of the axial load is observed. Other researchers report similar findings for other systems of this type (Cedarbaum and Mond 1994, Sun, Berg, and Hanson 1973). In fact, small changes in the initial conditions may alter the subsequent response from a stable motion to an unstable motion and *vice versa*. Also, depending on the initial system properties, we may see different pathways to instability. This dependence is discussed further below.

Another phenomenon we notice with the geometrically exact system is that the motion does not become unbounded. For the model with linearized geometry,

we could discern when the system became unstable because,with continued time, the displacement and velocity of the system tended toward infinity. With geometrically exact model, the rotation may become large, but it remains finite. Thus, we need an appropriate means of identifying instability for the geometrically exact system and a suitable definition for "dynamic instability." First, if the system becomes unstable before undergoing at least one complete cycle of motion (see Figure 26) or becomes unstable after the external excitation has ceased, then this will not be considered a case of dynamic instability. If, on the other hand, the system undergoes at least one complete cycle of motion without becoming unstable and then becomes unstable while excited by external forces, then this will be known as *dynamic instability*. Furthermore, instability for the system under consideration will be defined as the case where the column has undergone a rotation around the base of $\theta = \pm \pi$. Although this value of the rotation is much larger than the rotation any real structure would ever be expected to withstand, it makes good sense, from a behavioral point of view, to consider such large displace-

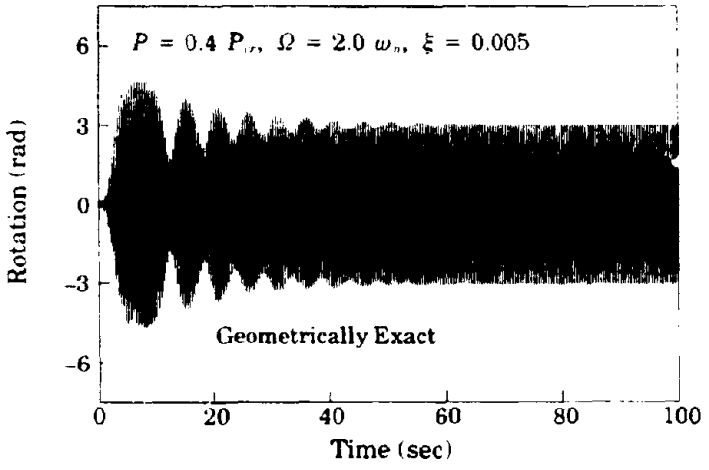

Figure 25 - Effects of damping on nonlinear, elastic analysis

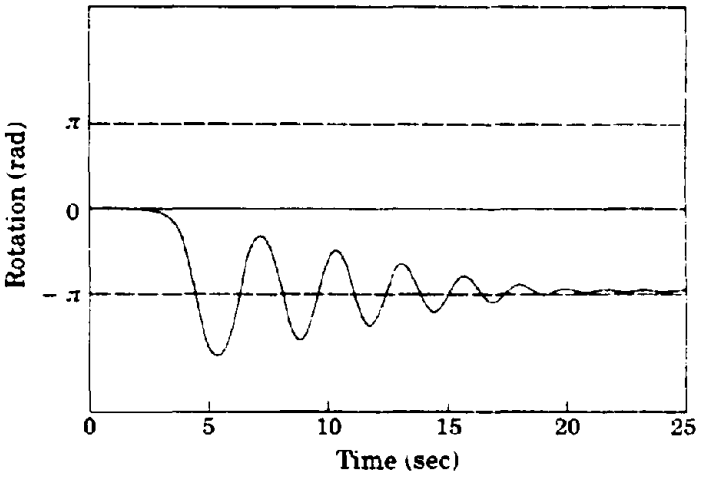

Figure 26 - System *not* considered to be a case of dynamic instability

ments. Only in this position does the axial load stabilize the motion in the sense that the system will oscillate about the configuration $\theta = \pm \pi$ (see Figure 26). Had a smaller limit been chosen, this condition would not hold. This limit is appropriate especially in light of the response indicated by the static stability bifurcation diagram (see Figure 3). For the static system, after the buckling load is exceeded, increased axial load will cause the system to tend toward the configuration $\theta = \pm \pi$. Therefore, we are simply applying Lyapunov's stability criterion for this particular dynamic system. From this point forward, we will be most concerned with loss of stability in the dynamical sense.

Exact Geometry and Nonlinear Material Properties. It is quite reasonable to assume that inelastic material response will occur in a system undergoing large deformations. When nonlinear material properties are included, the model will be more representative of a real structural material (*e.g.*, steel). Especially recently, there has been a sizeable amount of effort devoted to understanding the

behavior and stability characteristics of dynamical systems that have an elastic-plastic material model (Bernal 1987, Jones and Reis 1980, Karagiozova and Jones 1992, Yue and Zheng 1992, Newmark and Hall 1982, Maier and Perego 1992, Capecchi 1993, MacRae 1994). In fact, many researchers have made their observations and conclusions based upon a simple structure similar to the one presented here. However, most researchers have simplified the geometry of the problem to the linear case. As shown above, using linearized geometry can be helpful in determining some possible regions of instability, but the linearized model cannot give an accurate representation of the system once the rotations have become large.

The fact remains that we have no clear-cut measure that can accurately predict whether a given set of model parameters will lead to large or small rotations once inelastic material response occurs. Although it is challenging even for the elastic case, the results will show that it is almost impossible to predict the results of the nonlinear system based simply on the input parameters. In fact, under some circumstances, the elastic case is a poor predictor of the inelastic model whereas under other circumstances, it can serve as a good predictor.

Consider first some of the results that one might expect once inelastic material properties are included. We will initially concentrate on the elastic-plastic model. Doing so will allow a comparison of our results to those of previous studies. For this system, we would expect the maximum rotation to increase with increasing axial load. Results show, however, that this relationship does not always exist. The correlation between the maximum displacement and axial load is shown in Figure 27. Clearly, when the driving frequency is twice the natural frequency, the value of the maximum displacement is nearly the same for all axial loads. Additionally, we would expect that the displacements would be the largest for the fre-

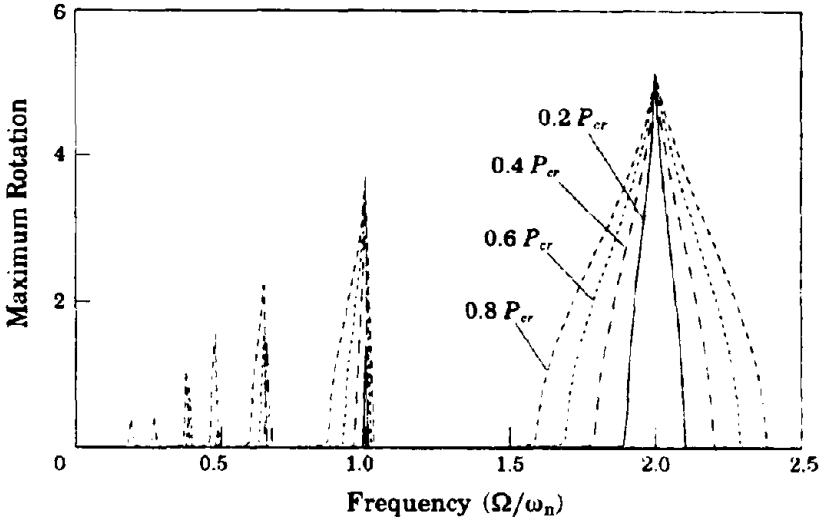

Figure 27 - Effect of axial load magnitude on maximum displacement for elastic-plastic model

quencies that correspond to the regions of instability in Figure 20. The instability regions indicate the system properties that lead to large displacements. Since yielding in the system will not occur unless the displacements exceed a certain level, and since once yielding occurs the displacements will become large, we can see that the elastic model provides a good estimate of the stability regions for the case where the material is elastic-plastic.

Figure 20 shows for the linear-elastic case that the primary region of instability occurs when the frequency of the axial load is twice the natural frequency of the system. Instability under these circumstances will occur for any magnitude of the axial load greater than zero. The next region of instability occurs when the axial load frequency is equal to that of the natural frequency of the system. However, under these conditions, instability will occur only if the magnitude of the axial load is greater than approximately 40% that of the static buckling load. It is these two regions that are of primary interest in the material that follows. In par-

ticular, we will be focusing on the following four pairs of driving frequency and axial load magnitude:

1. Axial load frequency is twice the natural frequency and the magnitude is 80% of the static buckling load;
2. Axial load frequency is twice the natural frequency and the magnitude is 50% of the static buckling load;
3. Axial load frequency is equal to the natural frequency and the magnitude is 80% of the static buckling load;
4. Axial load frequency is equal to the natural frequency and the magnitude is 50% of the static buckling load.

Understanding these four cases will improve our understanding of the system and contribute to our ability to recognize general trends in the response of this structure. Just as the linear-elastic case served as a good starting point in trying to understand the significance of including nonlinear geometry in our formulation of the problem, these test cases will help form the foundation of our understanding of the significance of including nonlinear material properties.

Let us first examine the behavior of these four cases when the material responds elastically. Figure 28 shows the displacement versus time for these test cases. Besides those differences mentioned above, all other parameters are the same for each test case (*i.e.*, there is no damping, each system starts from rest, *etc.*). Although the exact dependence of the response on the driving force amplitude and frequency is not clear, one can observe some interesting facets of behavior regarding Figure 28. First, the number of beats increases as the axial load increases. Second, the number of beats increases when the applied frequency of the axial load increases. The occurrence of more beats implies that the duration of an individual beat decreases with increasing axial load magnitude and driving frequency. Hence, each individual beat builds up and dissipates more rapidly under

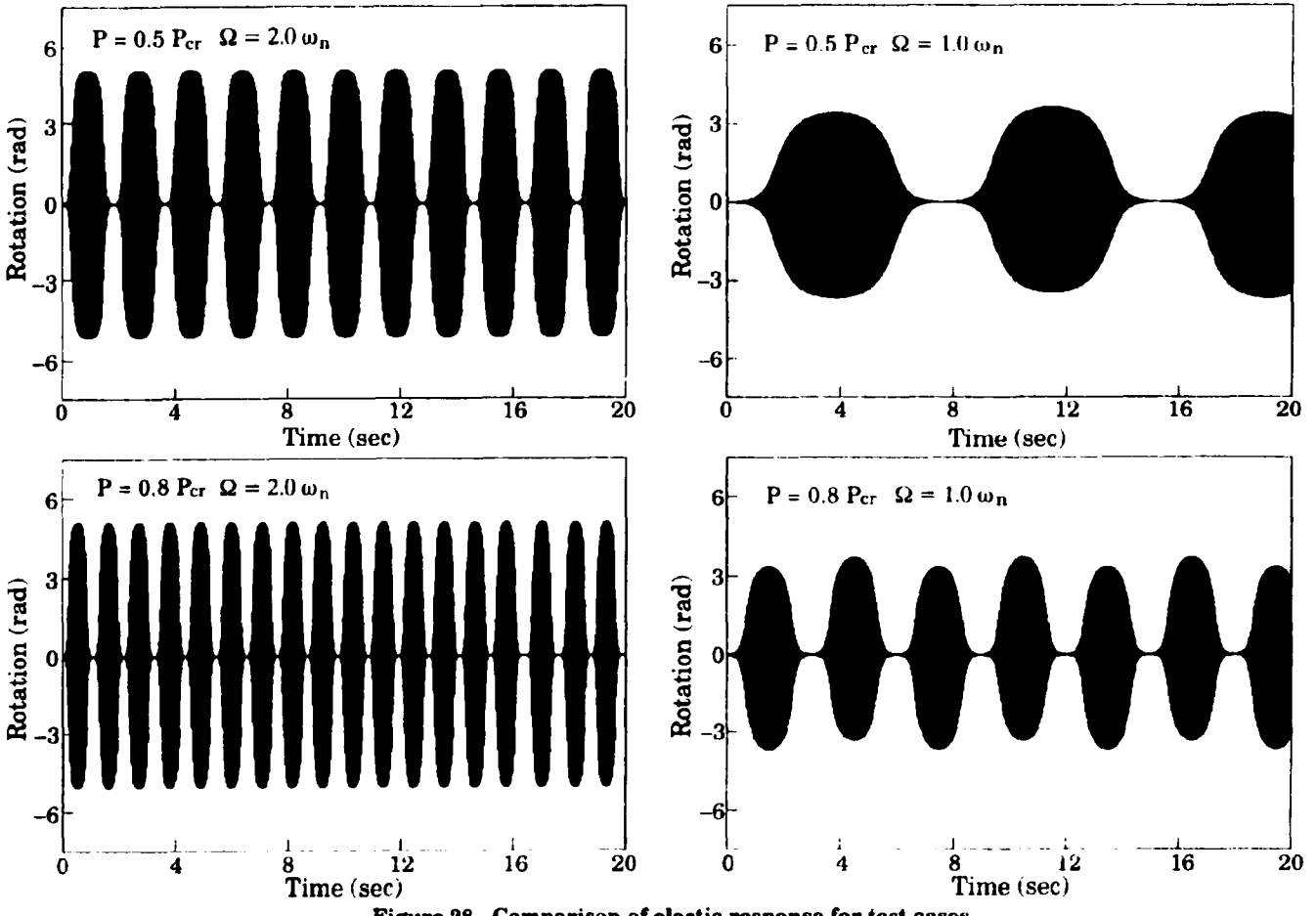

Figure 28 - Comparison of elastic response for test cases

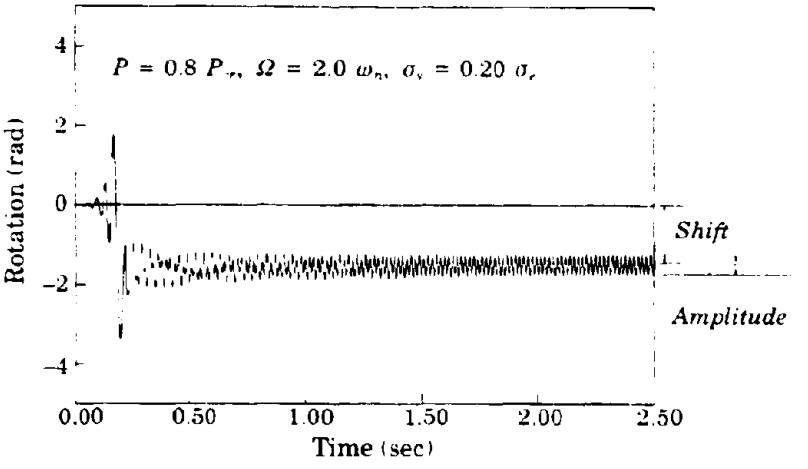

Figure 29 - Shift and steady state amplitude after yielding

these conditions. This property is very important. Its significance will be explained below.

We can characterize the inelastic response of the system with three quantities — the maximum rotation, the *displacement shift*, and the *steady state amplitude* after yielding occurs. The displacement shift and steady state amplitude are defined pictorially in Figure 29. Figure 30 also shows these two quantities but on a plot of the spring moment versus the rotation using the Ramberg-Osgood material model. Although not shown, these values are defined the same way for the elastoplastic model.

Figure 31 shows a comparison between the results obtained using the elastic-plastic material model and the Ramberg-Osgood material model. Results are shown for two different hardening exponents. For $n = 25$, the Ramberg-Osgood equation models a material with essentially no hardening. A plot of the stress versus the strain looks almost like that of the elastic-plastic model with the exception that the transition from the elastic state to the plastic state does not occur at a

sharp corner (see Figure 32). For $n = 9$, the Ramberg-Osgood equation more accurately models a material that strain hardens. Figure 11 shows the response of a material with a hardening exponent $n = 9$. The results for $n = 25$ have been included in Figure 31 in order to compare the results obtained using the elastoplastic model.

As one can clearly see, when $n = 25$, there is very good agreement between the elastic-plastic model and the Ramberg-Osgood model. The slight differences between the two are attributed to the fact that the transition from the elastic state to the plastic state is much smoother for the Ramberg-Osgood material model. The right hand portion of the figure is consistent with the model presented in Chapter 2 to model a material that strain hardens (*e.g.*, structural steel). As one would expect, the results obtained from the elastic-plastic material model are much different from those obtained using the Ramberg-Osgood model with hardening. Historically, the elastic-plastic constitutive relationship has been employed because it is assumed that the elastic-plastic model *conservatively* esti-

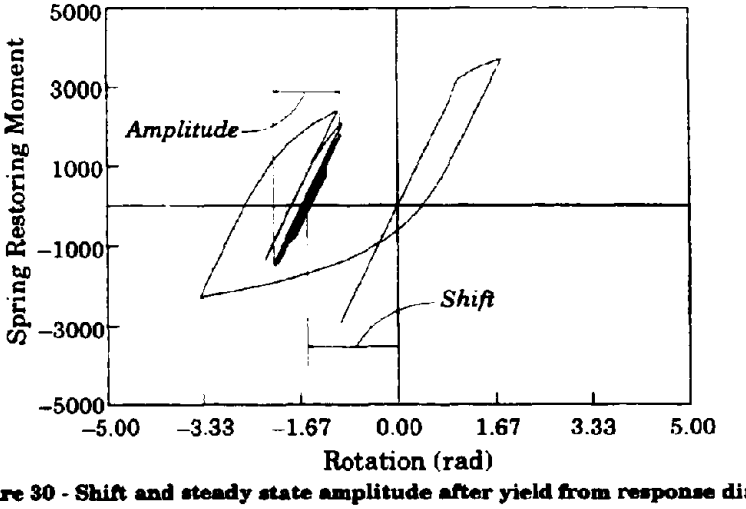

Figure 30 - Shift and steady state amplitude after yield from response diagram

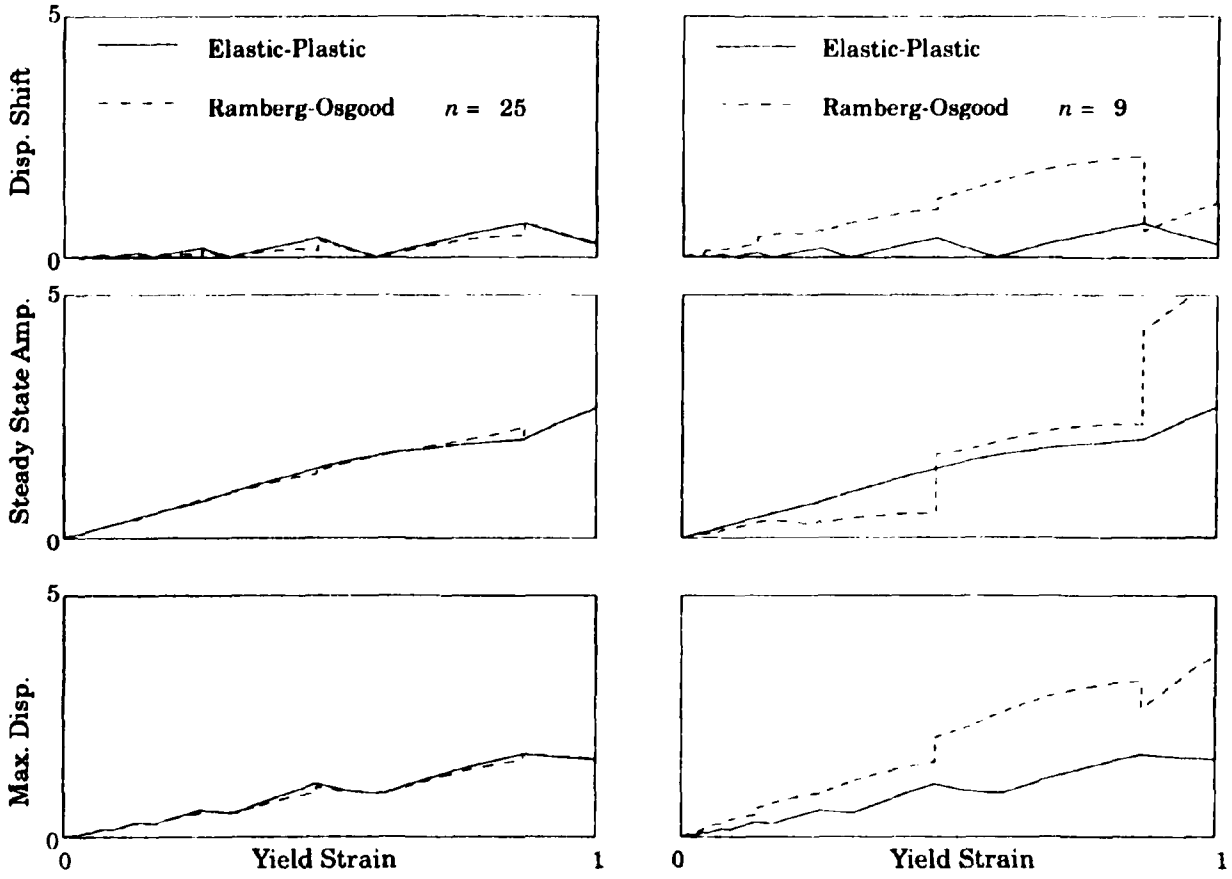

Figure 31 - Comparison between elastic-plastic and Ramberg-Osgood models

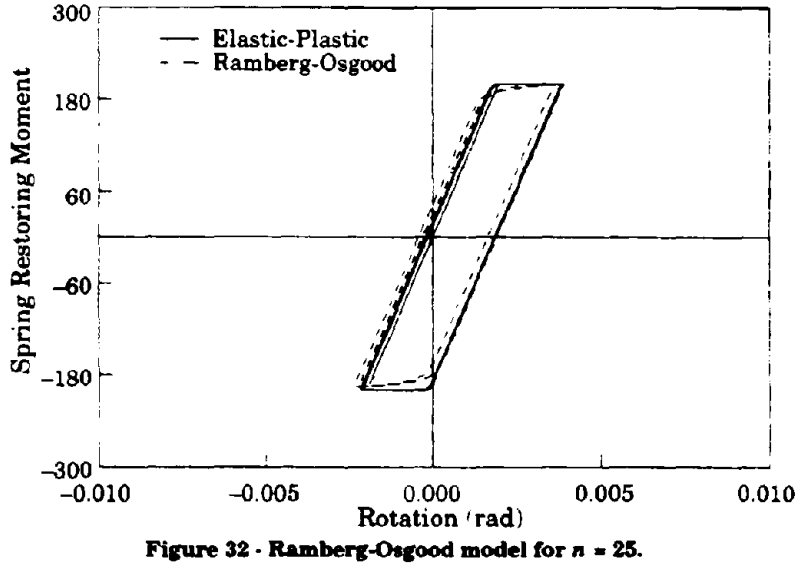

Figure 32 - Ramberg-Osgood model for $n = 25$.

mates the displacements the actual structure is likely to experience. Relative to the elastic-plastic model, the real material will strain harden, and thus, will have some reserve strength capacity that is not accounted for by the elastic-plastic model. Accordingly, the real structure *should* experience smaller displacements than those computed using the elastic-plastic model under the same loading conditions. While this observation always holds true for monotonic loading conditions, it does not necessarily hold for the case of cyclic loads. One can clearly see that these results are much different from the left hand portion of the figure.

The results have been plotted against the strain at which yielding occurs because the computed response is most sensitive to small changes in this parameter. A more in-depth discussion regarding the sensitivity of the computed results to the yield strain is included below. In addition, the reason we see large jumps in the data for the different displacement quantities is also considered below. For all yield strains considered, the maximum displacement calculated with the Ram-

berg-Osgood model is always greater than that computed using the elastic-plastic model. For the quantities of displacement shift and steady state amplitude, sometimes the elastic-plastic model gives a larger value and sometimes the Ramberg-Osgood model computes a greater value. Thus, based on these three criteria, it is clear that the choice of material model greatly affects the computed response of the structure. From the results presented above, the presence of the sharp corner in the transition regions for the elastoplastic model does not lead to significantly different behavior than for the case where this transition is smooth. However, the presence of strain hardening does lead to significantly different behavior.

For this research, each of the variables associated with the physical structure was assumed to be a parameter that could vary. Therefore, for any particular analysis, it is necessary to define the parameters that describe the physical structure (*i.e.*, the elastic stiffness, the length of the column, the magnitude of the mass, and the axial load magnitude and frequency). Some of the parameters associated with the inelastic material models though were fixed. For example, in using the cyclic Ramberg-Osgood model, only two different hardening exponents were considered – namely $n = 9$ and $n = 25$. Although it is possible for the parameter n to take on other values, different values were not considered in this research. The only parameters for the inelastic material response that could vary from analysis to analysis were the moment and rotation at which yielding occurs (these two quantities are related by the initial elastic stiffness), the maximum allowable moment capacity, and the maximum allowable rotation of the material. In this investigation, the ultimate moment and rotation capacities were set large enough so that the response of the structure would not be limited by a failure of the material.

The system response clearly depends upon the choice of parameters. Variation of each of the parameters that describes the physical structure, however, changes only the initial natural frequency of the system. Accordingly, it is possible to predict the initial elastic response of the structure by knowing the relationship between the external loads and the natural frequency of the system. Once yielding occurs, results have shown that the most important factor controlling the response is the yield strength of the system. Again, since we are not modeling any one material in particular, the yield strain is a parameter that is allowed to vary. Because the analyses did not account for the possibility of failure of the material, it is clear why the rotation at which yielding occurs is the most important parameter controlling the inelastic response of the structure.

Intuitively, one might anticipate that the lower the yield strength of the system, the greater the magnitude of response. Thus, given two systems with equal stiffness, one would expect that the system that yields first to experience a greater rotation or displacement. For both material models considered, however, it is interesting to note that the maximum response decreases with decreasing yield strain. This result is the opposite of what one would expect under monotonic or static loading conditions. For dynamic loadings with inelastic material response, the maximum displacement *increases* with increasing yield strain. Therefore, we see that information obtained from static loading conditions may not provide a good indication of the dynamic stability properties of an inelastic system.

Figure 33 through Figure 40 compare the results for the four different test cases considering different yield strengths and the Ramberg-Osgood material model. The percentage of the yield strength plotted as the abscissa in these eight figures is based upon the yield strength required to keep the system elastic when the axial load is $0.8P_{cr}$. When the applied axial load magnitude is only $0.5P_{cr}$, the

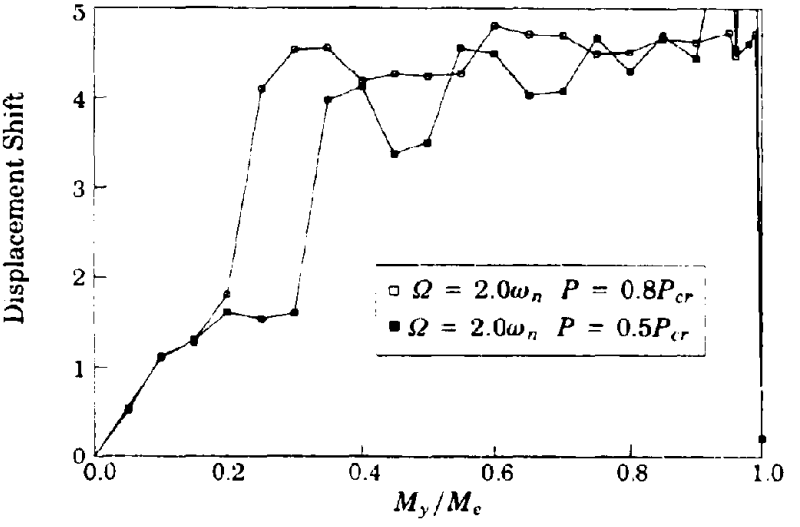

Figure 33 - Displacement shift as a function of yield strength

system does not require as much strength to remain elastic. Consequently, this would explain why the system response for the case of the lower axial load levels off at what appears to be a value less than that required for elastic response. Put another way, the results have been normalized against the case where the axial load is $0.8P_{cr}$.

Looking at Figure 33 through Figure 40, we immediately notice the large variability in the data. Furthermore, we see large jumps in the displacement shift for relatively small differences in the yield strength of the system. Reexamining Figure 28 may help to explain why this occurs. When the yield strength is less than a certain value, yielding will occur before the displacements have had a chance to grow very large. However, if the yield strength is higher, the system will remain elastic longer. Consequently, the displacement at the time of yield will be greater, thereby causing the displacement shift to be larger (see Figure 41). This effect is greatest at the beginning portion of the beat when the rate of change of the rotations is greatest. Toward the middle portion of the beat, the rate of change

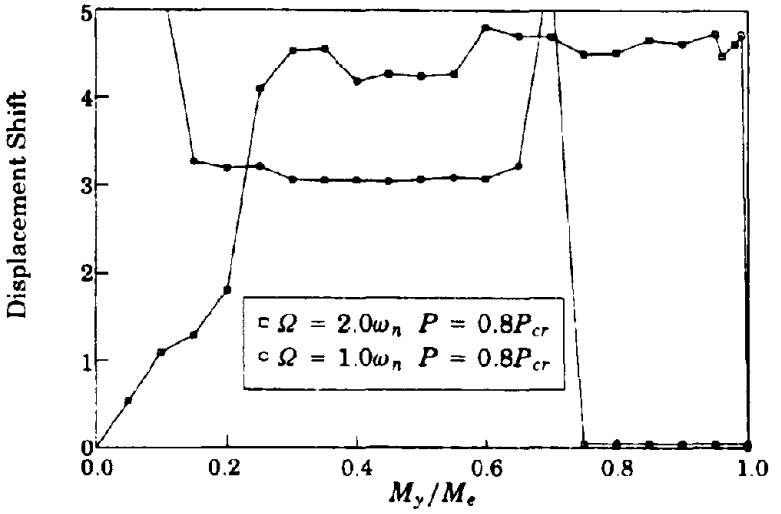

Figure 34 - Displacement shift as a function of yield strength

of rotations is relatively small (the amplitude remains essentially unchanged over this time period), and the differences in the displacement shift are much smaller. The relatively flat portion of the beat corresponds directly to the relatively

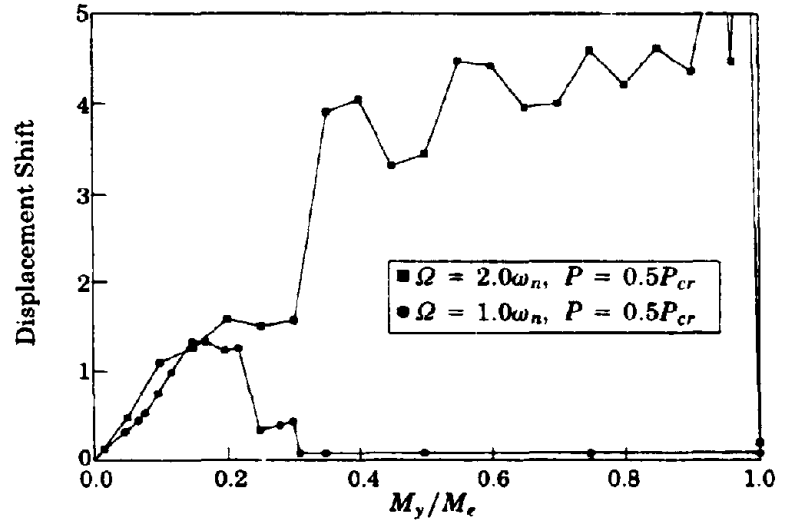

Figure 35 - Displacement shift as a function of yield strength

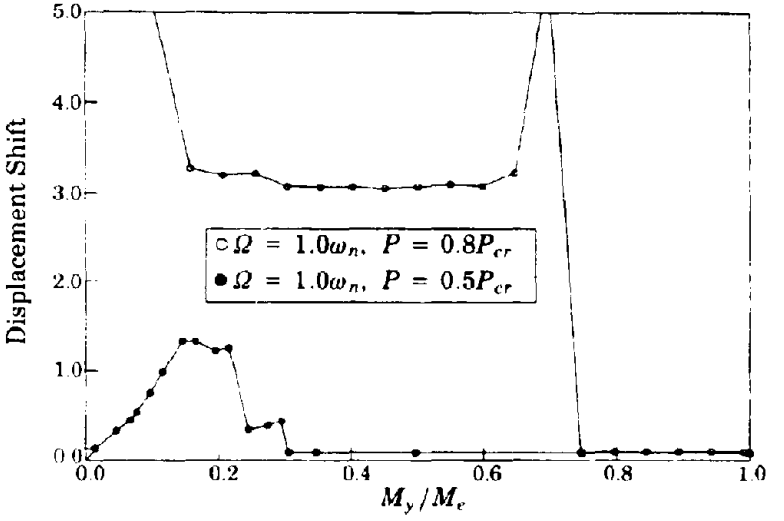

Figure 36 - Displacement shift as a function of yield strength

constant portion of the curves in Figure 33 through Figure 36. These results help illustrate why the rate at which the beats build up and dissipate for the elastic case is significant.

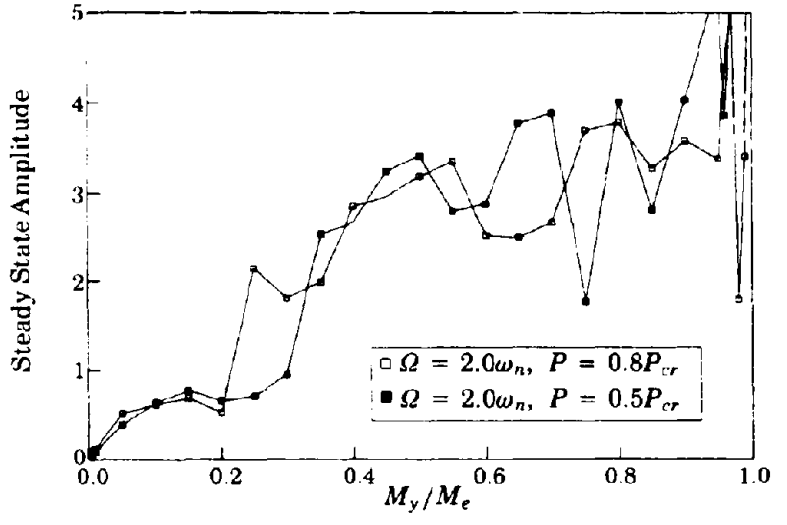

Figure 37 - Steady state amplitude as a function of yield strength

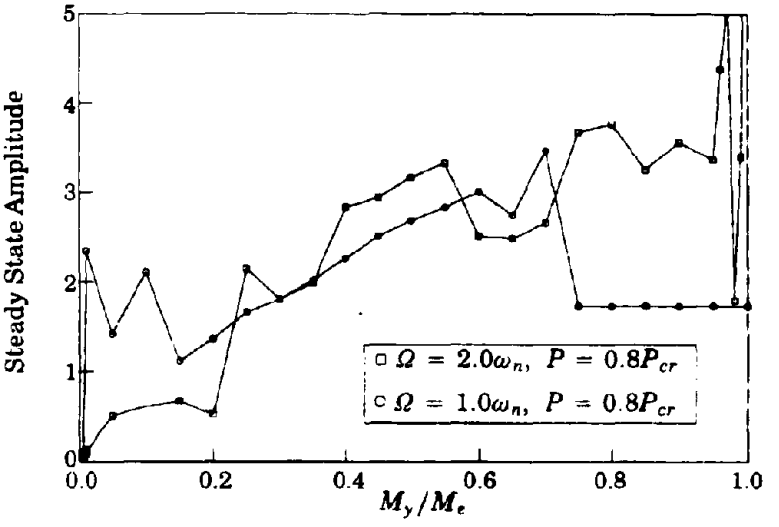

Figure 38 - Steady state amplitude as a function of yield strength

Also, with few exceptions, the motion subsequent to yielding remains elastic. For most of the cases considered, when yielding occurs, there is a large nonlinear excursion followed by motion that remains bounded within the new yield surface

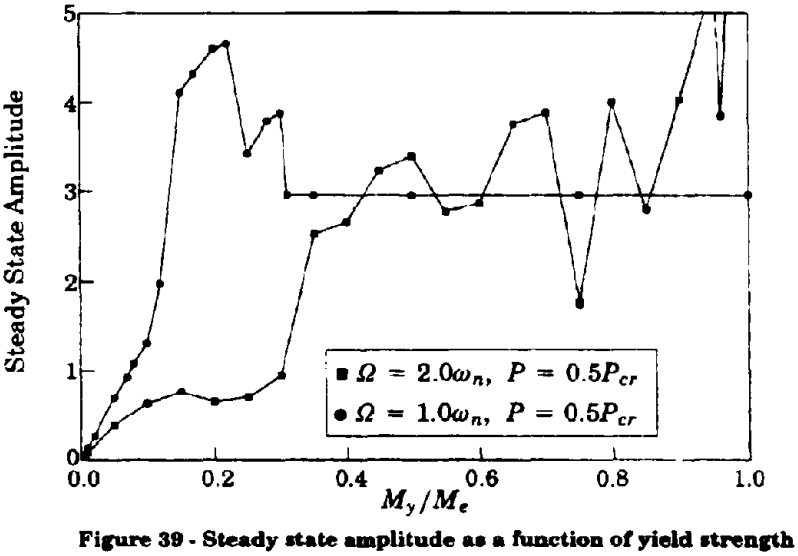

Figure 39 - Steady state amplitude as a function of yield strength

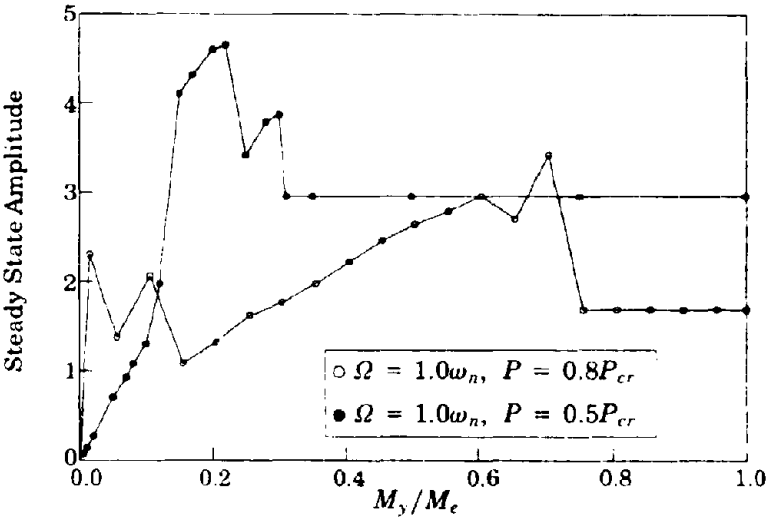

Figure 40 - Steady state amplitude as a function of yield strength

without beating (Figure 29). Although there are some exceptions, this type of response is the general trend. Therefore, we witness a steady state response after yielding for much the same reason we did before when we considered the elastic system with damping. Yielding of the material dissipates the energy of the system as does damping. Thus, the transient portion of the response no longer plays as

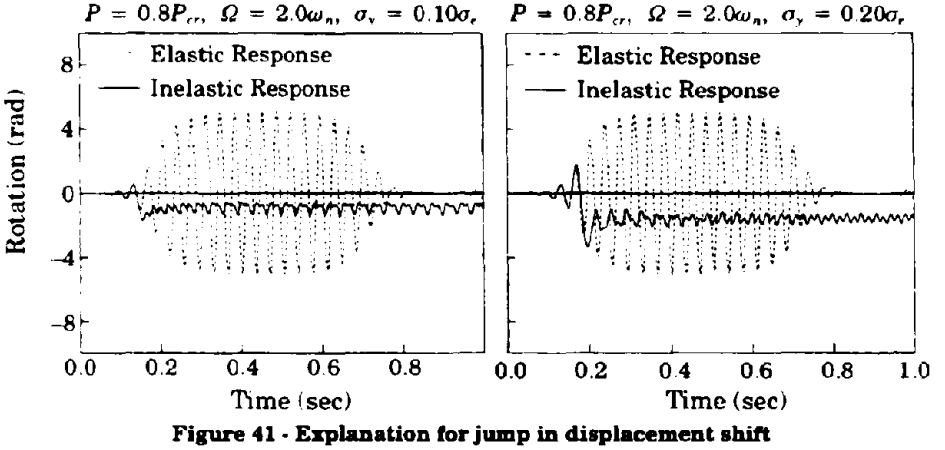

Figure 41 - Explanation for jump in displacement shift

important a role in the behavior of the system once yielding takes place. Furthermore, after a large yield excursion, the nature of the system changes, and the frequency of the axial load does not excite the system in the same way it did before yielding occurred.

Another interesting facet of behavior we see in studying Figure 33 through Figure 40 is that there does not appear to be an "almost elastic" system (see Figure 42). That is, we see that the displacement shift and amplitude of the steady state motion are large for values of yield strength that are very close to the strength required to prevent yielding. The reason we see such large displacements under these circumstances can best be explained from a total energy perspective. Sun, Berg, and Hanson (1973) used this approach for their study of the free vibration of elastoplastic systems. Initially, based upon its properties, the system is capable of dissipating a certain amount of energy. Systems that experience large rotations are more efficient at capturing energy from the external forces. Oscillations occur because of the exchange of strain energy and kinetic energy with

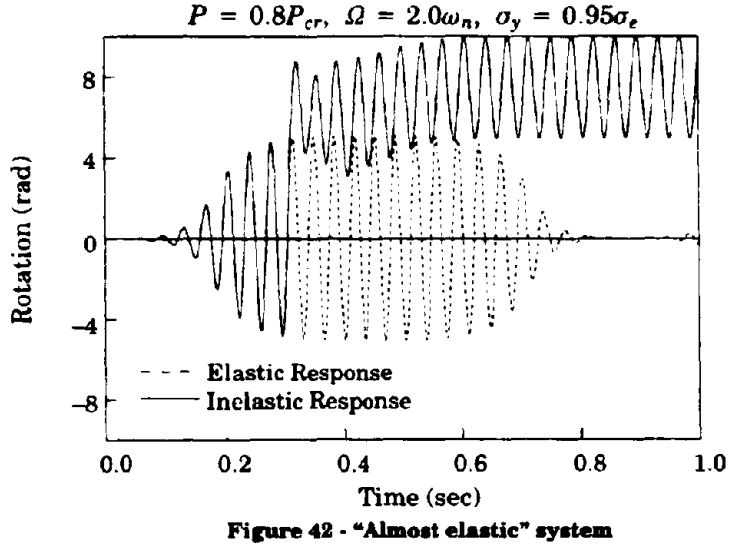

Figure 42 - "Almost elastic" system

a balance to total *captured* energy. Yielding dissipates captured energy. In the case of the "almost elastic" system, prior to yielding, there is a large build-up of kinetic energy. Once yielding occurs, the system can only dissipate energy in accord with the energy available to dissipate. Consequently, unlike before, the restoring forces are not sufficient to arrest the motion of the system.

Now consider the system behavior for very small yield strengths (*e.g.*, $< 25\%\ M_0$) and an axial load magnitude of $0.8P_{cr}$. Thus, the main focus here is to examine the differences in the behavior of the system for the following two situations with all other properties being the same: (1) the frequency of the axial load is twice the natural frequency; and (2) the frequency of the axial load is equal to the natural frequency. These frequencies correspond to the first two critical regions of Figure 20. Figure 34 shows a dramatic difference in the behavior of the system for these two cases. When the driving frequency is twice the natural frequency, if the yield strength of the system is continually lowered, one notes that the displacement shift and the rotation of the system also become smaller and smaller. Therefore, one could say that lowering the yield strength causes the system to tend toward a more favorable configuration. On the other hand, when the driving frequency is equal to the natural frequency, the opposite effect occurs. Thus, as the yield strength of the system is lowered, the displacement shift grows and grows to a very large value. Consequently, one might say that lowering the yield strength under these circumstances causes the system to tend toward a less favorable configuration. What is quite peculiar about these results is that they do not occur when the axial load magnitude is decreased to $0.5P_{cr}$ (see Figure 35). That is, for either frequency considered, lowering the yield strength of the system tends to decrease the magnitude of the rotation of the system. These observations

alone give a good indication why it is so difficult to discern trends in the behavior of this system.

Another interesting observation worth noting is that for all four test cases considered, the steady state amplitude following yielding in the spring, in general, increases with increasing yield strength. Initially, at low yield strengths, the amplitude is less than that for the elastic case. With increasing yield strength though, the steady state amplitude continues to grow, and it eventually exceeds the amplitude observed for the elastic case. Thus, provided any magnitude displacement shift can be tolerated, systems with yield strengths much lower than that required to keep the system elastic will display steady state oscillations smaller than the system would undergo if the spring did not yield. However, systems with yield strengths of intermediate value will display steady state oscillations that are larger in magnitude than those of the elastic case.

Lastly, another intriguing result to consider is that under some circumstances, the magnitude of the axial load does not greatly affect the maximum response of the system. For other conditions though, it does seem to have an important effect. To illustrate, when the driving frequency is twice the natural frequency, there is little difference in the size of the displacement shift for either axial load magnitude considered (see Figure 33). This result contradicts our intuition concerning the relationship between displacement and axial load. Contrary to this observation, when the driving frequency is equal to the natural frequency, we see that the results are more in line with what is expected (see Figure 36). That is, the rotations are smaller when the axial load is smaller.

Dynamic Response with Base Excitation

In the beginning part of this chapter, we discussed that even though the linear-elastic model may not provide a good indication of the true structural response, it does furnish valuable insight regarding the nature of the system. Analyzing the system with assumed linear-elastic behavior points out potential regions of instability. Initially, if it is assumed that the lateral ground motion is sinusoidal, the axial load is constant with time, and the system is undamped, then the linear-elastic analysis indicates only one region of instability – the case in which the frequency of the lateral ground motion is close to the natural frequency of the structure. Of course, from Eq. (27), it is noted that the natural frequency of the structure is dependent upon the axial load. Specifically, the natural frequency of the system is computed from the relationship

$$\omega_n = \sqrt{\frac{1}{m\ell}\left(\frac{k}{\ell} - P\right)} \tag{65}$$

Since the static buckling load occurs when the natural frequency of the system is equal to zero, Eq. (65) confirms that $P_E = k/\ell$.

In the previous sections, for a sinusoidally varying axial load, we found that the most important parameter affecting the dynamic stability properties of the inelastic system is the value at which yielding occurs. Although other factors have a strong influence on the computed results, it is the yield strength that is the most influential. In this section of the chapter, we are interested in determining whether or not the results obtained for the pulsing axial load correspond to this different load case of lateral base excitation Accordingly, we could go through the same procedure as above for the other load case. Without needlessly including this preliminary material, we find again that, for the case of laterally base-excited structures, the yield strength is the parameter for which small variations lead to significant

changes in the computed response. The response of the SDOF model to a sinusoidal lateral base excitation is summarized in Figure 43.

Similar to our previous results, Figure 43 indicates that the maximum displacement increases with increasing yield strength. Furthermore, these results also show that, once yielding occurs, the magnitude of the axial load does not impact the results as greatly as it would for an elastic system. Thus, one may conclude that high strength can be detrimental to the dynamic stability of the system, and it is more important to have greater ductility than greater strength. When the system has a relatively large strength, the displacements become fairly large before yielding occurs. It is the P-Δ effect of the axial loads acting through these large displacements that leads to the dynamic instability. If the system is allowed to yield earlier, then the displacements will remain small, and the system will remain stable. From the results presented in Figure 43, we see that the nature of the response for the two different loading cases is similar, and the trends

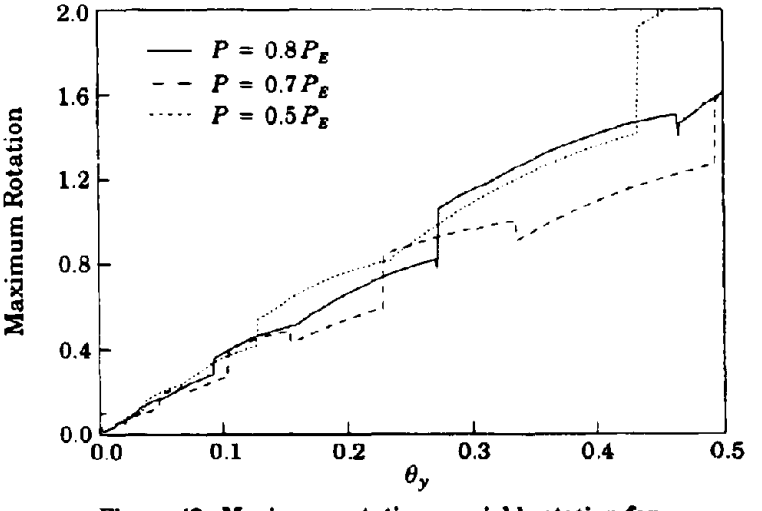

Figure 43 - Maximum rotation vs. yield rotation for sinusoidal lateral ground motion

in the results described previously also hold for the case of laterally base-excited systems.

Stability of Systems with 2-DOF

Although the single degree-of-freedom system that has been considered up until this point has provided us with some insight into dynamic stability problems, the extension to multiple degree-of-freedom problems is essential. All real structural systems consist of many degrees of freedom, and it is important to study the dynamic stability characteristics of such systems.

In the preceding chapter, the governing equations of motion for the 2-DOF model were presented. Recall that the terms in the equations of motion for each mass are nonlinear and coupled. Also, note that the damping matrix is non-zero even in the absence of velocity proportional damping. Furthermore, the mass matrix is *not* diagonal as it normally would be in the case of the linearized analysis. Unlike the typical linear-elastic analysis of MDOF systems, the system here cannot be easily uncoupled into the solution of of two SDOF systems. Because of the general form of the governing differential equations, previous studies into the behavior of MDOF systems have been sparse (Kalathas and Kounadis 1991).

In order to gain further insight on the dynamic stability properties of this 2-DOF system, four basic situations are considered: (1) the bottom spring is stiffer than the top spring; (2) the top spring is stiffer than the bottom spring; (3) both springs have equal stiffness; and (4) the spring properties vary so that yielding in both springs occurs at approximately the same time. Clearly, each one of these situations comprises many individual examples. The number of free parameters for this problem is quite large. Including an additional member with an added degree-of-freedom not only introduces twice the number of variables, but it more

than doubles the complexity of the problem because one must also consider various combinations of these parameters. Thus, in order to *quantitatively* describe which parameters and which combination of parameters most significantly impact the results as we did for the SDOF system, an excessively large number of analyses would be required. In order to avoid this situation, in this section, we will study the response of the MDOF structure by means of a few examples that fall into each of the four situations described above. Of course, this will just give us an overall indication or a *qualitative* indication of the behavior of this 2-DOF model.

Bottom spring stiffer than the top spring. Certainly, if the bottom spring is much stiffer than the top spring, then, in the limit as the stiffness of the bottom spring approaches infinity, the top member responds like the SDOF system studied earlier. Therefore, under these circumstances, results obtained previously can be used to ascertain the stability characteristics of the system. Figure 44 shows the response of the top member of the 2-DOF system for different ratios of spring stiffness between the top and bottom springs. The response is shown for a sinusoidal ground motion and a constant axial load on the top member only. Aside from these differences, all other parameters were assumed equal for the two members.

Certainly, Figure 44 indicates that when the spring stiffness of the bottom spring is much larger than that of the top spring, the response of the top member is very well approximated as a SDOF system. Even as the relative difference in spring stiffness between the two members becomes smaller, the SDOF response gives a reasonably good estimate of the response of the top member. Physically, as the stiffnesses of each of the springs become more similar, we would not expect the MDOF system to behave identically like the SDOF system. When the stiffness

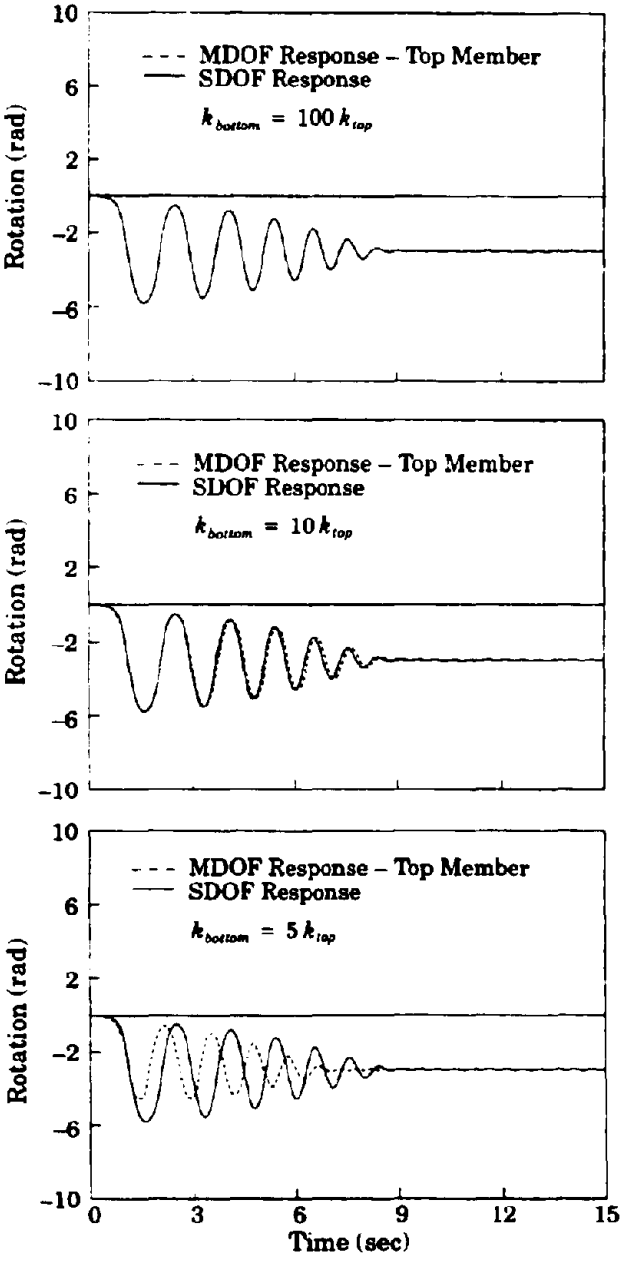

Figure 44 - Comparison of SDOF response to MDOF response for different spring stiffnesses

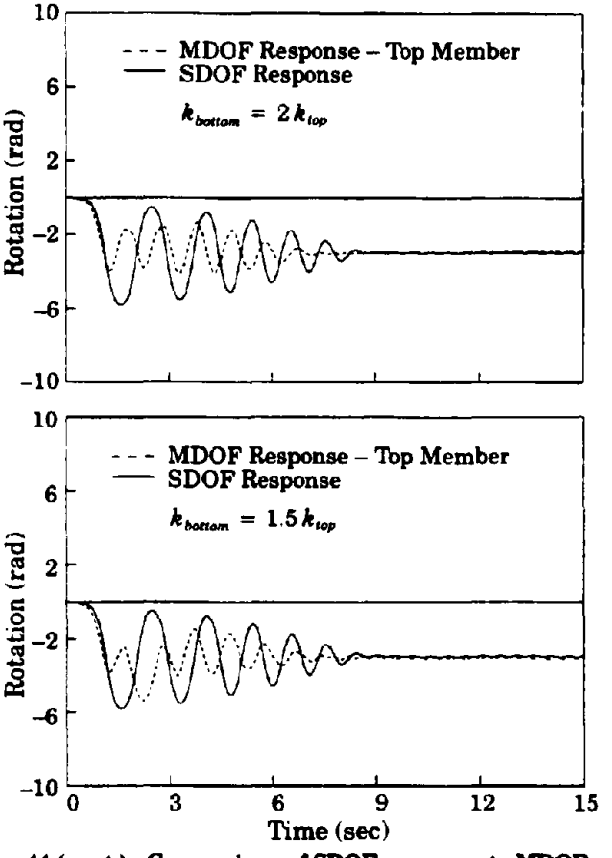

Figure 44 (cont.) - Comparison of SDOF response to MDOF response for different spring stiffnesses

of the lower spring is decreased, the bottom member begins to undergo larger displacements. Thus, because the motion of the two members is coupled, the inertia of the lower member has a greater impact on the top member. Even though the responses are not exact, both systems realize the same pathway to instability. Thus, under these circumstances, the SDOF system gives a good indication of the type of response we can expect for the MDOF system.

Top spring stiffer than the bottom spring. Similarly to the previous case, in the limit as the stiffness of the top spring approaches infinity, there will be no relative rotation between the top and bottom members. Consequently, the response of the system should be well approximated by the SDOF system studied earlier. In making this comparison, the height of both columns for the MDOF case should be equal to the height of the the column for the SDOF system. Additionally, in order for the MDOF system to behave exactly as the SDOF system, the mass

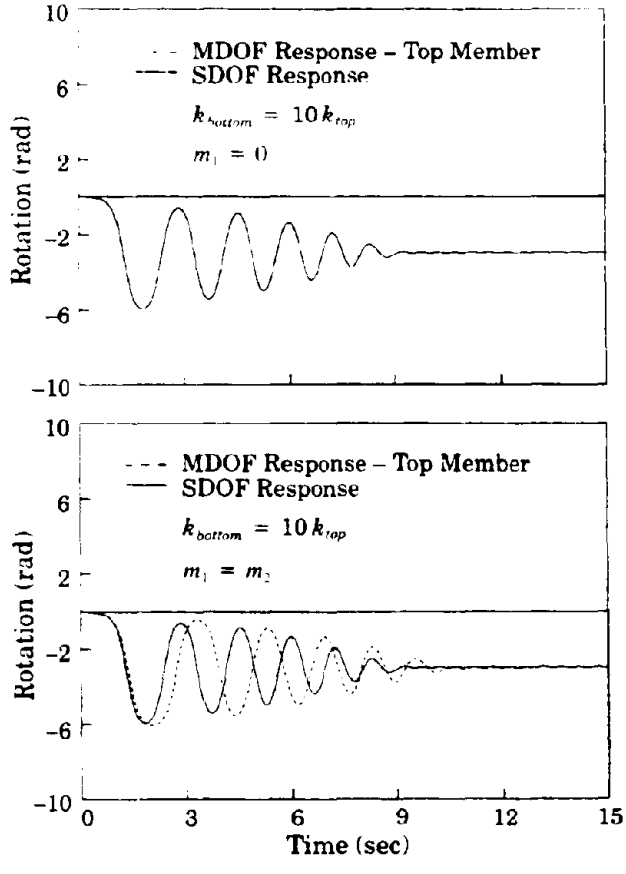

Figure 45 - Comparrison of response using different masses for m_1

on top of the lower column must be set equal to zero. Otherwise, we will not be modeling the SDOF previously studied. Instead, we will be modeling a SDOF system that has a mass both at the top of the column and at the mid-height. Figure 45 shows a comparison of the responses for assuming that the lower mass is equal to zero and for assuming that the lower mass is equal to the top mass. Because assuming both masses are equal is a more realistic assumption, it is appropriate to develop an alternate method for relating the results with the SDOF system. For the sake of comparison, it is reasonable to assume that an "equivalent" SDOF system would be one that has the same total mass as the the 2-DOF system with a column height that is equal to the height of the location of the center of mass for the 2-DOF system (see Figure 46). The responses of the system for different relative stiffnesses between the top spring and bottom spring are shown in Figure 47.

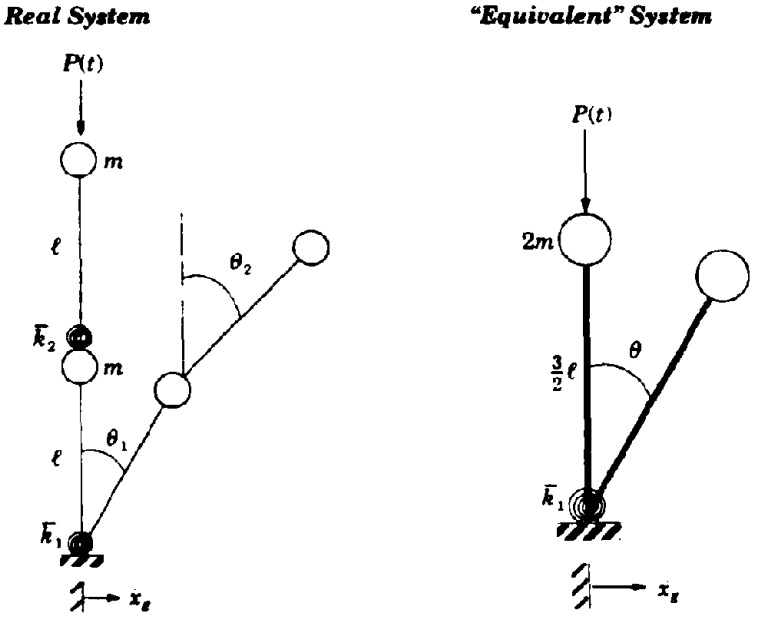

Figure 46 - "Equivalent" SDOF system

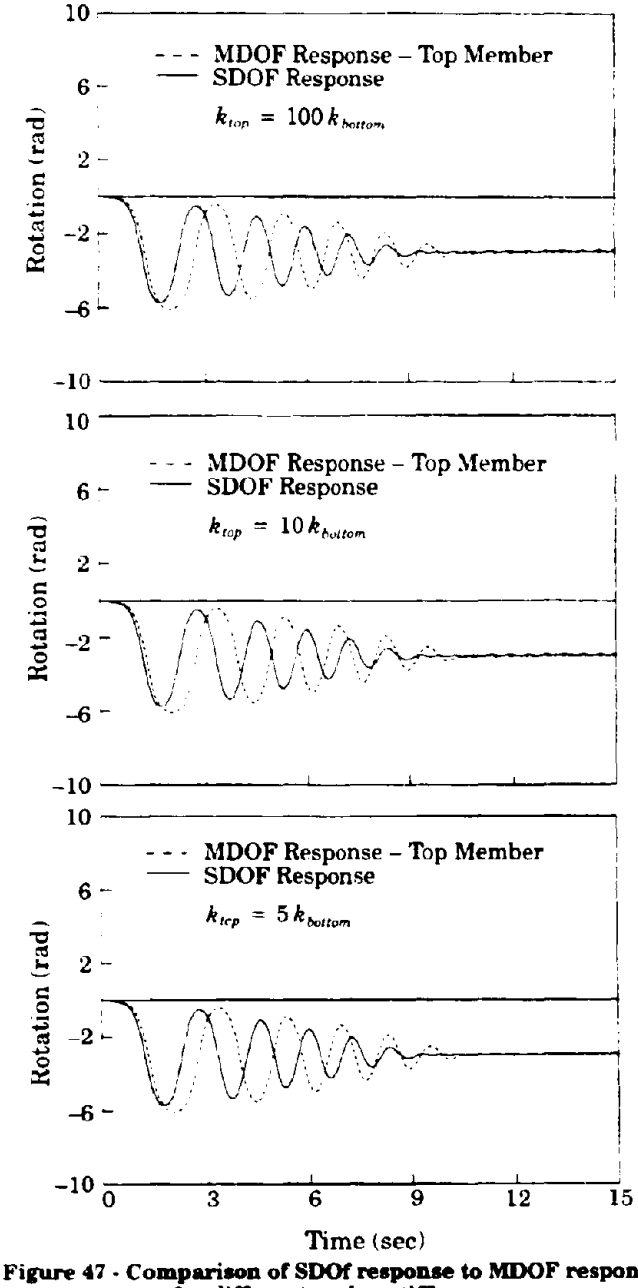

Figure 47 - Comparison of SDOf response to MDOF response for different spring stiffnesses

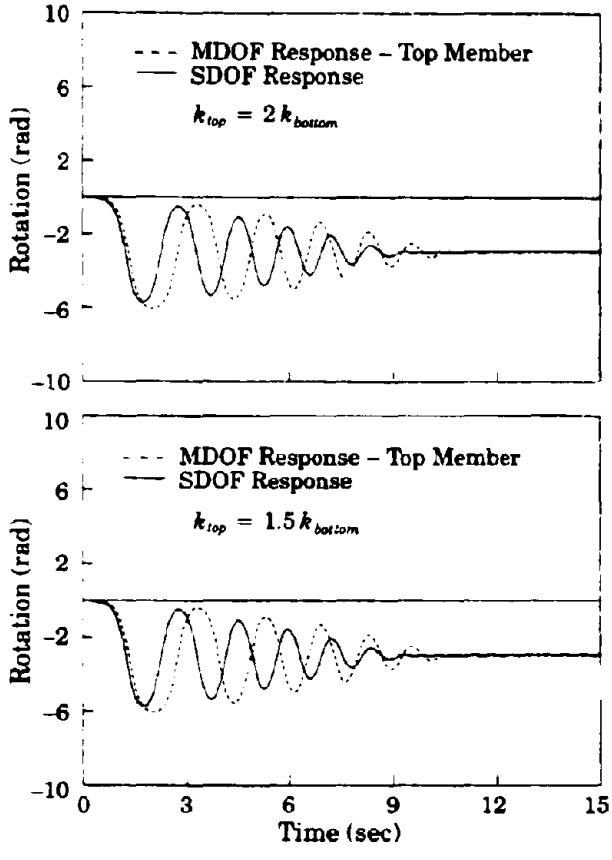

Figure 47 (cont.) - Comparison of SDOF response to MDOF response for different spring stiffnesses

The results are compared with the *equivalent* SDOF system. Once again, even though the responses are not exact, both systems realize the same pathway to instability. Thus, when the top spring is stiffer than the bottom spring, the SDOF system provides valuable insight to the type of behavior we can expect for the MDOF system.

Both members are the same. When both members share identical properties, then the structure truly responds as a multi-degree-of-freedom system. Un-

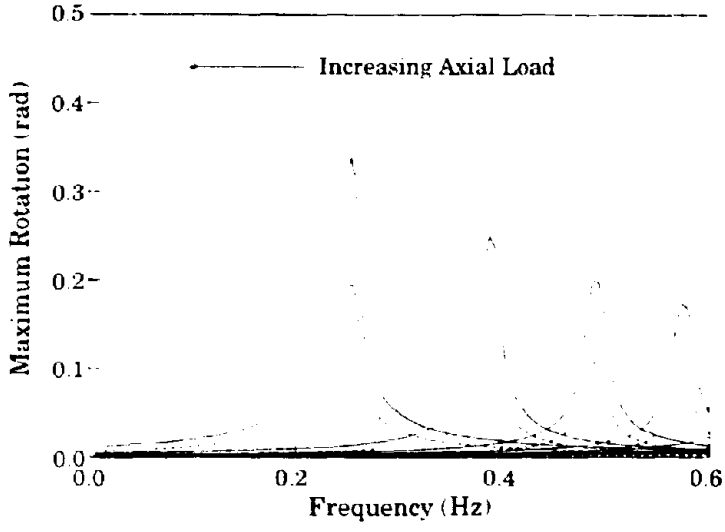

Figure 48 - Elastic response of MDOF system with identical members

der these circumstances, it may be difficult for the SDOF model to accurately predict the response of the MDOF structure. Because of this difficulty, it may be helpful to first look at the elastic response of the 2-DOF model. Figure 48 shows the elastic response of the system. In Figure 48, the dashed lines correspond to the rotation of the top member, and the solid lines correspond to the rotation of the bottom member. As one would expect, the elastic response increases with increasing axial load. The important thing to note concerning Figure 48 is that the maximum response of the top member remains bound within the response of the lower member. Therefore, the bottom member dominates the response. Comparing these results to the linearized case, this implies that the first mode or lower energy mode controls the dynamic response of the system.

The maximum response of the MDOF system including nonlinear material properties is shown in Figure 49. As the figure clearly shows, even for the inelastic

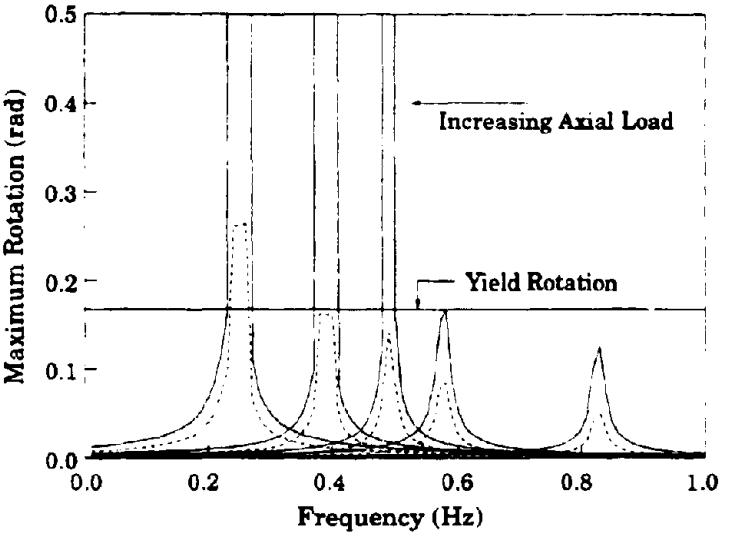

Figure 49 - Inelastic response of MDOF system with identical members

system, the bottom member dominates the response. This is true not only for the case in which the bottom spring yields and the top spring remains elastic, but it also holds for the case in which both springs yield. These results hold only when the top member yields well after the bottom member. The case in which both springs yield at approximately the same time is discussed below. Like the elastic case, Figure 49 indicates that the first mode or lower energy mode also controls the dynamic stability characteristics of the inelastic system. Furthermore, the results are very similar to those obtained earlier for the SDOF system. Thus, once again, the results obtained from the SDOF system can be used to predict the nature of the response of the MDOF system when both members are the same.

To further illustrate, the typical elastic response of the 2-DOF system is shown in Figure 50. The system is excited by a sinusoidal ground motion and a constant axial load. As Figure 50 clearly shows, the system responds primarily in the first

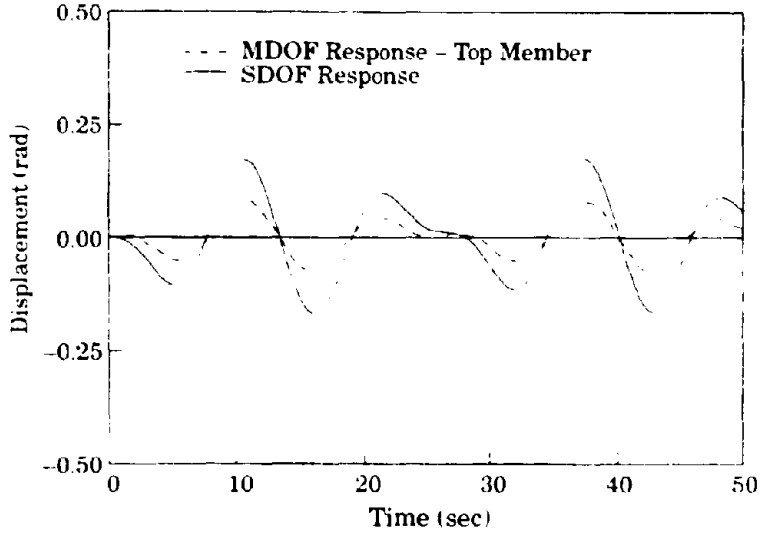

Figure 50 - Typical elastic response for 2-DOF system with identical elements

mode. Accordingly, the rotation in the lower spring always exceeds the rotation of the top spring. Consequently, if both members have the same yield strength, then the bottom spring will yield first. Should the bottom spring yield, then this helps dissipate energy. As a result, the elastic response of the top member diminishes. This phenomenon is illustrated in Figure 51. Under these circumstances, the stability of the system is governed by the response of the bottom member. Even if the top member also yields, provided the yield strength is not so small that both members yield at nearly the same time, the 2-DOF system realizes the same pathway to instability as the SDOF system. A comparison of the results between the top and bottom members of the 2-DOF system is illustrated in Figure 52. Consequently, under these circumstances, our knowledge of the stability properties of the SDOF system can be used to predict the nature of the response for the 2-DOF system.

Both Springs Yield at Approximately the Same Time. Both springs yielding at approximately the same time can occur in two different ways. First, if both

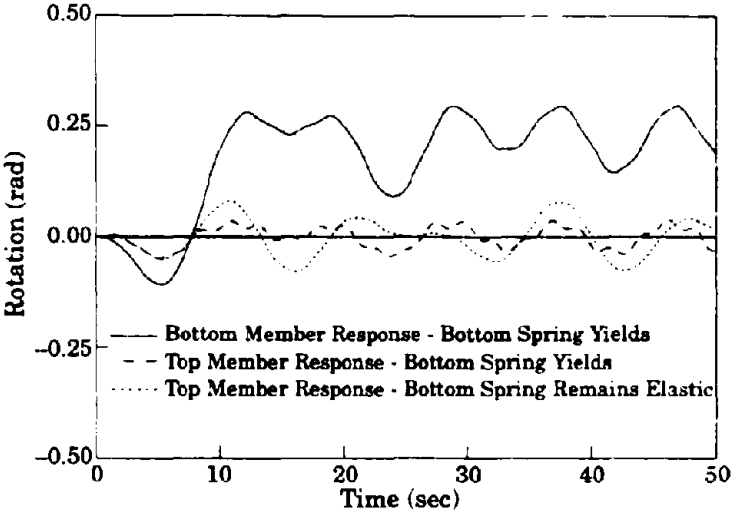

Figure 51 - Reduced elastic response of top member after bottom member yields for two identical members

members have identical properties, then both springs can yield at approximately the same time if the yield strength of each spring is small. Second, this situation

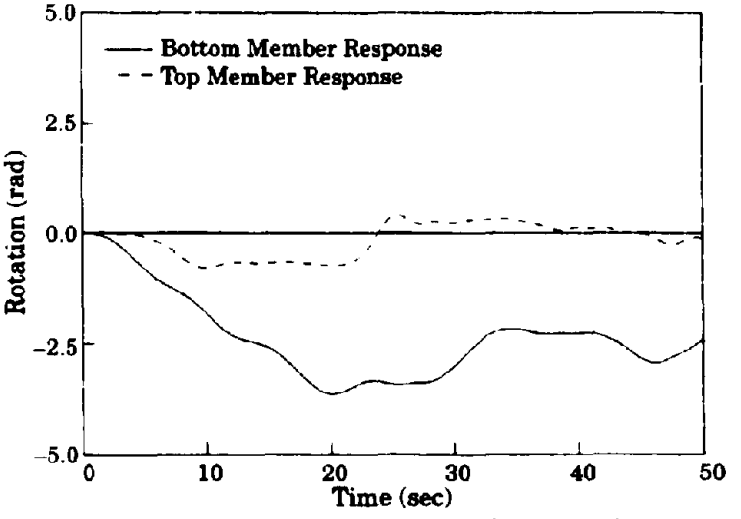

Figure 52 - Dynamic instability of 2-DOF model with two identical members. Both springs yield and response based upon Ramberg-Osgood model.

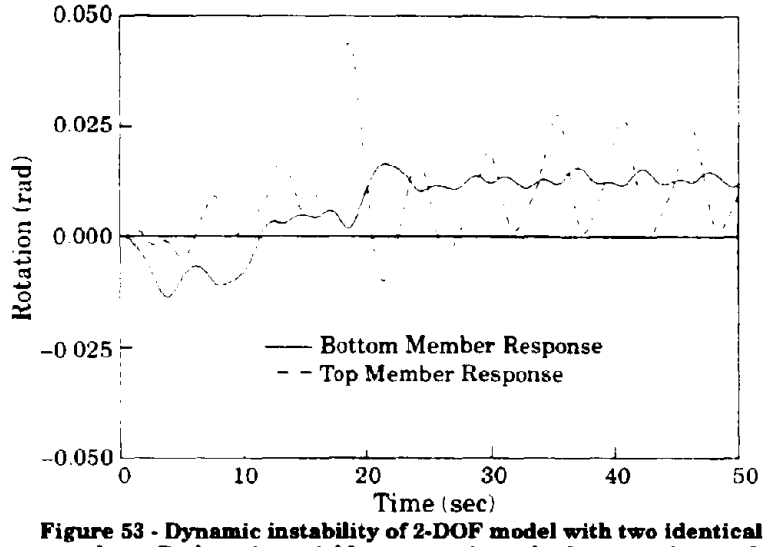

Figure 53 - Dynamic instability of 2-DOF model with two identical members. Both springs yield at approximately the same time and response based upon Ramberg-Osgood model.

may arise if the yield strength of the bottom member is relatively high and the yield strength of the top member is relatively low. Regardless of how the situation develops, the nature of the response is the same. Under these circumstances, the results from the SDOF response *cannot* be used to accurately predict the stability characteristics of the MDOF system because the response of the bottom member no longer controls the response of the entire system. For certain parameters, it is possible that the top member will undergo larger rotations than the bottom member. In addition, the system may also vibrate predominantly in the second mode. Consequently, the results obtained from the SDOF model no longer apply.

To illustrate these phenomena, we will first consider a case in which the top member response is greater than that of the bottom member. For this example, the yield strength of both members is relatively small, and yielding of both springs occurs at approximately the same time. Figure 53 shows the response of such a system. Clearly, the top member response is larger and not limited by the re-

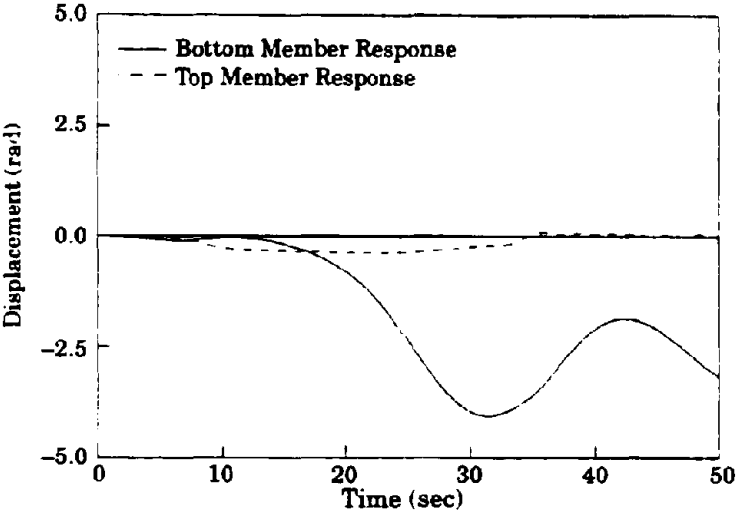

Figure 54 - Dynamic instability caused by bottom member with both members yielding at the same time using the Ramberg-Osgood model and two identical members

sponse of the bottom member. However, this situation does not always hold when both springs yield at nearly the same time. For other parameters, the response of the bottom member may be larger than that of the top member. Thus, instability in the 2-DOF system may be attributable to the top member, the bottom member, or both members when each spring yields at roughly the same time. These patterns of behavior are shown in Figure 54, Figure 55, and Figure 56 respectively.

One last phenomenon worth noting is, after yielding occurs in both springs, the system may oscillate primarily in the second mode. For the previous cases, the response of the bottom member was always in phase with the response of the top member. Figure 57 demonstrates that in-phase motion between the two members does not necessarily hold for the case in which the springs yield at nearly the same time.

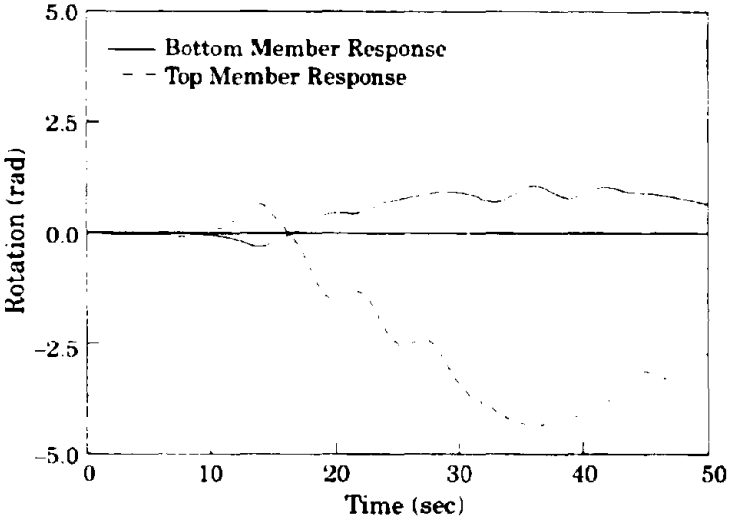

Figure 55 - Dynamic instability caused by top member with both members yielding at the same time using the ramberg-Osgood model and two identical members

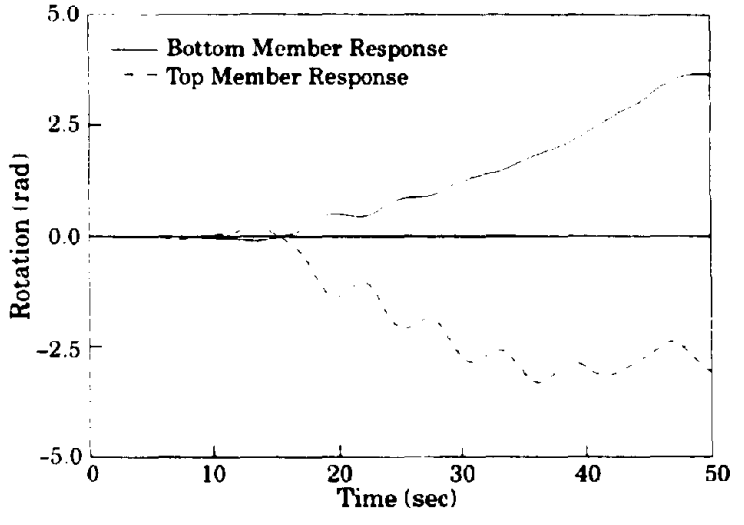

Figure 56 - Dynamic instability in both members with both members yielding at the same time using the Ramberg-Osgood model and two identical members

To summarize, for the case in which both springs yield at approximately the same time, various new patterns in behavior were observed. The type of behavior realized by the system is highly dependent upon the parameters of the system. Unfortunately, no clear relationship could be found between the parameters and the computed response. Furthermore, some of the conclusions reached earlier for the SDOF system do not hold for this particular case. For example, for the SDOF system, it was observed that lowering the yield strength of the system contributed to increased dynamic stability. This does not always hold for the case in which both springs yield at approximately the same time. Additionally, other pathways to instability exist under these conditions. That is, the top member may become dynamically unstable by itself, the bottom member may become dynamically unstable by itself, or both members may become unstable due to the coupling of their motions. Therefore, we can conclude from these results that we cannot use the re-

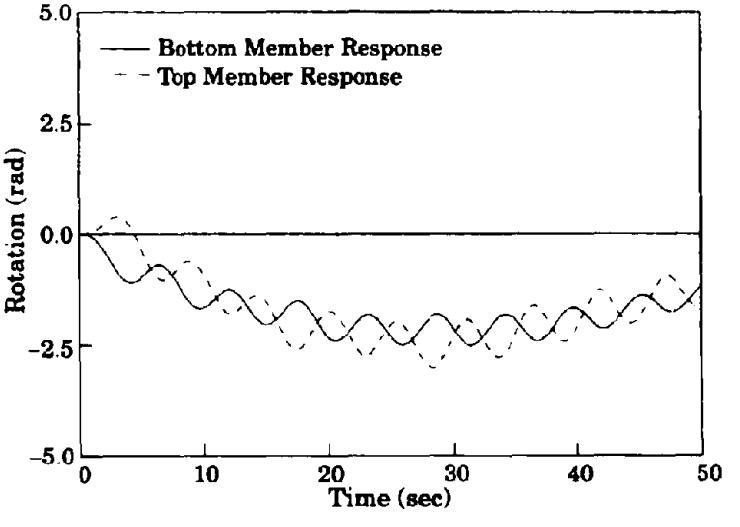

Figure 57 - Motion between members out of phase after both members yield at the same time using the Ramberg-Osgood model and two identical members

sponse from the SDOF model to effectively predict the response of the 2-DOF system when both springs yield at the same time. However, for the other cases considered, the SDOF model can accurately indicate the dynamic stability characteristics of the MDOF system.

Stability of Systems Prone to Damage

Compelling evidence exists to suggest that, with regard to arresting the potential for dynamic instability, damage is not necessarily bad. In fact, under dynamic excitation, damage of the system will help dissipate energy and may lessen the response. However, once damage occurs, the structure will not be able to dissipate the same amount of energy it could prior to the damaging event. If there is too much damage, the system will collapse. Collapse of a damaged system is shown in Figure 58. The system experiences so much damage that it simply can no longer support the axial load. The general trend of the results that include damage in the constitutive model is summed up in the following: the system that experiences damage will initially experience larger amplitude motion than for the case in which damage is not considered. Should the extent of the damage not be large enough to cause the system to become unstable, then the system that includes damage will undergo a motion that diminishes in comparison to the model without damage, and the displacements will remain small with time. If, however, the duration of the motion is long, extensive damage may lead to a situation in which the system becomes unstable due to a loss of restoring force. Consequently, the system becomes unstable in the sense that it cannot carry the loads, even statically, that it was originally designed to support.

To illustrate the dramatic effect that including damage can have on the computed results, consider Figure 59 and Figure 60. Immediately, one can recognize

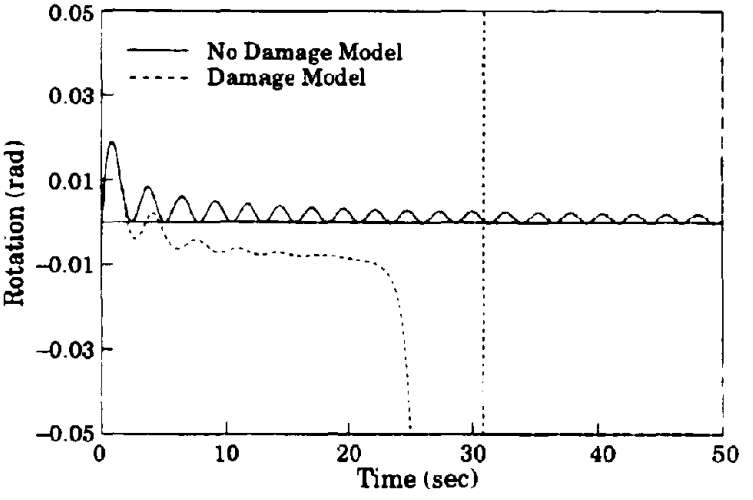

Figure 58 - Dynamic instability for damage model

that both the displacement shift and the steady state amplitude of the response after yielding are much smaller for the case in which damage has been included in the material model. Again, one should not be misled into believing that damage

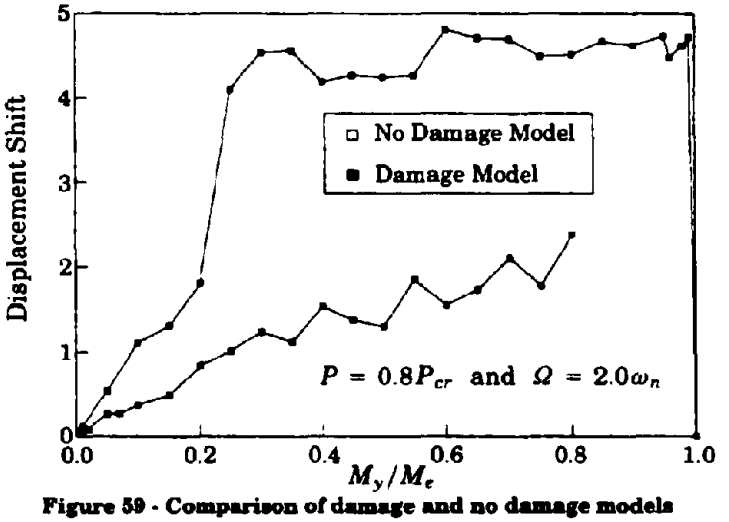

Figure 59 - Comparison of damage and no damage models

is always beneficial. For this particular plot, the motion was only considered while the external force was exciting the system, and the amount of damage was not sufficient to cause failure. Varying the system parameters could lead to very different results. For example, consider the case where the system accumulates a great deal of damage in response to the external exciting forces. Figure 58 shows the variation of displacement with time for the system under such conditions. The system accrues so much damage early on that it no longer has the ability to dissipate the input energy. As a result, dynamic instability is detected for this case. An interesting thing happens though if the system does not accumulate damage as quickly as that shown in Figure 58. If the values of α and β in the damage model are smaller, then the results are much different. To demonstrate, reconsider the system depicted in Figure 58. Keeping all system properties the same except for reducing the values of α and β, one would observe the response shown in Figure 61. Thus, depending on the nature of the system, similar loading condi-

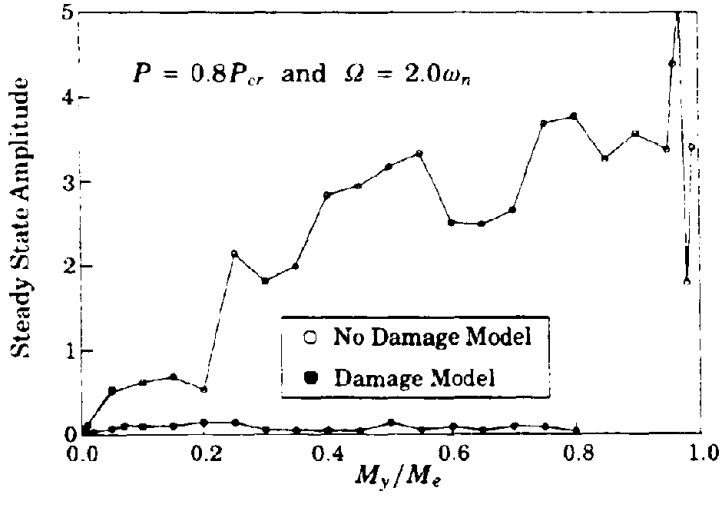

Figure 60 - Comparison of damage and no damage models

tions may produce two entirely different responses. Clearly, the response of the system depends greatly upon the parameters α and β.

It is also interesting to consider the response of the structure once the ground motion has ceased. This will provide some insight as to how a system may behave after an earthquake. For example, even though the damaged system of Figure 61 remains stable during the ground excitation, it may be possible for the structure to become unstable once the lateral base motion has ended. If the external exciting force stops when the system is in an unfavorable configuration, it is possible for the system to collapse even though it is perfectly stable during the excitation. The results again show that the parameters α and β play a crucial role on the behavior realized by the system. Figure 62 shows a system that is stable while the exciting force is acting but becomes unstable after the exciting force stops (the exciting force stops at $t = 50\ sec$). Once again, if the values of the damage parameters α and β are decreased, the system will remain stable after the ground motion

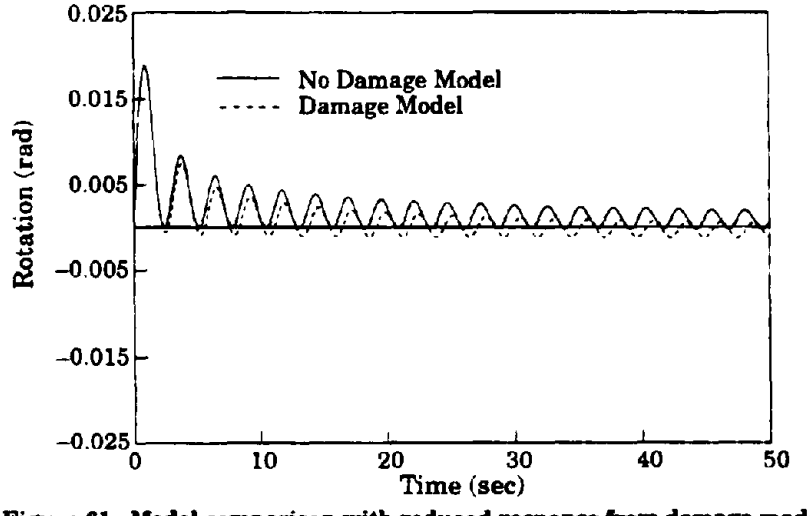

Figure 61 - Model comparison with reduced response from damage model

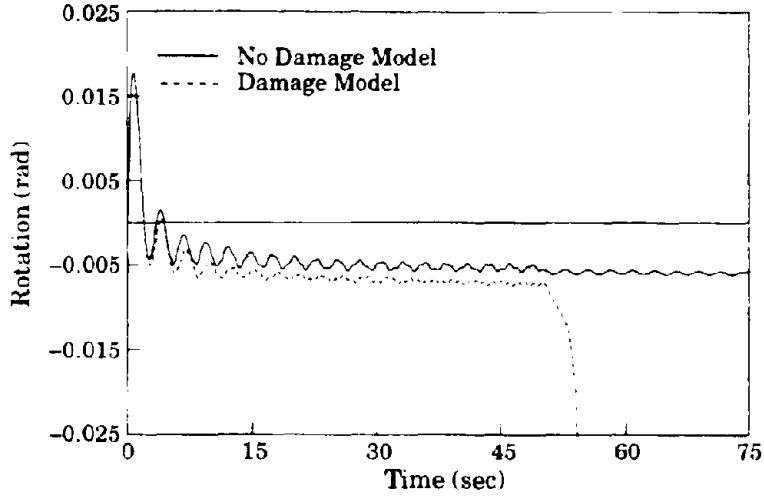

Figure 62 - Model comparison with damaged system becoming unstable after ground excitation ends with sinusoidal axial load

ends. For this particular system, the steady state oscillation will be smaller in amplitude but greater in displacement shift than the model without damage (see Figure 63). The response after the dynamic excitation stops will depend upon the axial load magnitude. When the axial load is large, the steady state amplitude and displacement shift are greater for the damage model after the ground motion ends. This result is shown in Figure 63. The contrary is observed when the axial load is small (see Figure 64). Thus, we again see how sensitive the computed response and stability characteristics are to including damage in the constitutive relationship.

Based upon the behavior illustrated in the previous plots, it is clear that the system can respond in a variety of ways depending upon the rate at which damage accumulates in the system. The rate of damage accumulation is entirely dependent upon the magnitude of the parameters α and β. Thus, the role of the damage model and its effects on the stability of the system can be observed for different

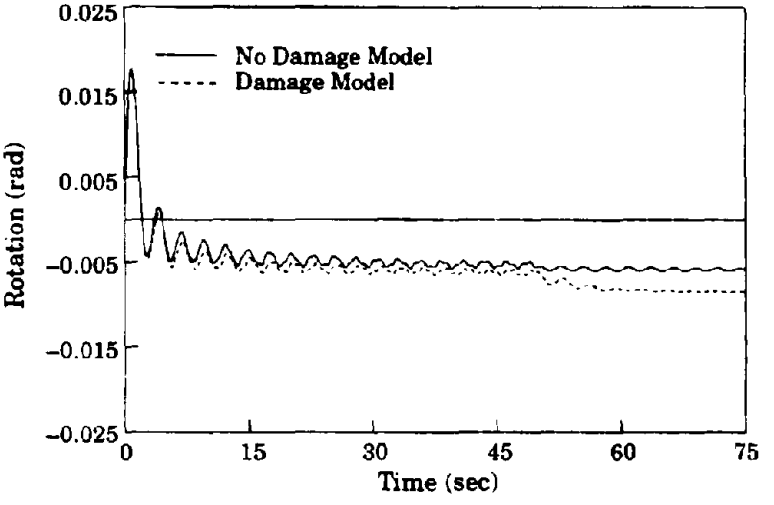

Figure 63 - Model comparison with damaged system remaining stable after ground excitation ends with sinusoidal axial load

values of α and β. For example, Figure 65 shows a plot of the stability regions for a sinusoidal lateral base acceleration acting at a frequency equal to the natural frequency with an amplitude of $0.2g$. The lateral base acceleration is assumed to

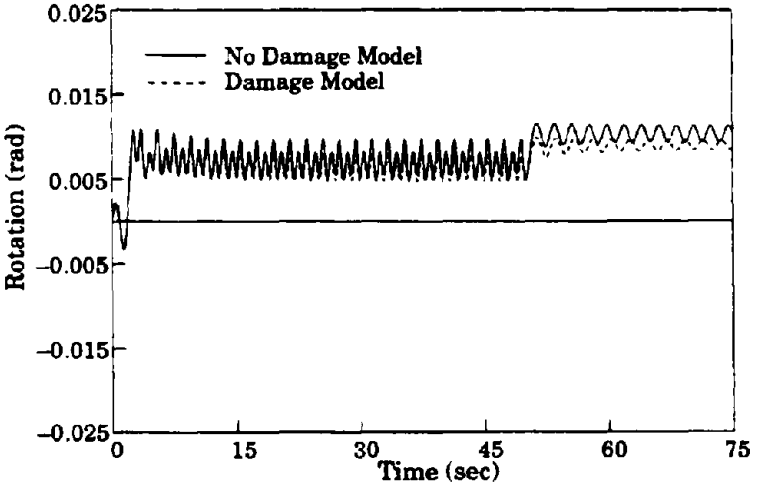

Figure 64 - Model comparison with damaged system undergoing smaller response after ground excitation ends with sinusoidal axial load

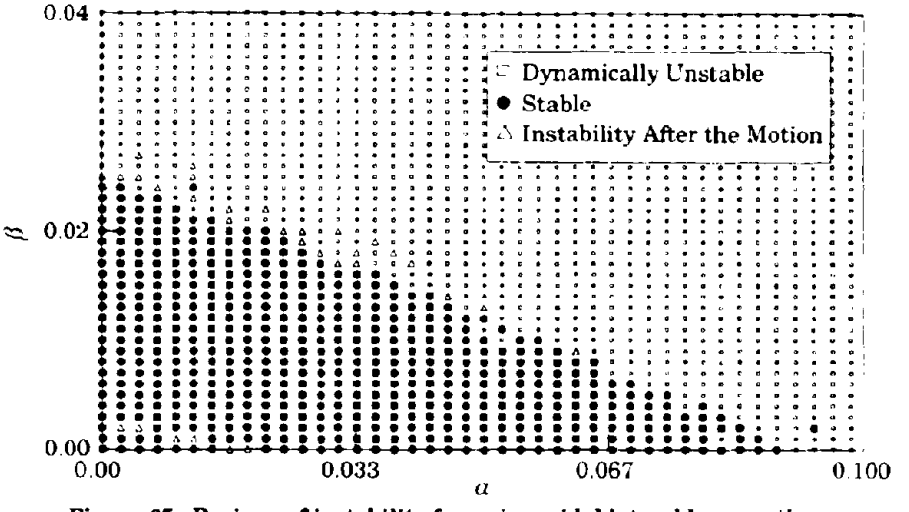

Figure 65 - Regions of instability for a sinusoidal lateral base motion with frequency equal to ω_n

act for a duration of 30 seconds, but the motion of the system is monitored for 50 seconds in order to determine if instability occurs after the ground motion stops. Furthermore, because the ground will not permit a rotation greater than $\pi/2$, this

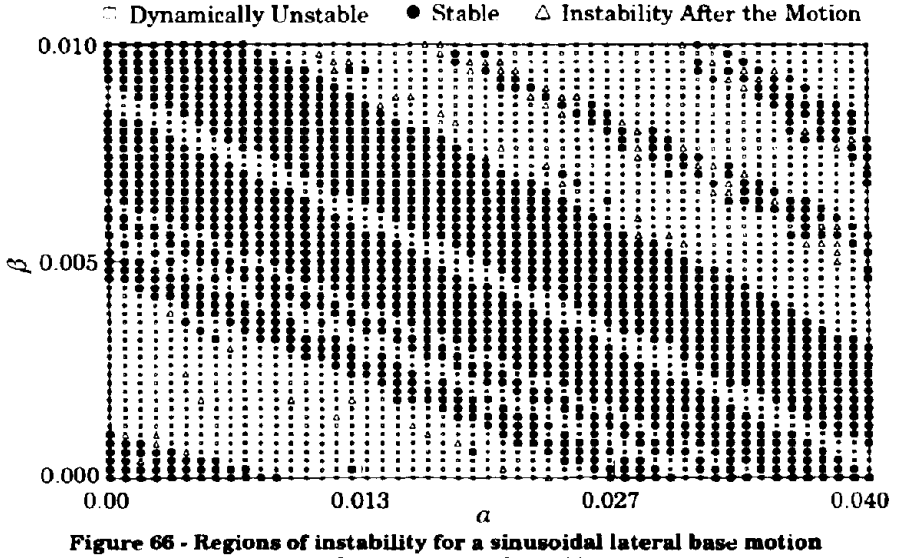

Figure 66 - Regions of instability for a sinusoidal lateral base motion with frequency equal to 0.75 ω_n

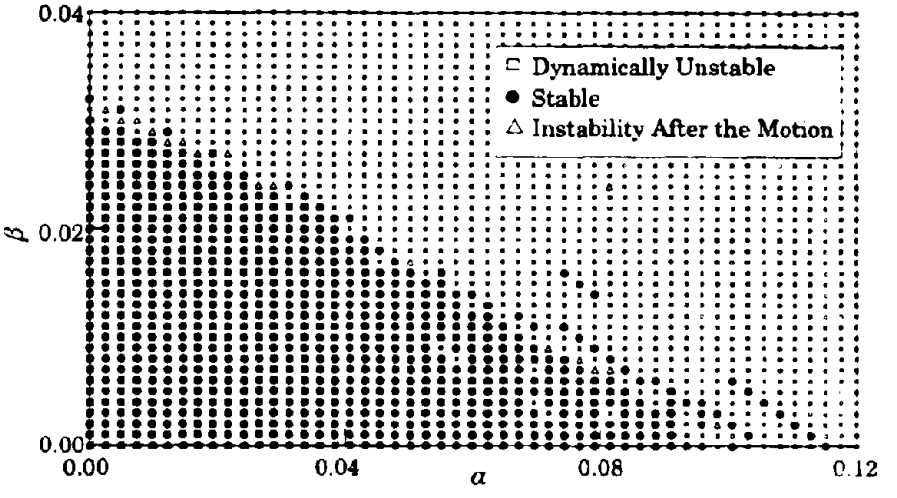

Figure 67 - Regions of instability for a sinusoidal lateral base motion with frequency equal to 1.07 ω_n

will be the new stability limit. Of course, the response of the oscillator will depend upon the frequency of the lateral base motion. For a lateral base frequency of $0.75\omega_n$, the results are much different and much more interesting. The stability regions for the this case are shown in Figure 66. From this figure, it is easy to see that the mere presence of damage does not necessarily lead to instability. The rate at which the damage accumulates has a tremendous impact on the dynamic stability characteristics of the system. Finally, the regions of stability for a lateral base motion acting at a frequency equal to $1.07\omega_n$ are shown in Figure 67.

In order to understand why we observe the dynamic stability characteristics illustrated by the previous plots, it is useful to study the response for some particular cases. The response of the structure when no damage accumulation is included in the material model is shown in Figure 68. The dashed horizontal lines in Figure 68 correspond to a rotation of $\theta = \pi/2$, and the vertical line at $t = 30$ *sec* is a reminder that the sinusoidal ground motion ends at this time. Figure 68

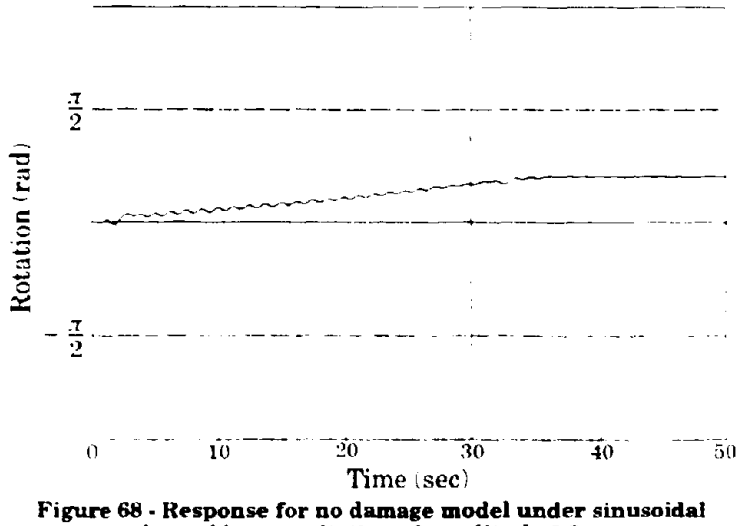

Figure 68 - Response for no damage model under sinusoidal lateral base excitation of amplitude 0.2 *g*

clearly shows that the motion of the system is stable, both in a dynamic sense during the motion and in a static sense after the ground motion ceases.

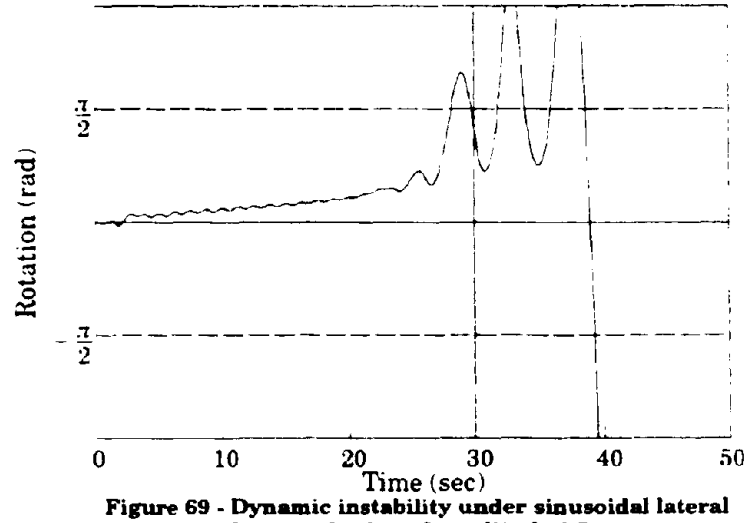

Figure 69 - Dynamic instability under sinusoidal lateral base excitation of amplitude 0.2 *g*

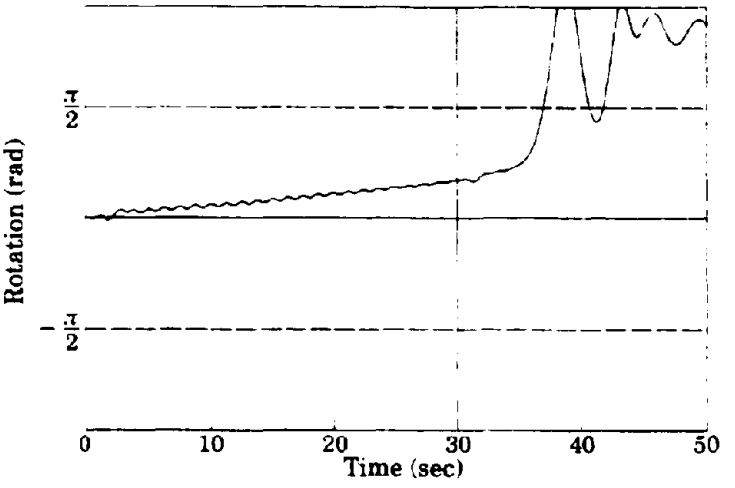

Figure 70 - Instability after ground motion ceases under sinusoidal lateral base excitation of amplitude 0.2 *g*

One peculiarity we see in studying the stability regions, especially Figure 66, is regions of stability between regions of instability. For smaller values of α and β that correspond to the first region of instability, the system becomes unstable fairly late in the response (*i.e.*, for $t > 20$ *sec*). Thus, just enough damage occurs in the system such that shortly before the ground motion ends, the system becomes unstable in a dynamic sense (see Figure 69). For slightly larger values of α and β, the motion of the system is stable. Figure 70 shows instability after the ground motion stops acting. If the values of α and β are increased further, the system becomes unstable in a dynamic sense. However, under these conditions, the motion of the system becomes unstable earlier than the first region of instability (see Figure 71). The reason we see this pattern of behavior is due to the dynamic nature of the problem, the nature of the dynamic loading, and the way in which the stiffness of the system varies in response to the loads.

When α and β are large, dynamic instability occurs because the system undergoes so much damage that it is incapable of supporting loads of any kind. For the

first region of dynamic instability, the pathway to instability is different. The damage parameters for this case are such that the stiffness of the system decays, but not particularly fast. For the sinusoidal ground motion, the system is excited primarily by one particular driving frequency – namely, the initial natural frequency of the linear-elastic system. Once yielding occurs and the system begins to accumulate damage, the effective period of the structure, and, hence, the frequency that most excites the structure changes. Since the stiffness of the system is changing with the load history and damage accumulation, the effective period of the system must also change. If the damage parameters happen to fall into the first region of dynamic instability, the stiffness of the system is altered just enough that the constant-frequency ground motion still excites the system, and the displacements grow. As the displacements grow, the system experiences more damage, and the damaged structure cannot support the axial load of the system once the displacements are large. For the region of stability between the two regions of dynamic instability, the damage that occurs is such that the stiffness of

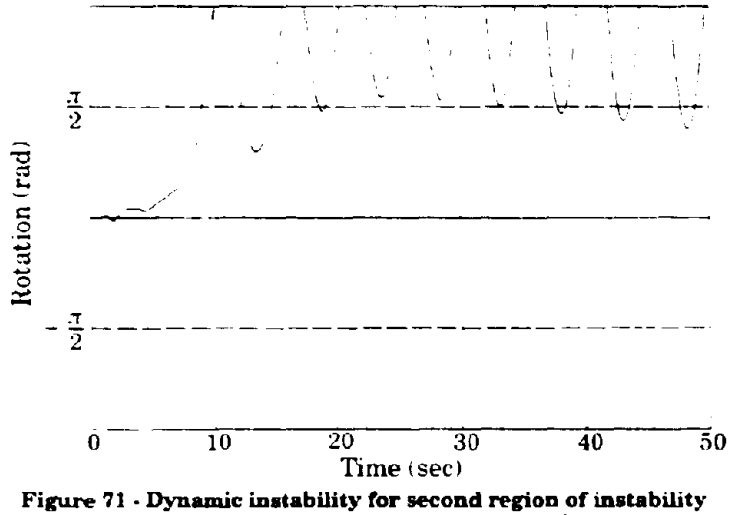

Figure 71 - Dynamic instability for second region of instability under sinusoidal lateral base excitation of amplitude 0.2 *g*

the system is altered early enough in the response in a way that the displacements have not had a chance to grow very large, but the stiffness of the system is different enough so that it is no longer excited by the frequency of the ground motion. Therefore, as these results indicate, the rate of damage accumulation and the nature of the dynamic loads can greatly affect the behavior and stability properties of this system.

Summary and Conclusions

Certainly, the inclusion of geometric and material nonlinearity has a tremendous impact on the analysis results for the model considered in this study. The results have shown that this system is capable of displaying very complex behavior. In order to apply the results we have obtained to real structures, it is clear that we need a thorough understanding of MDOF systems. Unfortunately, merely including one additional degree-of-freedom greatly complicates the analysis. The problem is not only made more difficult due to the fact that we have twice as many free parameters as the SDOF system, but we must also be concerned with the combination of these parameters. Further complicating the problem is the form of the governing differential equations. If we account for large rotations and inelastic material response, then the governing differential equations are highly nonlinear and coupled. Accordingly, traditional solution methods cannot be used to obtain the response.

Given these complications, it would appear that we would have little success in predicting the response of the 2-DOF system. However, our analyses showed otherwise. Under most circumstances, we can use the results from the SDOF model to accurately assess the stability properties and nature of the response for the 2-DOF system. Only for the case in which both springs yield at approximately

the same time does this condition not hold. Fortunately, this is a situation that is seldom encountered. In order to have both springs yield at approximately the same time, either both springs have to have a very small yield strength, or the springs need to be of much different properties. Neither of these scenarios is realistic in an actual structure. Therefore, in general, the response of a MDOF system can be approximated reasonably well by a SDOF system, which, from a physical point of view, makes good sense. A good example to consider is the response of a cantilever column. For the cantilever column, the maximum moment in the section occurs at the fixed end. For inelastic material modeling under these circumstances, it is reasonable to assume the formation of a plastic hinge at the base. Thus, based on this approximation of the plastic hinge, a SDOF oscillator like the one considered in detail in this chapter can model the continuos cantilever column. Details for making this comparison are given in Chapter 4.

Inclusion of a damage mechanism in the constitutive relationships can lead to very interesting results. In fact, the way in which damage accumulates directly controls the dynamic stability characteristics of a damage-prone system. As the results of this chapter have shown, the reduction in stiffness caused by damage does not necessarily lead to dynamic instability. Under certain circumstances, inclusion of the damage mechanism may actually reduce the response computed as compared to the case when damage is not included in the constitutive relationship. What is interesting about the results obtained in this study is that many are counter-intuitive and contradict the results one would obtain under static or monotonic loading conditions. From the findings presented in this chapter, it is clear that additional parameters are needed to characterize the dynamic stability properties of a damage-prone system over those needed to characterize the static stability properties.

4

Application to Earthquake Engineering

All things have second birth;
The earthquake is not satisfied once.
- William Wordsworth

Before seeing how some of the results from the previous chapter may be applied to seismic engineering problems, it is important to understand the current philosophy behind the design of structures to resist earthquake loadings. For earthquakes considered to be small, the strength of the structure should be large enough that the building remains safe and stable without experiencing any damage. For a moderately sized earthquake, it is considered acceptable if the building experiences some damage provided this damage is limited to non-structural elements. For example, yielding of the structural steel should not occur, but cracking of plaster walls may take place. Under very large seismic motions, the system will likely experience some structural damage in dissipating the energy of the earthquake. Thus, it is fully expected that steel will yield and that concrete will crack during a very strong ground motion. The major concern is that even though the structural system has been damaged, it should not collapse. The structure must remain safe after the largest of earthquakes. Otherwise, there exists a great potential for the loss of human life. This philosophy forms the basis of building code provisions regarding the design of structures to resist earthquakes.

There is good reason why structures are designed this way. If structures were designed to resist elastically the forces that arise from an earthquake, then in certain areas of high seismicity, designers would have to include a lateral force resisting capability equal to or larger than the weight of the structure itself. Since it is customarily assumed that the design life of most structures is no more than 50 years, and since the likelihood of occurrence of an extremely large earthquake is small, it would be prohibitively expensive to require that structures be built to elastically withstand such large earthquake forces.

The building owner, of course, must weigh this approach against the cost of repairing the structure in the event that a large earthquake actually does occur. Under some circumstances, it may be more cost effective to design the structure in such a way that even a severe earthquake will not damage the structure so much that it is incapable of meeting its original design intent. For example, in the manufacturing of computer chips, having the production line shut down may equate to millions of dollars lost, and the owner of such a facility may find it a wise investment to guard against this possibility. In addition, some structures are considered to be so essential that they must remain fully operational even after the largest of earthquake. Examples of such structures include hospitals and nuclear power plants. In an attempt to address some of the issues of allowable damage versus initial cost, new philosophies have emerged regarding the design of seismic-resistant structures. These new approaches try to optimize the cost of the structure taking such factors as performance and acceptable level of damage into consideration.

The procedure most often used for designing structures to resist earthquake forces is the *Equivalent Lateral Force* (ELF) method (UBC 1994, FEMA 1992). With the ELF method, lateral forces are applied *statically* to the structure to ac-

count for the earthquake motion. In using this method, the dynamic response of the structure need not be computed. Furthermore, when using the ELF procedure, code requirements are satisfied if the structure can *elastically* withstand the statically applied lateral forces. According to the code provisions, even though yielding may take place during the actual earthquake, the structure will remain stable and capable of supporting the gravity loads if it can adequately resist these lateral forces. The code, therefore, does not require a nonlinear analysis for design. Thus, if one is designing a steel column to resist seismic loads, the stability of the column is based upon its ability to resist the lateral and vertical loads without directly accounting for the fact that the loads are actually varying with time and the structure is responding dynamically. Analytical results from the previous chapter have shown that, under certain circumstances, the results obtained from static analyses do not give a good indication of the dynamic stability properties of a mechanical system. Consequently, understanding how this finding correlates to the current seismic design procedure is a problem that warrants special consideration.

Currently, earthquake resistant design procedures incorporate the concept of damage simply by means of a *ductility factor*. The ductility factor is defined as the ratio of the maximum displacement to the yield displacement. The advantage to using such a measure is its simplicity. Incorporating this value into the design, in effect, attempts to account for the nonlinear material behavior the structure is likely to experience during the course of an earthquake. The ductility factor theory is based on the assumption of equality between the maximum displacements of two SDOF systems – one having an purely linear-elastic behavior, the other having an elastic-perfectly-plastic one (Newmark and Hall 1982). Use of the ductility factor, though, has received a great deal of criticism. The main thrust of

this criticism is that the design of the structure is based on a single value. Hence, there is no accounting for the duration and frequency content of the dynamic loading when the ductility factor is used by itself. Furthermore, it is based upon a simple elastic-perfectly-plastic material model. The underlying hypothesis of the ductility factor approach loses its validity in both the case of very stiff and very flexible structures (McCabe and Hall 1992). Proper use of the method implicitly assumes structural regularity and a global collapse mechanism (Balio and Castiglioni 1994).

Other measures have been suggested that better account for damage than the ductility factor (McCabe and Hall 1992, Balio and Castiglioni 1994, Castiglioni and Loas 1992, Fajifar 1992, Loh and Ho 1990, Park, Ang, and Wen 1984). Some of these measures are modified forms of the ductility factor. For example, the *cumulative displacement ductility index* (Loh and Ho 1990), which is simply the sum of all absolute inelastic deformations normalized by the yield strain, accounts for damage that results from cycles of inelastic deformation. Most other measures that have been introduced incorporate the energy absorbed by the structure into the damage model. Many aspects of *low cycle fatigue theory* lend credibility to this approach. Furthermore, results from the previous chapter for the sinusoidally varying ground acceleration have shown that the dynamic stability characteristics of a system depend strongly upon the hysteretic energy dissipated through inelastic material response. Therefore, a damage model that is based upon the displacement ductility *and* the energy dissipated may be better able to model damage during an earthquake than a model that depends solely on the displacement ductility.

An example of a damage model that includes a dependence upon the hysteretic energy dissipated is the McCabe and Hall (1992) model. McCabe and Hall (1992) suggest a damage measure that depends quadratically upon the dissipated ener-

gy. This quadratic formulation, according to McCabe and Hall, agrees more closely to test results when many varying amplitudes of plastic strain are involved. Results from this study are based upon an assumed elastoplastic material response. Another model that is used quite frequently is the Park and Ang (Park, Ang, and Wen 1984) damage model. This model takes both displacement ductility and hysteretic energy dissipated into account for determining the extent of damage. This model has received much validation as to its accuracy by many researchers. In fact, the damage model presented in Chapter 2 is a modified form of the Park and Ang model.

Comparison with Current NEHRP Design Provisions

Perhaps one of the best ways to evaluate the findings presented in this research is to study the dynamic response of a structure designed in accord with the current NEHRP (FEMA 1992) design provisions. In doing so, we will simply design the SDOF system presented in the last chapter in accord with the ELF procedure. Based upon this design, we will evaluate the dynamic performance of the structure in response to two separate earthquake motions, and we will determine the role of damage accumulation on the dynamic stability characteristics of the system. Following the presentation of the dynamic analyses, interpretation of how these results may apply to real, MDOF systems is considered.

In comparing the results of our analyses of the SDOF system with the NEHRP code provisions, it is important to recognize some inherent limitations of this approach. The NEHRP provisions have been developed based upon our experiences regarding the performance of actual structures to previous earthquakes. Though a SDOF model will give us insight into the behavior of real structures, a SDOF model cannot include all the features of a real building. Unlike our model, real

structures are at least slightly damped and are composed of many elements. The system we will be studying neglects velocity proportional damping because we are only considering a system that yields, and, in the inelastic response of structures, the amount of energy dissipated through velocity proportional damping is negligible compared to the amount of energy dissipated through inelastic material response. Damping in a real structure, however, may be important in that it may reduce the response so that the material never yields. Thus, for the sake of these analyses, the NEHRP provisions are being used as a guideline for design, and the results are not necessarily a reflection on the adequacy of the code equations. Rather, we are trying to determine whether or not the *philosophy* of a static design procedure is appropriate under seismic excitations.

SDOF System Example

Static Design using ELF Method. For this example, the SDOF system studied in the preceding chapter is designed in accord with the current NEHRP design provisions using the ELF procedure. To begin, we first need to determine the base shear. The base shear depends upon the soil conditions at the site, the type of structure and structural system incorporated, the importance of the structure, and the fundamental period of the structure. Mathematically,

$$V = C_s W \tag{66}$$

where C_s is the seismic design coefficient, and W is the total dead load of the structure. According to the code, our system is an *inverted pendulum type structure.* This means that we have a structure that has a large portion of the mass concentrated at the top, and, thus, has essentially one degree-of-freedom. Accordingly, it is appropriate to assume that the axial load of the column is due entirely to dead load.

The seismic design coefficient (C_s), which depends upon the fundamental period of the structure, is determined from the following formula:

$$C_s = \frac{1.2A_vS}{RT^{2/3}} \leq \frac{2.5A_a}{R} \tag{67}$$

where A_v is the coefficient representing effective peak velocity-related acceleration, A_a is the coefficient representing effective peak acceleration, S is the coefficient for soil profile characteristics, R is the response modification factor for the type of structural system, and T is the fundamental period of the structure. According to the NEHRP provisions, the natural period can be estimated using the code equation, or the code allows us to compute the natural period exactly. The fundamental period of the SDOF structure can be computed exactly from the relationship

$$T = \frac{2\pi}{\sqrt{\frac{k}{m\ell^2} - \frac{P}{m\ell}}} \tag{68}$$

The axial load P is simply the total dead load or total weight of the structure. Using the NEHRP guidelines, the governing load case for this model is

$$(1.1 + 0.5A_v)Q_D + \left(\frac{2R}{5}\right)Q_E \tag{69}$$

where Q_D is the dead load effect due to the axial load, and Q_E is the laterally applied earthquake load effect. For the design of steel structures, the NEHRP code incorporates the AISC LRFD design procedure with some slight modifications. Therefore, once the base shear has been calculated, the AISC LRFD code is used to complete the design.

Table 1 - NEHRP Coefficients and Section Properties

Example					
Drift Limit	***S***	***R***	C_D	***h***	***k***
0.015 *h*	1.5	2.5	2.5	15 *ft*	300,000 *k-ft*
P_{cr}	A_v	A_a	***V***	***T***	***W***
20,000.0 *kip*	0.4	0.4	120 *kip*	0.529 *sec*	300 *kip*

Through trial and error, it was determined that in order for the structure to satisfy the code requirements, the axial load of the system must be small. The reason why the load must be small is that the earthquake load contributes significantly to the overturning or stability of the cantilever column. For this example, it was assumed that the axial load of the structure was only $\approx 1.5\%$ of the static buckling load, or that $W = Q_D = 300$ *kips*. The system parameters for this example are summed up in Table 1. With the axial load known, we can determine the period of the structure. Using Eq. (68), the period of the structure is given as

$$T = \frac{2\pi}{\sqrt{\frac{(300{,}000)(12)(386.1)}{(300)(180)^2} - \frac{386.1}{180}}} = 0.53 \; sec$$

From Eq. (67), the value C_s is calculated as follows:

$$\frac{(1.2)(0.4)(1.5)}{(2.5)(0.5294)^{2/3}} = 0.44 > \frac{2.5A_a}{R} \Rightarrow C_s = \frac{(2.5)(0.4)}{(2.5)} = 0.4$$

Finally, Eq. (66) tells us that the base shear is

$$V = C_s W = (0.4)(300) = 120 \; kips.$$

Now that the base shear is known, the NEHRP provisions allow the structure to be designed using the AISC LRFD provisions. For the load combination shown in Eq. (69), the factored axial load is $P_u = 1.3Q_D = 390$ *kips*, and the lateral earthquake load is $Q_E = 120$ *kips*. The adequacy of the column is verified by its compliance with the controlling interaction equation. To verify the interaction

equation, we must calculate the factored axial load and the amplified moment from the earthquake load. The controlling interaction equation is based upon the level of axial load in the column. Since

$$\frac{P_u}{\phi P_n} = \frac{300}{(0.85)(20,000)} = 0.018 < 0.15$$

the governing interaction equation is

$$\frac{P_u}{2\phi P_n} + \frac{M_u}{\phi_b M_n} \leq 1 \tag{70}$$

According to the specification, the required flexural strength is determined as follows:

$$M_u = B_1 M_{nt} + B_2 M_{lt} \tag{71}$$

where M_{nt} is the required flexural strength in the member assuming there is no lateral translation of the frame, M_{lt} is the required flexural strength in a member as a result of lateral translation of the frame only, and B_1 and B_2 are amplification factors. For this example, it is assumed that the the flexural resistance is provided completely by the rotational spring at the bottom. The column itself is rigid. Accordingly, when there is no lateral translation of the frame, no moment is developed in the spring, and M_{nt} is zero. When lateral translation does occur, a moment is developed in the rotational spring, and we must determine the amplification factor B_2. The code presents two different formulas to calculate B_2. The formula used in this example is

$$B_2 = \frac{1}{1 - \frac{\Sigma P_u}{\Sigma P_e}} \tag{72}$$

where ΣP_u is the required axial load strength for all columns in a story, and ΣP_e is the sum of the critical loads in a story for the case where joint translation is permitted. Thus, for this example

$$B_2 = \frac{1}{1 - \frac{300}{20,000}} = 1.015$$

Even if we assume that the maximum moment that this structure can support is the yield moment, then the interaction equation is

$$\frac{(300)(1.3)}{2(0.85)(20,000)} + \frac{(120)(15)(1.015)}{0.9(7200)} = 0.29 \leqslant 1.00 \Rightarrow OK$$

Therefore, according to the code, this column has adequate strength to safely carry the applied loads. The column must also satisfy certain serviceability criteria including a maximum drift criterion. We can calculate the rotation in the spring by summing moments about the base because we know the relationship between rotation and moment for the elastic spring. Doing so, we determine a tip deflection of 1.08 *in.* The NEHRP code utilizes the following drift criterion:

$$\delta_x = C_d \delta_{xe} \leq 0.015 h_{sx} \tag{73}$$

where δ_x is the calculated inelastic deflection, C_d is the deflection amplification factor (based on properties of the structural system), δ_{xe} is the deflection determined by elastic analysis, and h_{sx} is the story height. Using Eq. (73), the inelastic deformation is calculated as

$$(2.5)(1.08) = 2.7 \ in < \delta_{allowable} \Rightarrow OK.$$

Finally, the code requires a check to determine if we need to consider P-Δ effects. P-Δ effects need not be considered when the stability factor $\theta < 0.10$. The stability factor is defined as

$$\theta = \frac{P_x \Delta}{V_x h_{sx} C_d} \tag{74}$$

where P_x is the total vertical design load above level x (for the purposes of these calculations, factored loads need not be considered), Δ is the design story drift occurring along with V_x, and V_x is the seismic shear force. Accordingly,

$$\frac{(300)(1.08)}{(120)(180)(2.5)} = 0.006 < 0.10 \Rightarrow OK.$$

Thus, we have just verified the adequacy of this design by the current NEHRP provisions. Again, in order to satisfy the code provisions, only a very small axial load is permitted.

Dynamic Analyses. We are now ready to evaluate the dynamic performance of the structure designed statically in accord with ELF procedure of the code. In doing so, two separate earthquake records are considered – El Centro and Mexico City. The N-S component of the 1940 Imperial Valley earthquake, El Centro station ground accelerogram is shown in Figure 72. The 1985 Mexico City ground motion, E-W component measured at the SCT1 station is given in Figure 73.

The response of the system to the El Centro earthquake is shown in Figure 74 when no damage is included in the constitutive model. The rotations have been plotted between +2 and –2 because we are defining instability for the case where $\theta \geq \pi/2$. For a real structure, of course, a *much* smaller limit would be set. Recall, however, that we are interested in studying the behavior of this system and understanding how the *philosophy* behind the code provisions relates to the computed dynamic response. In studying Figure 74, one would classify the motion of this system as stable. However, even though the motion is stable, the system experiences a much larger rotation than that estimated by the NEHRP code using

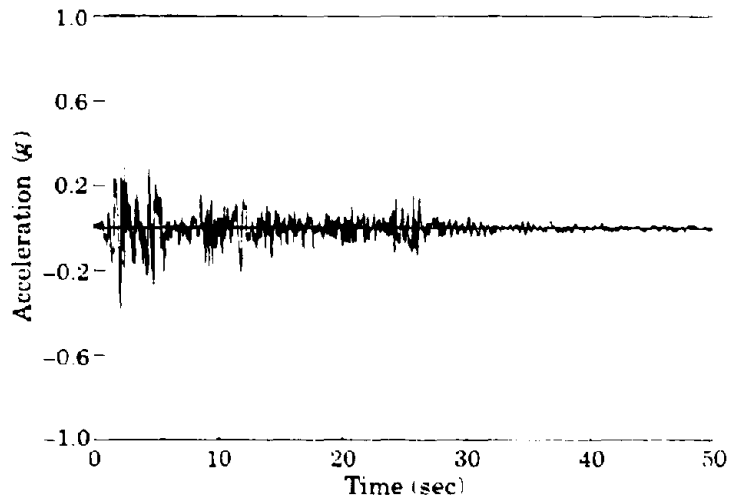

Figure 72 - El Centro ground record

Eq. (73). The steady state displacement after yield is approximately 0.10 *rad*. For a column that is 15 *ft* tall, this amounts to a tip deflection of 18 *in*. This value exceeds the inelastic displacement calculated using Eq. (73) by more than 15 *in*. In addition, if damage is included in the constitutive relationship, it is possible to get

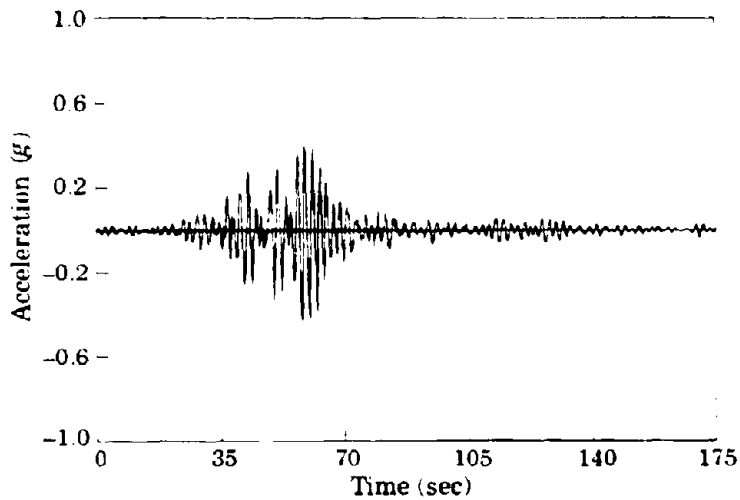

Figure 73 - Mexico City ground record

even larger displacements and, possibly, instability. As we saw in the last chapter, the type of behavior that results depends highly upon the damage parameters α and β. The dynamic stability properties as a function of α and β for the El Centro ground motion are shown in Figure 75. This plot demonstrates that the dynamic stability properties depend upon both the displacement ductility and the energy dissipated by the spring. Plots of instability after the ground motion subsides and dynamic instability are shown in Figure 76 and Figure 77 respectively.

The response of the undamaged system to the Mexico City earthquake is shown in Figure 78. We again see that the motion of the system is stable. However, we note that the steady state tip displacement for this case is also quite large ($\approx 14\ in$). Once damage is included in the constitutive relationship, the steady state amplitude after yielding occurs increases, and instability can result. Interestingly though, the damage parameters that lead to instability for the Mexico City earthquake are different from those for the El Centro earthquake. The main reason for this difference is that the Mexico City earthquake is of a much longer

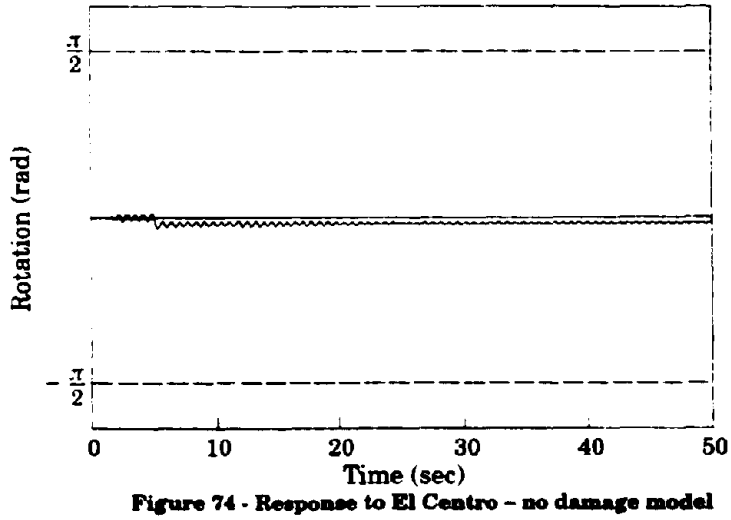

Figure 74 - Response to El Centro – no damage model

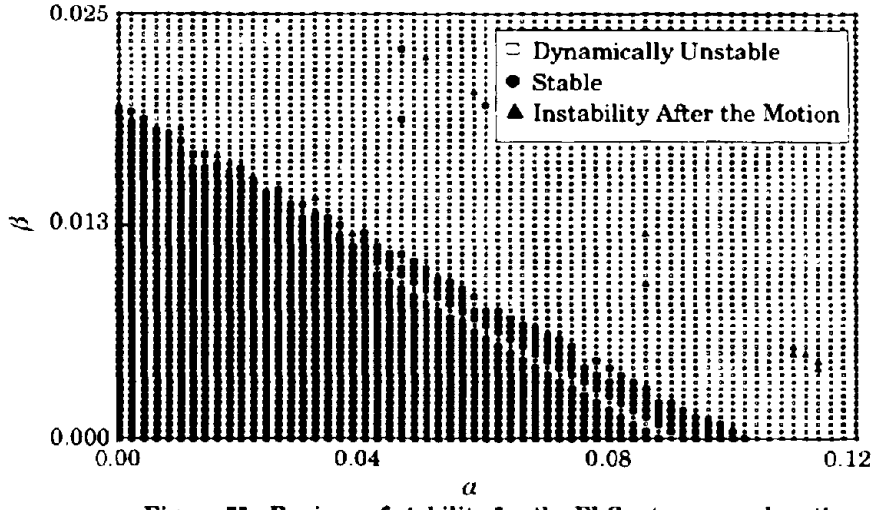

Figure 75 - Regions of stability for the El Centro ground motion

duration, and the frequency content of the motion is also different from the El Centro motion. The response of the structure to the Mexico City earthquake as a function of α and β is shown in Figure 79. The response for $\alpha = 0.04$ and $\beta = 0.001$ is shown in Figure 80. Clearly, for this choice of damage parameters,

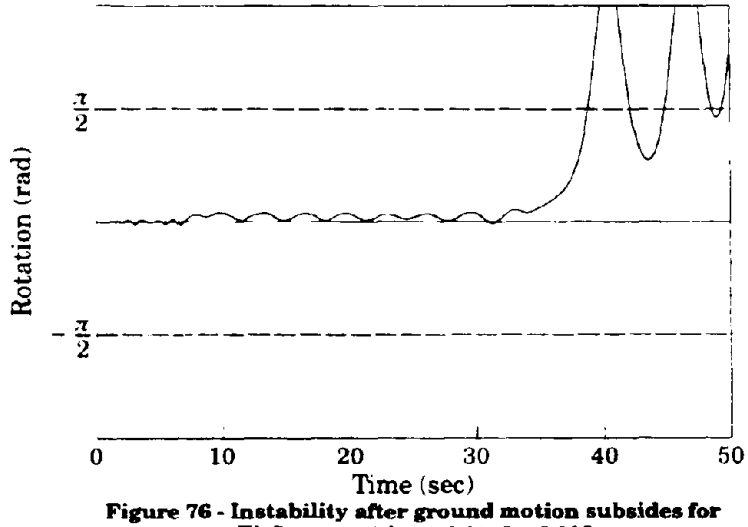

Figure 76 - Instability after ground motion subsides for El Centro with α = 0.01, β = 0.018

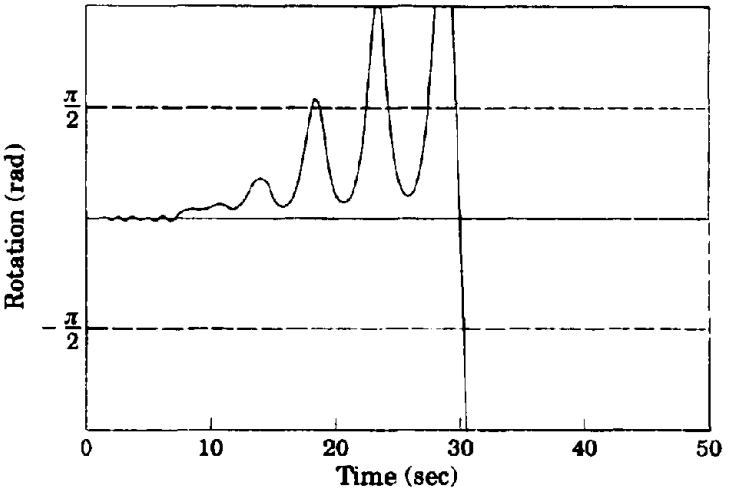

Figure 77 - Dynamic instability for El Centro with $\alpha = 0.02$, $\beta = 0.01$

we observe dynamic instability. Figure 79 shows that while the dynamic stability properties depend upon both the displacement ductility and the energy dissipated by the spring, the dependence is much stronger upon the displacement ductility (the values of α are ≈ 10 times the values of β in the region of dynamic instabili-

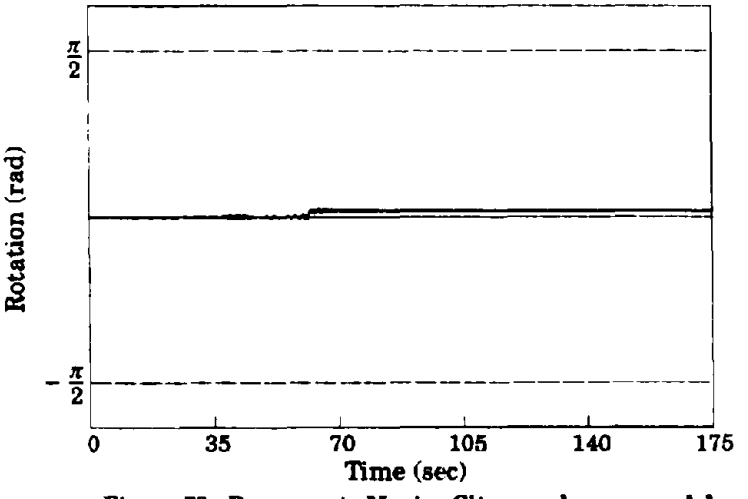

Figure 78 - Response to Mexico City - no damage model

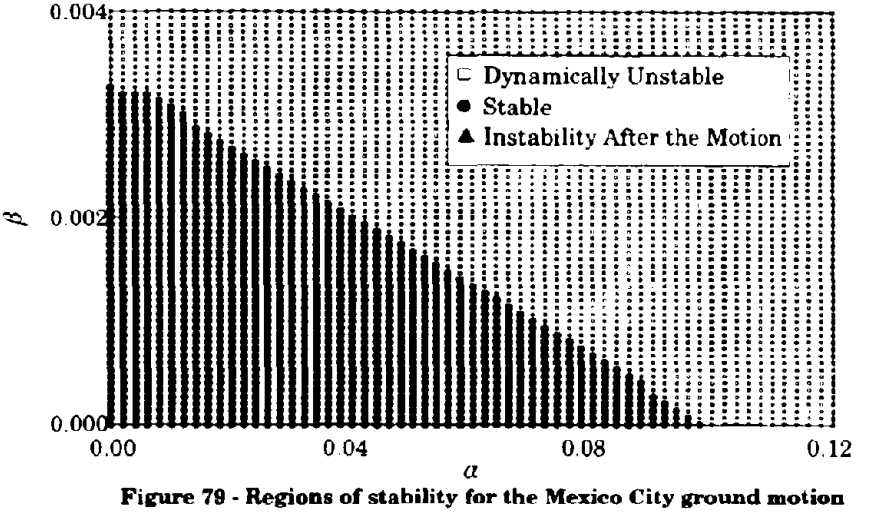

Figure 79 - Regions of stability for the Mexico City ground motion

ty). The response to the El Centro motion also showed a greater dependence upon the displacement ductility but not to the extent as that for the Mexico City motion. The differences between the two result from the fact that the dynamic character-

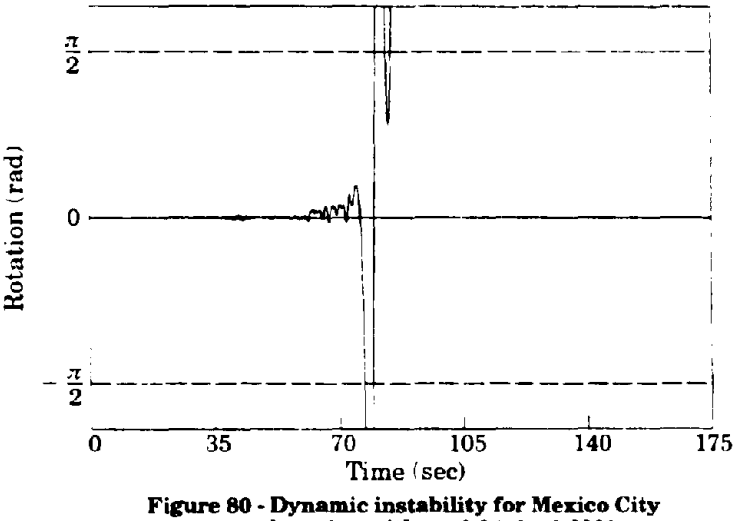

Figure 80 - Dynamic instability for Mexico City ground motion with α = 0.04, β = 0.0001

istics of the two ground motions are much different. Clearly, the choice of ground record plays an important role on the dynamic stability properties of the damage-prone system.

Application of Results to Continuous Systems

Results from the last chapter indicated that the dynamic stability characteristics of a MDOF damage-prone system can be well approximated by analyzing the dynamic performance of a suitably chosen SDOF system. In fact, the SDOF approximation is often used in structural dynamics problems (Clough and Penzien 1993). Under certain circumstances, even the response of a continuous system with continuous displacements over the domain of the structure can be well approximated using a SDOF system. The requirement for such an approximation to be accurate is that the structure behaves essentially like a SDOF system in that the structural displacements, though continuous, are capable of being expressed in a single form or shape. If this approximation holds, then the solution will simply give the amplitude of the assumed displaced shape. For these conditions, the structure may be analyzed in exactly the same way as a true SDOF system.

An example of a continuous system having an infinite number of degrees of freedom that can be well approximated by SDOF system behavior is the cantilever tower shown in Figure 81 (Clough and Penzien 1993, Berg 1989). For the case of elastic material response, the governing equation of motion takes the form

$$m^*\ddot{Z} + c^*\dot{Z} + \left(k^* - k_G^*\right)Z = p_{eff}^* \tag{75}$$

where m^* is the generalized mass, c^* is the generalized damping, k^* is the generalized flexural stiffness, k_G^* is the generalized geometric stiffness, and p_{eff}^* is the generalized effective load. The expressions for each of the generalized variables

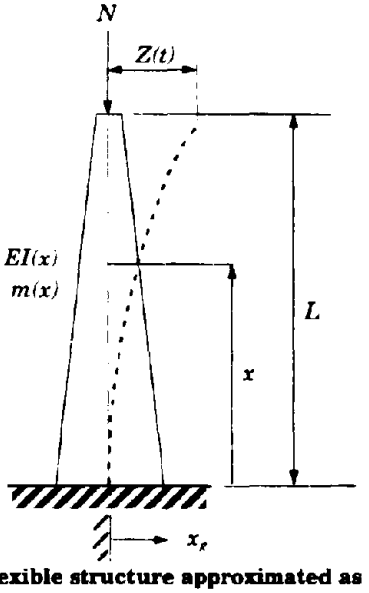

Figure 81 - Flexible structure approximated as a SDOF system

is dependent upon the assumed displaced shape. To illustrate, the generalized variables are computed as follows:

$$
\begin{aligned}
m^* &= \int_0^L m(x)(\chi(x))^2 dx \\
k^* &= \int_0^L EI(x)(\chi''(x))^2 dx \\
k_G^* &= N \int_0^L (\chi'(x))^2 dx \\
p_{eff}^* &= -\ddot{x}_g \int_0^L m(x)\chi(x) dx
\end{aligned}
\tag{76}
$$

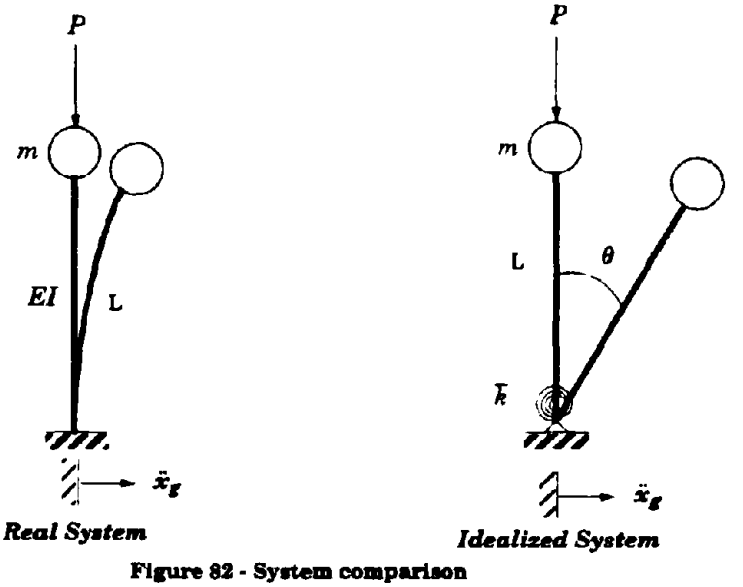

Figure 82 - System comparison

where $m(x)$ is the distributed mass per unit length, $\chi(x)$ is the assumed displaced shape, and N is a constant vertical load applied at the top of the structure that is positive when acting in compression.

Consider now the cantilever column shown in Figure 82. Physically, this could represent a bridge pier or perhaps a water tower. For the real cantilever column, the largest moment occurs at the base. Thus, should the loads be large enough to cause the elastic limit of the material to be exceeded, the section at the base will be the first to yield or form a plastic hinge (Gaylord, Gaylord, and Stallmeyer 1992, Chen and Lui 1987). Once a plastic hinge forms, the column can rotate. Under these conditions, the total rotation of the column will be due mainly to the inelastic response at the base. The additional elastic deformation in the top portion of the column is negligible in comparison to the inelastic deformation. Consequently, the SDOF model developed in the previous chapter can be used to model the dynamic response of the real cantilever column.

To model such a system requires the appropriate choice of model parameters for the idealized SDOF structure. In choosing the parameters, we need to match the principal dynamical variables of the cantilever column with the idealized system. The appropriate choice of variables, however, will involve some trade-offs. It will not be possible to match exactly the variables of the continuous system with the idealized system, but, by making good choices, we can minimize the error between the two systems. For a dynamic, yielding system, our previous results indicate that the two variables that most significantly control the response are the initial natural frequency of the structure and the strain at which yielding occurs. The initial, elastic response of the structure will depend upon the relationship between the frequency content of the external loads in relation to the natural frequency of the system. As we saw in the last chapter, the frequency is important for both linear and nonlinear systems. If the external loads are not in the frequency range that excites the structure and leads to large displacements, then yielding will not occur. If yielding does not occur, one does not need to resort to numerical techniques to determine the response because a closed-form solution exists under these conditions. In addition to matching the frequencies of both the idealized system and the continuous system, we would like both systems to have the same load intensity and yield strain.

For the cantilever column, the transverse displacement $u(x,t)$ is a function of both position and time. Because we are assuming that the cantilever column has no distributed mass along its length, the only inertial force of the system is due to the tip mass. The governing equation of motion is obtained by requiring equilibrium of a free-body diagram of the tip mass (see Figure 83). Assuming that the rotary inertia, j, of the tip mass is zero implies the following relationships:

$$M(L,t) = 0$$
$$N(L) = P \tag{77}$$
$$V(L) + f_I = 0$$

If we assume that EI and P are constant and that the moment at any cross section of the beam can be calculated from the relationship $M(x,t) = \partial^2 u/\partial x^2$, then the governing equilibrium equation is

$$EI\,u'''' + P\,u'' = 0 \tag{78}$$

where a prime (') indicates partial differentiation of $u(x,t)$ with respect to x. The general solution to Eq. (78) is

$$u(x,t) = a_1(t) + a_2(t)x + a_3(t)\sin\lambda x + a_4(t)\cos\lambda x \tag{79}$$

where $\lambda = \sqrt{P/EI}$. Applying the boundary conditions will allow us to solve for the coefficients $a_i(t)$ for $i = 1,4$. For the cantilever column, the fixed-end boundary conditions require the displacement and rotation to be equal to zero. At the free-end, the moment must be equal to zero, and the shear plus the inertial force must also be equal to zero. For a uniform beam with a constant axial load, Eq. (78) implies that the shear at any cross section can be determined from the relationship

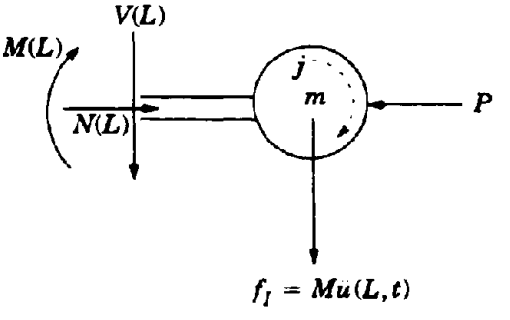

Figure 83 - Free-body diagram of tip mass

$V = -EIu''' - Pu'$. Mathematically stated, the boundary conditions require the following:

$$u(0,t) = 0 \Rightarrow a_1 + a_4 = 0 \tag{80}$$

$$u'(0,t) = 0 \Rightarrow a_2 + \lambda a_3 = 0 \tag{81}$$

$$M(L,t) = EIu''(L,t) = 0 \Rightarrow a_3 \sin\lambda L + a_4 \cos\lambda L = 0 \tag{82}$$

$$V(L,t) + f_I = -EIu'''(L,t) - Pu'(L,t) + mu(L,t) = 0 \tag{83}$$

where a dot $(\cdot)$ indicates partial differentiation with respect to time. Solving Eqs. (80) through (82) in terms of a_4 and substituting these values into Eq. (83) allows us to determine the governing differential equation of motion

$$a_4 + \left[-\omega_o^2 \frac{(\lambda L)^3 \cos\lambda L}{\lambda L \cos\lambda L - \sin\lambda L} \right] a_4 = 0 \tag{84}$$

where $\omega_o^2 = EI/mL^3$ is the natural frequency when no axial load is present. Therefore, the natural frequency of the continuous system as function of the load is

$$\omega^2(\lambda) = \omega_o^2 \frac{(\lambda L)^3 \cos\lambda L}{\lambda L \cos\lambda L - \sin\lambda L} \tag{85}$$

The expression for the static buckling load for an inelastic cantilever column, using the tangent modulus theory, is given as

$$(P + m)_{cr} = \overline{P}_{cr} = \frac{\pi^2 E_t I}{4L^2} \tag{86}$$

where E_t is the tangent modulus of the material (Chen and Lui 1987). Of course, the critical buckling load could also be calculated by setting the natural frequency

equal to zero (Meirovitch 1986, Clough and Penzien 1993). Finally, we can designate the moment at which yielding occurs at the critical section to be M_y.

Recall that for the SDOF system that the natural frequency is given as

$$\omega^2_{SDOF} = \frac{k}{mL^2}\left[1 - \frac{P}{P_{cr}}\right], \tag{87}$$

the critical buckling load is

$$(P + m)_{crSDOF} = \overline{P}_{crSDOF} = \frac{k_t}{L} \tag{88}$$

and that the yield moment is M_{ySDOF}.

By considering the first two terms in the Taylor series expansion for $\sin\lambda L$ and $\cos\lambda L$, it is possible to express the natural frequency of the continuous cantilever column in terms of its critical load as

$$\omega^2 \approx \frac{3EI}{mL^3}\left[1 - \frac{\pi^2}{8}\frac{P}{P_{cr}}\right] \tag{89}$$

Of course, we get a better approximation of the natural frequency by considering more terms in the expansion. As mentioned earlier, modeling the cantilever column as a SDOF system requires us to match the key dynamic variables for both systems. The variables we are most interested in matching are the initial natural frequencies, the moments at which yielding occurs, and the load intensities. From the relationships derived above, we can get a measure of the error in our approximation by comparing these dynamic variables for the two systems. Since the frequency of both the continuous system and the SDOF system both depend explicitly upon the load, we can simply define the error as the square root of the sum of the squares of the differences between the key dynamic variables. Accordingly,

$$Error = \left[\left(\frac{\hat{\omega}^2 - \tilde{\omega}^2}{\hat{\omega}^2} \right)^2 + \left[\frac{\hat{M}_y - \tilde{M}_y}{\tilde{M}_y} \right]^2 \right]^{1/2} \tag{90}$$

where, for convenience, the quantities with a hat (^) refer to the cantilever column and the quantities with a tilde (~) refer to the SDOF system. The combination of model parameters that produces the smallest error will result in the best approximation of the continuous system's response by the SDOF system.

By means of a few assumptions, Eq. (90) can be simplified considerably. First, define the equivalent stiffness of the cantilever column as $\hat{k} = EI/\hat{L}$. Further, let us assume that the column length and mass are the same for both the cantilever column and the SDOF system so that $\hat{L} = \tilde{L} = L$ and $\hat{m} = \tilde{m} = m$. By way of these assumptions, the error in Eq. (90) is minimized (= 0) for the choice of parameters

$$\tilde{k} = 3\hat{k}, \quad \tilde{\eta} = \frac{\pi^2}{8}\hat{\eta}, \quad \text{and} \quad \tilde{M}_y = \hat{M}_y \tag{91}$$

where $\eta = P/P_{cr}$. For this choice of parameters, we would expect the analysis results of the SDOF system to correlate best with the results for the continuous case. We could make the results even better by using a better approximation of the frequency of the continuous system. From this derivation, it is easy to see how the analysis results of the SDOF system may be applied to understanding the behavior of a MDOF or continuos system.

Summary and Conclusions

In this chapter, a SDOF system was designed in accord with the current NEHRP equivalent lateral force procedure, and the dynamic performance of this design was investigated. The results showed that the response of the system, ne-

glecting damage, was stable. The displacements, however, were larger than those calculated using the code equation. Once damage was introduced into the constitutive relationship, we saw that the system could become unstable dynamically as well as after the motion stopped. These results are consistent with the results obtained in the previous chapter in that, under certain circumstances, the static model does not provide a good indication of the dynamic response. Based upon these results, as well as those obtained earlier, we can conclude that additional parameters are required to ascertain the dynamic stability characteristics of a damage-prone system over those needed to classify the static stability properties.

In the latter portion of the chapter, we saw that the response of a MDOF or continuous system may be approximated by a SDOF model. The approximation will be best for structures that have a dynamic response that is well described by a single shape. In order to have the SDOF model best represent the MDOF system, it is necessary to match the key dynamic variables for the two systems.

5

Summary and Conclusions

It is the engineer's constant challenge to conceive the new from the old, and it is his lot to worry about his curious kind of time travel that transcends the instruments of calculation and forces him always to think about the future to avoid the failures of the past.

– Henry Petroski

The dynamic stability characteristics of a nonlinear system have been investigated by means of a simple mechanical model. Although the system was simple, it contained many of the essential features of the the behavior of more complex systems. The governing differential equations of motion were derived for the general N-dimensional system, and detailed analyses were performed for the one-degree-of-freedom and two-degree-of-freedom systems. In this study, both large rotations and inelastic material properties were included. Consequently, the resulting differential equations were highly nonlinear, and, for the MDOF case, coupled. As a result, these equations could only be solved numerically.

Numerical integration of the governing differential equations must be done with care. Traditional numerical solution techniques for structural dynamics problems can result in a loss of accuracy. Accordingly, special techniques have been employed to eliminate these problems, and criteria for discerning numerical inaccuracy from structural stability have been established.

Because the number of free parameters was quite large, even for the SDOF system, analyses were performed to determine which of the variables most significantly influenced the computed results. At first, a very simple system was studied. Then, the effects of including nonlinear geometry, and then both nonlinear geometry and inelastic material response were investigated.

Initially, by assuming small rotations, elastic material response, and an axial load of the form $P_o \cos \Omega t$, the governing differential equation took the form of the well studied Mathieu Equation. Analyzing the response of the system described by the Mathieu Equation provided a means of verifying our results and developing an appropriate definition of dynamic instability. Once the geometrically exact model was considered, the system response was characterized by a beating phenomenon.

The type of material model chosen to represent the inelastic response played a major role in determining the dynamic stability characteristics of the system. In this research, two separate material models were considered – an elastoplastic model and a cyclic Ramberg-Osgood model. In its original form, the Ramberg-Osgood model is incapable of modeling cyclic response, and special provisions were employed to remedy this problem. By studying these two material models, we were able to observe the importance that strain hardening has and that a kink in the loading curve has on the dynamic stability properties of the system. The results obtained using the two separate material models under the same loading conditions were quite interesting. Normally, one would anticipate that, under the same loading conditions, the elastoplastic model would displace more than the Ramberg-Osgood model because the elastoplastic model does not account for the additional strength capacity that results from strain hardening. The results showed, however, that this assumption does not necessarily hold under cyclic

loading conditions. In fact, for the examples considered in this study, the maximum displacement that was computed with the Ramberg-Osgood model was always larger than the maximum displacement computed using the elastoplastic model. Although the inclusion of strain hardening had a dramatic impact on the computed results, the presence of a kink in the loading curve did not lead to significantly different results (see Figure 31).

Based on the responses of a large number of systems, using a wide variety of different model parameters, it was determined that the initial natural frequency and the yield strength are the two most important quantities controlling the behavior of the structure. The frequency is important because it will dictate whether or not the dynamic loading will lead to large or small rotations. If the rotations are large enough to causing yielding of the material, the dynamic stability characteristics of the system will depend upon the value of the yield strength. Contrary to the conclusion one would draw for static or monotonic loading conditions, a more favorable dynamic response can be achieved for lower yield strengths. If yielding occurs early, the displacements and velocities have not had a chance to become very large, and the inelastic response of the spring is able to dissipate the energy of the system. However, if the yield strength of the system is large, prior to yielding, the system will have had ample time to generate large displacements and velocities. The inelastic response of the spring cannot dissipate this higher energy state, and the system is more prone to dynamic instability.

The extension to multiple-degree-of-freedom systems was made. Formulating the governing equations for the 2-DOF case revealed that introducing an additional degree of freedom did not simply double the difficulty of the problem. Not only did we have to deal with twice the number of free parameters, but we also had to be concerned with the different combinations of these parameters. Again,

based upon the analyses of a large number of systems, it was concluded that, under most circumstances, the results obtained from the SDOF model could be used to assess the nature of the response for the 2-DOF system. Only when both springs yielded at approximately the same time were we not able to predict the results of the 2-DOF structure using the SDOF model. However, physically, this case is seldom encountered. Consequently, one can usually gain a good understanding of the response of a MDOF system by analyzing an appropriate SDOF system.

Under large amplitude strain cycling, experimental evidence has shown that certain metals, such as structural steel, experience cyclic softening. Cyclic strain softening was accounted for in the constitutive relationships by means of a damage mechanism. Many different factors can contribute to damage of the material, however, many researchers agree that the two most important factors are related to the maximum displacement of the system and the energy dissipated by the spring in response to the cyclic loading. As a result, it was assumed that a reasonable damage measure would depend linearly upon these two variables.

Analysis results have shown that the dynamic stability properties of the system are highly sensitive to the rate of damage accumulation. The mere presence of damage though does not necessarily lead to larger displacements. Of greater importance is how the damage manifests itself during the dynamic response. Compared to analyses that do not include damage, it is possible for the model that does include damage to experience either greater or smaller displacements depending upon the development of damage during the response. Damage in the system will help dissipate energy in response to the current loads even though the structure's ability to dissipate future loads is diminished because of the damage. Certainly, when too much damage occurs, the structure will collapse.

Based on the model that included damage in the constitutive relationship, the SDOF system was designed in accord with the current NEHRP provisions. The dynamic performance was evaluated by studying the response of the structure to two earthquake motions. The capacity of the structure was well above the code requirements, but the structure was found to become unstable for various amounts of damage accumulation in the system. In response to the earthquake loadings, the results showed an increased potential for dynamic instability as the rate of damage accumulation increased. However, instability resulted for values of displacement ductility well below those specified in the code for this type of structure. These results, along with those obtained from the other loading cases indicate that the response of a dynamic system, prone to damage, cannot easily be predicted using the results from static analyses. In fact, what is interesting about many of the results obtained in this study is that they contradict the results one would obtain under static or monotonic loading conditions. This result is important given that current building codes utilize an equivalent static design procedure for structures required to resist earthquakes.

The parameters that have the greatest influence on the response have been identified. In their current state, the results are not directly applicable to design. More empirical data are needed to accurately determine how damage accumulates under dynamic loadings. Accordingly, possible future research will focus on developing design criteria that will take into account when nonlinear, inelastic systems may be prone to dynamic instability. Also, in order to develop a general design criteria, a greater variety of model parameters will need to be studied as will more MDOF systems. James Thurber once wrote that, "It is better to know some of the questions than to know all the answers." Certainly, questions remain that need to be answered regarding the behavior of dynamic systems prone to

damage. It is hoped that the research presented here has provided some insight to the problem and has demonstrated the need to study such systems.

A1

Successive Symmetric Quadratures (SSQ)

If in other sciences we should arrive at certainty without doubt and truth without errors, it behooves us to place the foundations of knowledge in mathematics.

– Roger Bacon

As discussed in Chapter 2, the key reason why the Newmark Method has problems with the elastoplastic model is that the integration scheme cannot precisely determine the corners that define the transitions between the plastic and elastic states. Over a particular time step, a rapid change occurs in the restoring moment that is not accurately captured. Therefore, if the effects of this rapid variation can be diminished, then the errors associated with not correctly determining the corners of the stress-strain curve will also be diminished. Based upon this idea, Chen and Robinson (1993) first integrate the conventional equations of motion twice over time in order to smooth the effects of the rapid changes in the restoring function. These integrated equations are then used in the numerical integration scheme to determine the new variables (the integrated displacements, velocities, and accelerations), and the rapid variations in the functions do not appear in the solution to these new differential equations. Once the integrated values are determined, the results are then simply converted back to actual system displacements, velocities, and accelerations. Using this procedure, the time step size does

not have to remain small enough to try to capture the corners of the stress-strain curve. Larger time step sizes can be used with accurate results because the twice integrated equations of motion are much more smooth.

In addition to smoothing the data by means of time integration, Chen and Robinson (1993) also introduce an improved quadrature rule to numerically integrate the integrated equations of motion. This method, like the Newmark Method for linear systems, is unconditionally stable. The basic idea behind the new scheme is that more accurate results can be obtained if the accelerations over the time step are allowed to vary quadratically instead of linearly as in the Newmark Method. Thus, for each time step increment, the system properties are determined at both the mid-point and end-point of the time step. The following formulae are used to update the unknown variables:

$$U_{t+\Delta t/2} = U_t + \frac{1}{24}(5U_t + 8U_{t+\Delta t/2} - U_{t+\Delta t})\Delta t, \tag{92}$$

$$U_{t+\Delta t} = U_t + \frac{1}{24}(4U_t + 16U_{t+\Delta t/2} + 4U_{t+\Delta t})\Delta t, \tag{93}$$

$$U_{t+\Delta t/2} = U_t + \frac{1}{24}(5U_t + 8U_{t+\Delta t/2} - U_{t+\Delta t})\Delta t, \tag{94}$$

$$U_{t+\Delta t} = U_t + \frac{1}{24}(4U_t + 16U_{t+\Delta t/2} + 4U_{t+\Delta t})\Delta t. \tag{95}$$

The SSQ procedure requires approximately four times as many computations as the Newmark Method per time step. However, the SSQ method allows the use of larger time step sizes because errors caused by rapid variations in the resistance function are dramatically reduced. In order to obtain the same level of accuracy with the Newmark Method, a much smaller time step must be used. Thus, the overall computation time needed for accurate results is less for the SSQ Method. Figure 84 shows a comparison of the two methods for a nonlinear system that ex-

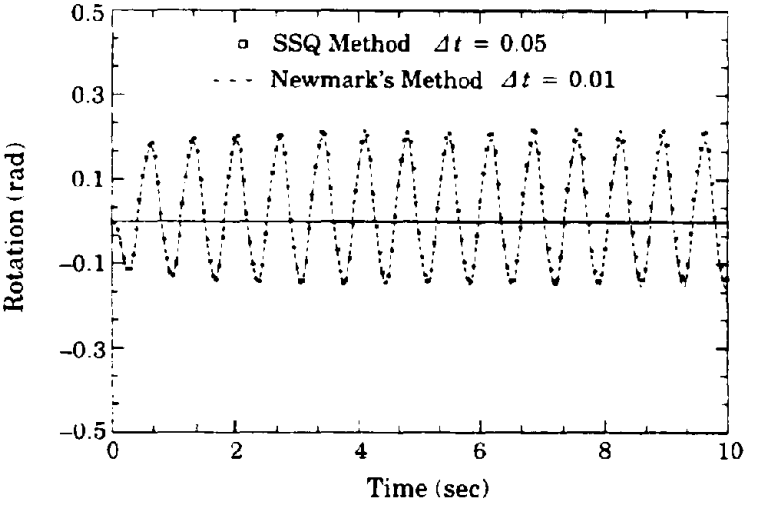

Figure 84 - Comparison of SSQ Method and Newmark's Method

periences many loading cycles in which yielding occurs. As the figure clearly shows, even for a time step that is five times larger than the one used for the Newmark Method, the SSQ Method gives very good results.

The procedure for employing the SSQ method for use with SDOF systems is easily summarized. The governing differential equation of motion for a nonlinear, SDOF system, in general, is given as

$$m\ddot{x} + c\dot{x} + R(x) = -m\ddot{x}_g \tag{96}$$

where m is the mass, c is the damping coefficient, $\ddot{x}_g$ is the acceleration of the ground, $\ddot{x}$ is the system acceleration, $\dot{x}$ is the system velocity, x is the system displacement, and $R(x)$ is the nonlinear restoring force. The integrated variables are defined in the following way:

$$P(t) = \int_0^t x(\xi)d\xi \tag{97}$$

$$Q(t) = \int_0^t P(t)d\xi = \int_0^t \int_0^\xi x(\eta)d\eta d\xi \tag{98}$$

Expressing (96) in terms of the system acceleration leads to the relationship

$$\ddot{x} = -\ddot{x}_g - \frac{c}{m}\dot{x} - \frac{1}{m}R(x). \tag{99}$$

The integrated variables can be expressed in terms of the actual variables in the following ways:

$$\begin{aligned} Q(t) &= P(t) = x(t) \\ \dot{Q}(t) &= P(t) \\ \ddot{P}(t) = x(t) &= -\int_0^t \ddot{x}_g dt - \frac{c}{m}\int_0^t x dt - \frac{1}{m}\int_0^t R(x)dt \end{aligned} \tag{100}$$

Based on these relationships, we can calculate the actual displacement and velocity as follows:

$$x = -\dot{x}_g + \dot{x}_o - \frac{c}{m}(x - x_o) - \frac{1}{m}\int_0^t R(x)dt \tag{101}$$

$$x = -x_g + x_o + \dot{x}_o t + \frac{c}{m}(x_o t - Q) - \frac{1}{m}\int_0^t \int_0^\xi R(x)d\xi dt \tag{102}$$

The SSQ solution algorithm, employing these relationships, is summarized in ***Algorithm A1***.

Algorithm A1

Assume that we are at a converged state and would like to advance the solution to the end of the next time step.

1. Using a subscript *1* and a subscript *2* to indicate the mid-point and end-point of the time step, respectively, update the values for $q_1, q_2, \dot{q}_1, \dot{q}_2$

based upon the values of q_1 and q_2. For the first iteration, the values of q_1 and q_2 are set equal to the converged value from the previous time step. Otherwise, they are set equal to the value calculated from the previous iteration. The unknown values are updated with the relationships

$$q_1 = q_t + \frac{1}{24}(5q_t + 8q_1 - q_2)\Delta t,$$

$$q_2 = q_t + \frac{1}{24}(4q_t + 16q_1 + 4q_2)\Delta t,$$

$$q_1 = q_t + \frac{1}{24}(5q_t + 8q_1 - q_2)\Delta t,$$

$$q_2 = q_t + \frac{1}{24}(q_t + 16q_1 + 4q_2)\Delta t.$$

A subscript t refers to the converged value from the previous time step.

2. Calculate the nonlinear restoring force in the spring at the middle and end of the time step based upon the approximated values for x_1 and x_2, which, from Equation (100), are simply equal to the values of q_1 and q_2 used in step (1). (For this particular research, the nonlinear restoring force could be based on either an elastoplastic model or the cyclic Ramberg-Osgood model.)

3. Evaluate the single integral of the restoring force using the same quadrature rules used to update the integrated displacements and velocities. Thus,

$$r_{I1} = r_{It} + \frac{1}{24}(5r_t + 8r_1 - r_2)\Delta t,$$

$$r_{I2} = r_{It} + \frac{1}{24}(4r_t + 16r_1 + 4r_2)\Delta t.$$

where r_{I1} is the integrated value of the restoring force at the mid-point of the time step, and r_1 is the calculated value of the restoring force at the mid-point of the time step determined in step (2). Likewise, the subscript t on a variable refers to the converged value from the last time step, and the subscript *2* still refers to the values at the end of the time step.

4. Calculate the double integral of the restoring force with the values from step (3).

$$r_{III} = r_{IIt} + \frac{1}{24}\left(5r_{It} + 8r_{I1} - r_{I2}\right)\Delta t,$$

$$r_{\int\int 2} = r_{\int\int t} + \frac{1}{24}\left(4r_{\int t} + 16r_{\int 1} + 4r_{\int 2}\right)\Delta t.$$

5. Based on these values, calculate $\ddot{q}_1$ and $\ddot{q}_2$.

$$\ddot{q}_i = -x_{g_i} + x_o + \dot{x}_o t_i + \frac{c}{m}(x_o t_i - q_i) - \frac{1}{m} r_{\int\int i}, \text{ where } i \in 1, 2$$

6. If the difference between the calculated values for $\ddot{q}_1$ and $\ddot{q}_2$ in step (5) and the ones used in step (1) are within an acceptable tolerance, then the solution has converged. Determine the real acceleration, velocity, and displacement from Equations (99), (101), and (102) respectively, and proceed to the next time step. Otherwise, return to step (1) using the new values for $\ddot{q}_1$ and $\ddot{q}_2$ calculated in step (5) as the new estimate.

Bibliography

A

Addison, P. S. (1995). "On the characterization of non-linear oscillator systems in chaotic mode." *Journal of Sound and Vibration*, **179**(3), 385-398.

Afolabi, D. (1995). "Sylvester's eliminant and stability criteria for gyroscopic systems." *Journal of Sound and Vibration*, **182**(2), 229-244.

Aktan, A. E., Karlson, B. I., and Sozen, M. A. (1973). "Stress-strain relationships of reinforcing bars subjected to large strain reversals." *Report No. SRS 397, UILU-ENG-73-2014*, University of Illinois at Urbana-Champaign, Urbana, IL.

Ariaratnam, S. T. (1967). "Dynamic stability of a column under random loading" in *Dynamic stability of structures* (Herrmann, G., ed.). Pergamon Press, Oxford, 254-266.

B

Baker, G. L. and Gollub, J. P. (1990). *Chaotic dynamics: An introduction*. Cambridge University Press, Cambridge.

Ballio, G. and Castiglioni, C. A. (1994). "An approach to the seismic design of steel structures based on cumulative damage criteria." *Earthquake Engineering and Structural Dynamics*, **23**(9), 969-986.

Balopoulou, S. and Grigoriu, M. (1994). "Sensitivity of seismic response to uncertainties in restoring force model: A monte carlo simulation case study." *Engineering Structures*, **16**(7), 518-533.

Bathe, K.-J. (1982). *Finite element procedures in engineering analysis*. Prentice-Hall, Inc., Englewood Cliffs, NJ.

Bazant, Z. P. and Cedolin, L. (1991). *Stability of structures: Elastic, inelastic, fracture, and damage theories*. Oxford University Press, New York.

Berdichevsky, V. L. and Kim, W.-W. (1995). "Dynamical potential for non-linear vibrations of cantilevered beams." *Journal of Sound and Vibration*, **179**(1), 151-164.

Bernal, D. (1987). "Amplification factors for inelastic dynamic P-Δ effects in earthquake analysis." *Earthquake Engineering and Structural Dynamics*, **15**, 635-651.

Bílý, M., ed. (1993). *Cyclic deformation and fatigue of metals*. Elsevier, Amsterdam.

Black, R. G., Wenger, W. A., and Popov, E. P. (1980). "Inelastic buckling of steel struts under cyclic load reversals." *Report No. UCB/EERC-80/40.* University of California at Berkeley, Berkeley, CA.

Bogoliubov, N. N. and Mitropolsky, Y. A. (1961). *Asymptotic methods in the theory of non-linear oscillations* (translated from Russian). Hindustan Publishing Corporation, India.

Bolotin, V. V. (1963). *Nonconservative problems of the theory of elastic stability.* Pergamon Press, Moscow.

Bolotin, V. V. (1964). *The dynamic stability of elastic systems.* Holden-Day, Inc., San Francisco.

Budiansky, B. (1967). "Dynamic buckling of elastic structures: Criteria and estimates" in *Dynamic stability of structures* (Herrmann, G., ed.). Pergamon Press, Oxford, 83-108.

Budiansky, B. (1976). *Buckling of Structures: Symposium Cambridge / USA June 17-21,1974.* Springer-Verlag, Berlin.

Butenin, N. V. (1965). *Elements of the theory of nonlinear oscillations.* Blaisdell Publishing Company, New York.

C

Capecchi, D. (1993). "Asymptotic motions and stability of the elastoplastic oscillator studied via maps." *International Journal of Solids and Structures,* **30**(23), 3303-3314.

Capecchi, D. and Vestroni, F. (1985). "Steady-state dynamic analysis of hysteretic systems." *ASCE Journal of Engineering Mechanics,* **111**(12), 1515-1531.

Carotti, A. and Chiappulini, R. (1994). "Brake systems for protecting large structures from seismic or aerodynamic instability." *Engineering Structures,* **16**(8), 625-636.

Castiglioni, C. A. and Losa, P. L. (1992). "Local buckling and structural damage in steel members under cyclic loading" in *Proceedings of the Tenth World Conference on Earthquake Engineering, July 1992, Madrid, Spain. Vol. 5.* A.A. Balkema, Rotterdam, 2891-2896.

Cederbaum, G. and Mond, M. (1994). "Instability and chaos in the elastica type problem of parametrically excited columns." *Journal of Sound and Vibration,* **176**(4), 475-486.

Chaboche, J. L. (1989). "Constitutive equations for cyclic plasticity and cyclic viscoplasticity." *International Journal of Plasticity,* **5**,247.

Chaboche, J. L. (1992). "On some modifications of kinematic hardening to improve the description of ratchetting effects." *International Journal of Plasticity,* **7**, 661.

Chan, C.-M., Sherbourne, A. N., and Grierson, D. E. (1994). "Stiffness optimization technique for 3D tall steel building frameworks under multiple lateral loadings." *Engineering Structures,* **16**(8), 570-576.

Chan, S. L. and Kitipornchai, S. (1988). "Inelastic post-buckling behavior of tubular struts." *ASCE Journal of Structural Engineering,* **114**(5), 1091-1105.

Chawla, J. P. (1951). "Numerical analysis of the process of buckling of elastic and inelastic columns" in *Proceedings of the 1st U.S. National Congress on Applied Mechanics*, 435-441.

Chen C. C. and Robinson, A. R. (1993). "Improved time-history analysis for structural dynamics: Treatment of rapid variation of excitation and material nonlinearity." *ASCE Journal of Engineering Mechanics*, **119**, 2496-2513.

Chen, C.-C. and Yeh, M.-K. (1995). "Parametric instability of a cantilevered column under periodic loads in the direction of the tangency coefficient." *Journal of Sound and Vibration*, **183**(2), 253-267.

Chen, W. F. and Lui, E. M. (1987). *Structural stability: Theory and implementation*. Elsevier Science Publishing Co., New York.

Cheng, J. K. and Wang, K. W. (1993). "Stability and nonlinear dynamics of a horizontally base-excited rigid rod with unsymmetric end stiffness." *Transactions of the ASME, Journal of Vibration and Acoustics*, **15**, 85-95.

Clough, R. W. and Penzien, J. (1993). *Dynamics of structures, second edition*. McGraw-Hill, Inc., New York.

Collins, J. A. (1981). *Failure of materials in mechanic design: Analysis, prediction, prevention*. John Wiley and Sons, New York.

Cruz, E. F. and Cominetti, S. (1992). "Nonlinear response of buildings, a parametric study" in *Proceedings of the Tenth World Conference on Earthquake Engineering, July 1992, Madrid, Spain, Vol. 7*. A.A. Balkema, Rotterdam, 3662-3666

Cunniff, P. F. and O'Hara, G. J. (1986). "Beating motion of a damped mechanical oscillator." *Journal of the Acoustical Society of America*, **80**(4), 1255-1257.

D

Dafalias, Y. F. (1992). "Bounding surface plasticity model for steel under cyclic loading" in *Stabi' 'y and ductility of steel structures under cyclic loading* (Fukamato and Lee). CRC Press, Boca Raton, FL, 25-36.

Dafalias, Y. F. and Popov, E. P. (1975). "A model of nonlinearly hardening materials for complex loading." *Acta Mechanica* **21**, 173-192.

Danielson, D. A. (1967). "Dynamic buckling loads of imperfection-sensitive structures from perturbation procedures." *AIAA Journal*, **7**(8), 1506-1510.

Davidson, B. J., Fenwick, R. C., and Chung, B. T. (1992). "P-delta effects in multi-storey structural design" in *Proceedings of the Tenth World Conference on Earthquake Engineering, July 1992, Madrid, Spain, Vol. 7*. A.A. Balkema, Rotterdam, 3647-3652.

de la Llera, J. C. and Chopra, A. K. (1994). "Using accidental eccentricity in code-specified static and dynamic analyses of buildings." *Earthquake Engineering and Structural Dynamics*, **23**(9), 947-968.

den Hartog, J. P. (1985). *Mechanical vibrations, fourth edition*. Dover Publications, Inc., New York.

Dodds, R. H. (1987). "Numerical techniques for plasticity computations in finite element analysis." *Computers and Structures*, **26**(5), 767-779.

E

Ellingwood, B. R. (1994). "Probability-based codified design for earthquakes." *Engineering Structures,* **16**(7), 498-506.

Elnashai, A. S. and Dowling, P. J. (1991). "Seismic design of steel structures" in *Structures subjected to dynamic loading: Stability and strength* (R. Narayanan and T. M. Roberts, eds.). Elsevier Applied Science, New York.

F

Fajfar, P. (1992). "Equivalent ductility factors, taking into account low-cycle fatigue." *Earthquake Engineering and Structural Dynamics,* **21**, 837-848.

Federal Emergency Management Agency (1992). *NEHRP recommended provisions for the development of seismic regulations for new buildings. Part 1: Provisions, 1991 ed.,* Report No. FEMA 222. Building Seismic Safety Council, Washington, D.C.

Federal Emergency Management Agency (1992). *NEHRP recommended provisions for the development of seismic regulations for new buildings. Part 2: Commentary, 1991 ed.,* Report No. FEMA 223. Building Seismic Safety Council, Washington, D.C.

Felippa C. A. (1994). "50 year classic reprint: An appreciation of R. Courant's 'Variational methods for the solution of problems of equilibrium and vibrations,' 1943." *International Journal of Numerical Methods in Engineering,* **37**, 2159-2187.

Fukumoto, Y. and Lee, G. C., eds. (1992). *Stability and ductility of steel structures under cyclic loading.* CRC Press, Boca Raton, FL.

G

Galambos, T. V., ed. (1988). *Guide to stability design criteria for metal structures.* John Wiley and Sons, New York.

Gaspersic, P., Fajfar, P., and Fishinger, M. (1992). "An approximate method for seismic damage analysis of buildings" in *Proceedings of the Tenth World Conference on Earthquake Engineering, July 1992, Madrid, Spain, Vol. 7.* A.A. Balkema, Rotterdam, 3921-3926.

Gaylord, E. H., Gaylord, C. N., and Stallmeyer, J. E. (1992). *Design of steel structures, third edition.* McGraw Hill, New York.

Gere, J. M. and Timoshenko, S. P. (1984). *Mechanics of materials, second edition.* PWS Engineering, Boston.

Goodier, J. N. (1967). "Dynamic plastic buckling" in *Dynamic stability of structures* (Herrmann, G., ed.). Pergamon Press, Oxford, 189-214.

Goel, S. C. (1969). "P-Δ and axial column deformation in aseismic frames." *ASCE Journal of Structural Engineering,* **95**, 1693-1711.

Gravador, E., Thywle, K.-Ξ., and Hökback, A. (1995). "Stability transitions of certain exact periodic responses in undamped Helmholtz and Duffing oscillators." *Journal of Sound and Vibration*, **182**(2), 209-220.

Greenwood, D. T. (1988). *Principles of dynamics, second edition*. Prentice-Hall, Inc., Englewood Cliffs, NJ.

Grimshaw, R. (1990). *Nonlinear ordinary differential equations*. Blackwell Scientific Publications, Oxford.

H

Hartz, B. J. and Clough, R. W. (1957). "Inelastic response of columns to dynamic loadings." *ASCE Journal of Engineering Mechanics*, **83** (EM 2), Pap. No. 1213.

Herrmann, G. and Nemat-Nasser, S., (1967). "Energy considerations in the analysis of stability of nonconservative structural systems" in *Dynamic stability of structures* (Herrmann, G., ed.). Pergamon Press, Oxford, 299-308.

Hill, R. (1958). "A general theory of uniqueness and stability in elastic-plastic solids." *Journal of the Mechanics and Physics of Solids*, **6**, 236-249.

Hill, R. (1950). *The mathematical theory of plasticity*. Oxford University Press, Oxford.

Hjelmstad, K. D. and Lee, S. (1990). "Lateral buckling of short I-beams under cyclic loading." *Report No. SRS 549, UILU-ENG-90-2001*, University of Illinois at Urbana-Champaign, Urbana, IL.

Hjelmstad, K. D. (1994) *What Newton never knew: a brief introduction to structurl mechanics*. University of Illinois, Urbana, IL.

Hoff, N. J. (1967). "Dynamic stability of structures" in *Dynamic stability of structures* (Herrmann, G., ed.). Pergamon Press, Oxford, 3-41.

Holzer, S. M. (1970). "Stability of columns with transient loads." *ASCE Journal of Engineering Mechanics*, **96** (EM 6), 913-929.

Hosseini, M. and Ghafory-Ashitany, M. (1992). "A method for prediction of hysteretic response to earthquake excitations." *Proceedings of the Tenth World Conference on Earthquake Engineering, July 1992, Madrid, Spain, Vol. 7*. A.A. Balkema, Rotterdam, 3689-3694.

Hughes, T. J. R. (1977). "A note on the stability of Newmark's algorithm in nonlinear structural dynamics." *International Journal of Numerical Methods in Engineering*, **11**(2), 383-386.

Huseyin, K. (1978). *Vibrations and stability of multiple parameter systems*. Noordhoff International Publishing, Netherlands.

Hwang, H. H. M. and Hsu, H. (1993). "Seismic LRFD criteria for RC moment-resisting frame buildings." *ASCE Journal of Structural Engineering*, **119**(6), 1807-1824.

I

Idriss, I. M. (1978). "Characteristics of earthquake ground motions." *Proceedings – Specialty Conference on Earthquake Engineering and Soil Dynamics*. ASCE, Pasadena, CA, 1151-1265.

Ishikawa, H., Sasaki, K., and Nakagawa, T. (1994). "Constitutive equation for cyclic plasticity considering memorization of back stress." *JSME International Journal Series A, Mechanics and Material Engineering* **37**(4), 347-354.

Ivanyi, M. and Skaloud, M. (1992). *Stability problems of steel structures.* Springer-Verlag, New York.

J

Johnston, B. G. (1983). "Column buckling theory: Historical highlights." *ASCE Journal of Structural Engineering,* **109**(9), 2086-2096.

Jones, N. and Reis, M. (1980). "On the dynamic buckling of a simple elastic-plastic model." *International Journal of Solids and Structures,* **16**, 969-989.

Joshi, A. (1995). "Constant frequency solutions of a uniform cantilever beam with variable tip mass and corrector spring." *Journal of Sound and Vibration,* **179**(1), 165-169.

K

Kachanov, L. M. (1986). *Introduction to continuum damage mechanics.* Martinus Nijhoff Publishers, Dordrecht, Netherlands.

Kahn, L. F. and Hanson, R. D. (1976). "Inelastic cycles of axially loaded steel members." *ASCE Journal of Structural Engineering,* **102**(5), 948-959.

Kalathas, N. and Kounadis, A. N. (1991). "Metastability and chaoslike phenomena in nonlinear dynamic buckling of a simple two-mass system under step load." *Archive of Applied Mechanics,* **61**, 162-173,.

Karagiozova, D. and Jones, N. (1992a). "Dynamic pulse buckling of a simple elastic-plastic model including axial inertia." *International Journal of Solids and Structures,* **29**(10),1255-1272.

Karagiozova, D. and Jones, N. (1992b). "Dynamic buckling of a simple elastic-plastic model under pulse loading." *International Journal of Non-Linear Mechanics,* **27**(6), 981-1005.

Keppel, M. and Dodds, R. H. (1990). "Improved numerical techniques for plasticity computations in finite element analysis." *Computers and Structures,* **36**(1),183-185.

Key, D. (1988). *Earthquake design practice for buildings.* Thomas Telford Limited, London.

Komarakul-na-nakorn, A. and Arora, J. S. (1990). "Stability criteria: A review." *Computers and Structures.* **37**(1), 35-49.

Kounadis, A. N. and Raftoyiannis. J. (1990). "Dynamic stability criteria of nonlinear elastic damped/undamped systems under step loading." *AIAA Journal* **28**(7), 1217-1223.

Kounadis, A. N., (1993a). "Static and dynamic, local and global bifurcations in nonlinear autonomous structural systems." *AIAA Journal,* **31**(8),1468-1477.

Kounadis, A. N. (1993b). "Nonlinear dynamic buckling of discrete structural systems under impact loading." *International Journal of Solids and Structures*, **30**(21), 2895-2909.

Kreyszig, E. (1993). *Advanced engineering mathematics, seventh edition*. John Wiley and Sons, Inc., New York.

Kutt, T. and Bieniek, M. P. (1988). "Cumulative damage and fatigue life prediction." *AIAA Journal*, **26**(2), 213-219.

Kuwamura, H. and Suzuki, T. (1992). "Low-cycle fatigue resistance of welded joints of high-strength steel under earthquake loading" in *Proceedings of the Tenth World Conference on Earthquake Engineering, July 1992, Madrid, Spain, Vol. 5*. A.A. Balkema, Rotterdam, 2851-2856.

L

Labé, P. and Noé, H. (1992). "Ductility and seismic design criteria" in *Proceedings of the Tenth World Conference on Earthquake Engineering, July 1992, Madrid, Spain, Vol. 7*. A.A. Balkema, Rotterdam, 3659-3662.

Lee, H. P. (1995). "Stability of a cantilever beam with tip mass subject to axial sinusoidal excitations." *Journal of Sound and Vibration*, **183**(1), 91-98.

Lee, K. C. and Poon, K. P. (1990). "Analysis of power system dynamic oscillations with beat phenomenon by Fourier transformation." *IEEE Transactions on Power Systems*, **5**(1), 148-153.

Lee, L. H. N. (1977). "Quasi-bifurcation in dynamics of elasto-plastic continua." *Transactions of the ASME, Journal of Applied Mechanics*, **44**, 413-418.

Lee, L. H. N. (1978). "Quasi-bifurcation of rods within an axial compressive wave." *Transactions of the ASME, Journal of Applied Mechanics*, **45**, 100-104.

Lee, L. H. N., (1981). "Dynamic buckling of an inelastic column." *International Journal of Solids and Structures*, **17** (3), 271-279.

Leipholz, H. H. E., ed. (1972a). *Stability: Fourteen special lectures presented at the University of Waterloo*. University of Waterloo, Waterloo.

Leipholz, H. H. E. (1972b). "Dynamic stability of elastic systems" in *Stability: Fourteen special lectures presented at the University of Waterloo from October 1970 to September 1971* (Leipholz,ed.). SM Study Series, University of Waterloo, Waterloo.

Leipholz, H. H. E., (1974). "On conservative elastic systems of the first and second kind." *Ingenieur-Archive*, **43**, 255-271.

Leipholz, H. H. E. (1976). "Some remarks on Liapunov stability of elastic dynamical systems" in *Buckling of Structures: Symposium Cambridge / USA June 17-21, 1974* (Budiansky, ed.). Springer-Verlag, Berlin, 208-216.

Lemaitre, J. and Chaboche, J.-L. (1994). *Mechanics of solid materials*. Cambridge University Press, Cambridge.

Liew, R. J. Y., White, D. W., and Chen, W. F. (1991). "Beam-column design in steel frameworks – insights on current methods and trends." *Steel Research for Construction*. **18**, 269-308.

Load & resistance factor design, first edition. (1986). American Institute of Steel Construction. Chicago, IL.

Loh, C. and Ho, R. (1990). "Seismic damage assessment based on different hysteretic rules." *Earthquake Engineering and Structural Dynamics.* **19**, 753-771.

Lu, S. and Hall, W. J. (1990). "Torsional effects in structures subjected to strong ground motions." *Report No. UILU-ENG-89-2006.* University of Illinois at Urbana-Champaign, Urbana, IL.

Lubarda, V. A. (1994). "An analysis of large-strain damage elastoplasticity." *International Journal of Solids and Structures,* **31**(21), 2951-2964.

Luenberger, D. G. (1984). *Linear and nonlinear programming, second edition.* Addison-Wesley Publishing Company, Reading, MA.

Lundqvist, S., March, N. H., and Tosi, M.P., eds. (1988). *Order and chaos in nonlinear physical systems.* Plenum Press, New York.

Lyapunov, A. M. (Fuller, A. T., ed.) (1992). *The general problem of the stability of motion.* Taylor and Francis, London.

M

MacRae, G. A. (1994). "P-Δ effects on single-degree-of-freedom structures in earthquakes." *Earthquake Spectra,* **10**(3), 539-568.

Maier, G. and Perego, U. (1992). "Effects of softening in elastic-plastic structural dynamics." *International Journal of Numerical Methods in Engineering,* **34**, 319-347.

Matsui, C. and Sakai, J. (1992). "Effect of collapse modes on ductility of steel frames " in *Proceedings of the Tenth World Conference on Earthquake Engineering, July 1992, Madrid, Spain, Vol. 5.* A.A. Balkema, Rotterdam, 2849-2854.

Matthies, H. G. and Nath, C. (1985). "Dynamic stability of periodic solutions of large scale nonlinear systems." *Computer Methods in Applied Mechanics and Engineering,* **48**, 191-202.

McCabe S. L. and Hall, W. J. (1987). "Evaluation of structural response and damage resulting from earthquake ground motion." *Report No. SRS 538, UILU-ENG-87-2009*, University of Illinois at Urbana-Champaign, Urbana, IL.

McCabe S. L. and Hall, W. J. (1989). "Assessment of seismic structural damage." *ASCE Journal of Structural Engineering,* **115**(9), 2166-2183.

McCabe S. L. and Hall, W. J. (1992). "Damage and reserve capacity evaluation of structures subjected to strong earthquake ground motion." *Proceedings of the Tenth World Conference on Earthquake Engineering, July 1992, Madrid, Spain, Vol. 7.* A.A. Balkema, Rotterdam, 3653-3658.

McIvor, I. K. and Bernard, J. E. (1973). "The dynamic response of columns under short duration axial loads." *Transactions of the ASME, Journal of Applied Mechanics,* **40** (3), 688-692.

Meirovitch, L. (1986). *Elements of vibration analysis.* McGraw-Hill Book Company, New York.

Mendelson, A. (1968). *Plasticity: Theory and application.* Robert E. Krieger Publishing Company, Malabar, FL.

Menegotto, M. and Pinto, P. (1973). "Method of analysis for cyclically loaded reinforced concrete plane frames including changes in geometry and non-elastic behavior of elements under combined normal force and bending." IABSE Symposium on the Resistance and Ultimate Deformability on Structures Acted on by Well-Defined Repeated Loads, Lisbon.

Mettler, E. (1967). "Stability and vibration problems of mechanical systems under harmonic excitation" in *Dynamic stability of structures* (Herrmann, G., ed.). Oxford: Pergamon Press, 169-188.

Miller, R. (1993). *Class Notes for TAM 314 – Advanced Dynamics for Engineers.* University of Illinois at Urbana-Champaign, Urbana, IL.

Mizuno, E., Shen, C., Tanaka, Y., and Usami, T. (1992). "A Uniaxial Stress-Strain Model for Structural Steels under Cyclic Loading" in Fukamato and Lee *Stability and ductility of steel structures under cyclic loading,* CRC Press: Boca Raton, pp. 37-48.

Mo, Y. L. (1995). "Effect of material properties on inelastic dynamic response of spandrel beams." *Engineering Structures,* **17**(2), 81-86.

Monti, G. and Nuti, C. (1992). "Nonlinear cyclic behavior of reinforcing bars including buckling." *ASCE Journal of Structural Engineering,* **118**(12), 3268-3284.

Mustafa, G. and Ertas, A. (1995). "Dynamics and bifurcations of a coupled column-pendulum oscillator." *Journal of Sound and Vibration,* **182**(3), 393-413.

N

Narayanan, R. and Roberts, T. M., eds. (1991). *Structures subjected to dynamic loading: Stability and strength.* Elsevier Applied Science, London.

Nataraju, B. S. and Nagaraj, B. P. (1994) "Elastoplastic analysis and cumulative damage study of a lanyard under dynamic conditions." *Journal of Guidance, Control, and Dynamics,* **17**, 411-414.

Newland, D. E. (1975). *An introduction to random vibrations and spectral analysis.* Longman Group Limited, London.

Newmark, N. M. and Rosenblueth, E. (1971). *Fundamentals of earthquake engineering.* Prentice-Hall, Inc., Englewood Cliffs, N. J.

Newmark, N. M. and Hall, W. J. (1982). *Earthquake spectra and design.* Earthquake Engineering Research Institute, Berkeley, CA.

Nonaka, T. (1973). "An elasti-plastic analysis of a bar under repeated axial loading." *International Journal of Solids and Structures,* **9**, 569-580.

O

Ohno, N. (1982). "A constitutive model of cyclic plasticity with a nonhardening strain region." *Transactions of the ASME, Journal of Applied Mechanics,* **49**, 721.

P

Panovko, Y. G. and Gubanova, I. I. (1965). *Stability and oscillations of elastic systems: paradoxes, fallacies, and new concepts.* Consultants Bureau, New York.

Papadrakis, M. and Chrysos, L. (1985). "Inelastic cyclic analysis of imperfect columns." *ASCE Journal of Structural Engineering*, **111** (6), 1219-1234.

Park, Y. J., Ang, A. H.-S., and Wen, Y. K. (1984). "Seismic damage analysis and and damage-limiting design of RC buildings."*Report No. SRS 516, UILU-ENG-84-2007.* University of Illinois at Urbana-Champaign, Urbana, IL.

Petyt, M. (1990). *Introduction to finite element vibration analysis.* Cambridge University Press, Cambridge.

Popov, E. P. (1977). "Mechanical characteristics and bond of reinforcing steel under seismic conditions." *Proceedings: Workshop on Earthquake-Resistant Reinforced Concrete Building Construction (ERCBC).* University of California at Berkeley, Berkeley, CA, 658-682.

Powell, G. H., Row, D. G., and Hollings, J. P. (1984). "Improved modeling of tubular brace elements under severe cyclic loading." *Transactions of the ASME, Journal of Energy Resources Technology*, **106**, 240-245.

Prasad, S. N. and Herrmann, G. (1972). "Adjoint variational methods in non-conservative stability problems." *International Journal of Solids and Structures*, **8**, 29-40.

R

Ramu, S.A. and Ganesan, R. (1992). "Stability analysis of a stochastic column subjected to stochastically distributed loadings using the finite element method." *Finite Elements in Analysis and Design*. 11, 105-115.

Ravindra, B. and Mallik, A. K. (1995). "Chaotic response of a harmonically excited mass on an isolator with non-linear stiffness and damping characteristics." *Journal of Sound and Vibration*, **182**(3), 345-353.

Reese, L. R., Chang, G. Y., and Dupuym D. L. (1989). "The oscillation of the synodic period of the moon: A 'beating' phenomenon." *American Journal of Physics*, **57**(9), 802-807.

Rehfield, L. W. (1973). "Nonlinear free vibrations of elastic structures." *International Journal of Solids and Structures*, **9**, 581-590.

S

Saaty, T. L. and Bram, J. (1964). *Nonlinear mathematics.* Dover Publications, Inc., New York.

Sewell, M. J. (1972). "A survey of plastic buckling" in *Stability: Fourteen Special Lectures Presented at the University of Waterloo* (Leipholz, H. H. E., ed.). University of Waterloo, Waterloo, 85-197.

Shibata, M. (1982) "Analysis of elastic-plastic behavior of a steel brace subjected to repeated axial force." *International Journal of Solids and Structures*, **18**(3), 217-228.

Shirts, R. B. (1993). "The computation of eigenvalues and solutions of Mathieu's differential equation for noninteger order." *ACM Transactions on Mathematical Software*, **19** (3), 377-390.

Simitses, G. J. (1990). *Dynamic stability of suddenly loaded structures.* Springer-Verlag, New York.

Simo, J. C. and Hughes, T. J. R. (1988). *Elastoplasticity and viscoplasticity· Computational aspects.* (Unpublished notes).

Sittipunt, C. and Wood, S. L. (1993). "Finite Element Analysis of Reinforced Concrete Shear Walls." *Report No. SRS 584, UILU-ENG-93-2015.* University of Illinois at Urbana-Champaign, Urbana, IL.

Sivakumaran, K. S. and Balendra, T. (1994). "Seismic analysis of asymmetric multistorey buildings including foundation interaction and P-Δ effects." *Engineering Structures*, **16**(8), 609-624.

Sridharan, S. and Ali, M. A. (1988). "Dynamic instability of frames having thin-walled columns." *Earthquake Engineering and Structural Dynamics*, **16**, 705-717.

Stoker, J. J. (1950). *Nonlinear vibrations in mechanical and electrical systems.* Interscience Publishers, New York.

Stubs, N. and Krajcinovic D. (1985). *Proceedings of the ASCE Engineering Mechanics Division: Damage Mechanics and Continuum Modeling,* American Society of Civil Engineers, New York, NY.

Sugiura, K., Chang, K. C., and Lee, G. C. (1991). "Evaluation of low-cycle fatigue strength of structural metals." *ASCE Journal of Engineering Mechanics*, **117**(10), 2373-2383.

Sujith, R. I. and Hodges, D. H. (1995). "Exact solution for the free vibration of a hanging cord with a tip mass." *Journal of Sound and Vibration*, **179**(2), 359-361.

Sun, C. K., Berg, G. V., and Hanson, R. D. (1973). "Gravity-effect on single-degree inelastic systems." *ASCE Journal of Engineering Mechanics*, **99**, 183-200.

Szemplinska-Stupnicka, W., Iooss, G., and Moon, F. C. (1988). *Chaotic motions in nonlinear dynamical systems.* Springer-Verlag, New York.

T

Tarnow, N. and Simo, J. C. (1994). "How to render second order accurate time-stepping algorithms fourth order accurate while retaining the stability and conservation properties." *Computer Methods in Applied Mechanics and Engineering*, **115**, 233-252.

Thompson, J. M. T. (1967). "Dynamic buckling under step loading" in *Dynamic stability of structures* (Herrmann, G., ed.). Pergamon Press, Oxford, 215-236.

Thompson, J. M. T. and Stewart, H. B. (1986). *Nonlinear dynamics and chaos: Geometrical methods for engineers and scientists.* John Wiley and Sons, New York.

Thylwe, K.-E. and Gravador, E. (1995). "Non-perturbative stability analysis of periodic responses in driven non-linear oscillators." *Journal of Sound and Vibration,* **182**(2), 191-207.

Timoshenko, S. P. and Gere, J. M. (1961). *Theory of elastic stability, second edition.* McGraw-Hill Book Co., New York.

Timoshenko, S. P. and Young, D. H. (1948). *Advanced dynamics.* McGraw-Hill Book Co., New York.

Torby, B. J. (1984). *Advanced dynamics for engineers.* Holt, Rinehart and Winston, New York.

V

Vierck, R. K. (1969). *Vibration analysis.* International Textbook Company, Scranton, PA.

W

Wakabayashi, M. (1986). *Design of earthquake-resistant buildings.* McGraw-Hill Book Co., New York.

Weigel, R. L., ed., (1970). *Earthquake engineering.* Prentice-Hall, Inc., Englewood Cliffs, NJ.

Y

Yue, Y. and Zheng, J. (1992). "Dynamic elastic-plastic buckling behavior illustrated by simple model." *ASCE Journal of Engineering Mechanics,* **118**(10), 2005-2016.

Z

Zayas, V. A., Shing, P.-S. B., Mahin, S. A., and Popov, E. P. (1981). "Inelastic structural modeling of braced offshore platforms for seismic loading." *Report. No. UCB/EERC-81/04.* University of California at Berkeley, Berkeley, CA.

Zuo, Q. H. and Schreyer, H. L. (1996). "Flutter and divergence instability of nonconservative beams and plates." *International Journal of Solids and Structures,* **9**(33), 1355-1367.